Database-driven online safe flight envelope prediction and protection for enhanced aircraft fault tolerance

Zhang, Ye

DOI
10.4233/uuid:70778c5c-3f00-4854-a0fb-98b24c9ed1cb

Publication date
2019

Document Version
Final published version

Citation (APA)
Zhang, Y. (2019). *Database-driven online safe flight envelope prediction and protection for enhanced aircraft fault tolerance*. [Dissertation (TU Delft), Delft University of Technology].
https://doi.org/10.4233/uuid:70778c5c-3f00-4854-a0fb-98b24c9ed1cb

Database-driven Online Safe Flight Envelope Prediction and Protection for Enhanced Aircraft Fault Tolerance

DATABASE-DRIVEN ONLINE SAFE FLIGHT ENVELOPE PREDICTION AND PROTECTION FOR ENHANCED AIRCRAFT FAULT TOLERANCE

Proefschrift

ter verkrijging van de graad van doctor
aan de Technische Universiteit Delft,
op gezag van de Rector Magnificus prof. dr. ir. T.H.J.J. van der Hagen,
voorzitter van het College voor Promoties,
in het openbaar te verdedigen op woensdag 20 maart 2019 om 10:00 uur

door

Ye ZHANG

Master of Science, Northwestern Polytechnical University, China
geboren te Xi'an, China

Dit proefschrift is goedgekeurd door de

promotor: prof. dr. ir. M. Mulder en dr. Q.P. Chu
copromotor: dr. ir. C.C. de Visser

Samenstelling promotiecommissie:

Rector Magnificus,	voorzitter
Prof.dr.ir. M. Mulder	Technische Universiteit Delft, promotor
Dr. Q.P. Chu	Technische Universiteit Delft, promotor
Dr.ir. C.C. de Visser	Technische Universiteit Delft, copromotor
Onafhankelijke leden:	
Prof.dr. E.M. Atkins	University of Michigan, USA
Prof.dr.ir. L.L.M. Veldhuis	Technische Universiteit Delft
Prof.dr.ir. M.H.G. Verhaegen	Technische Universiteit Delft
Dr.ir. G. Looye	Zentrum für Luft- und Raumfahrt (DLR), Duitsland
Prof.dr. R. Curran	Technische Universiteit Delft, reservelid

Keywords: flight envelope, loss-of-control, database, fault tolerance, machine learning...

Printed by: Ipskamp Printing

Front & Back: Ye Zhang

ISBN 978-94-028-1418-7

An electronic version of this dissertation is available at
http://repository.tudelft.nl/.

To my dear husband and my beloved parents.

CONTENTS

SUMMARY

Among all the contributors to fatal accidents, in-flight loss of control (LOC-I) remains one of the largest categories, as indicated by statistics of investigations into past civil aircraft accidents. In flight LOC generally refers to accidents in which the flight crew was unable to maintain control of the aircraft in flight, resulting in an unrecoverable deviation from the intended flight path. Compared with other accidents occurrence categories, LOC-I is more challenging to predict and prevent, since it is often the result of a highly complex combination of a wide range of contributing factors. Many in-depth researches into loss of control accidents have been conducted to find out how these events unfold, and to develop effective intervention strategies for preventing LOC.

An important characteristic of an aircraft transgressing into a LOC situation is that it moves to the boundaries, or even crosses the boundaries, of its safe flight envelope. The general definition of safe flight envelope is the set of states where an aircraft can be operated and controlled with guaranteed safety. Therefore, part of the research in LOC prevention focuses on how to determine the safe flight envelope. Knowledge about safe flight envelopes can be incorporated into a warning system, to increase the situation awareness of the pilots, and integrated into the flight control system, leading to flight envelope protection systems.

Currently, most modern commercial and military are equipped with some form of flight envelope protection system, to keep the aircraft within the limitations of flight states such as speed, angle of attack and load factor, which together characterize the aerodynamic performance of the aircraft. If a certain boundary is violated, e.g., due to some aggressive maneuvers, a warning will be given by the system. A number of flight envelope protection systems has been developed to enhance the safety level of aviation, which vary in ways of flight envelope determination and warning mechanism.

Current day flight envelope protection systems work with fixed flight envelopes, assuming that the intrinsic aircraft flight dynamics do not change under any circumstances. When abnormal cases like structural damage and icing occur, the performance of the aircraft may suddenly or slowly degrade, which is then ultimately reflected in a change of the flight envelope. If the new, mostly shrunken envelopes are not provided to the system or pilot in time, the aircraft risks to 'unconsciously' leave the safe region, and cause an LOC event. It is therefore essential to develop a method that can provide updated flight envelopes during flight, especially after the occurrence of abrupt events like system failures, or damage. This dissertation focuses on the design and validation of such online safe flight envelope prediction systems.

The development of an online safe flight envelope prediction system meets several challenges and limitations. First of all, in order to provide safe flight guidance across all the flight conditions, the safe flight envelope should be computed on the global model of the aircraft. When damage and failures occur, however, measurement data required for online system identification can realistically only be obtained in a limited region around

the current flight condition, because the impaired aircraft may not be able to maneuver freely. Hence, the onboard global model can only be updated locally in the direct neighborhood of the current flight condition, and the change to the remainder of the global model remains undiscovered. Without a globally updated model, the safe flight envelope computed online will be inaccurate for flight conditions in which the model is not updated.

Secondly, the computational load of computing flight envelopes on the fly is very heavy, as techniques suffer from the so-called curse of dimensionality in the sense that they scale badly with increasing state-space dimensions. This makes the computation infeasible online, especially in emergency situations where even one second of delay may lead to unrecoverable consequences.

Since the determination of flight envelopes during flight is impractical, this dissertation considers the computation of the envelopes *in advance*. To achieve this, a wide spectrum of damage and failure cases that might possibly occur will be considered. For each case, the safe flight envelopes are computed and stored in a database. Including such a comprehensive database in the envelope prediction system, allows the safe flight envelope to be quickly retrieved and used to prevent the aircraft from moving into a LOC situation, even in cases of damage and failures.

The main research goal is **to develop a database-driven safe flight envelope prediction system and apply it to the control and recovery of an impaired aircraft**. To achieve this goal, several questions need to be answered:

1. How to establish the aerodynamic model of an aircraft under damage/failures?

2. How to develop an online assessment system, to diagnose the current condition of the aircraft using identified parameters?

3. In which way to define and compute a safe flight envelope?

4. What should the database look like, and how can one interpolate between two flight envelopes in the database?

5. How to apply the retrieved flight envelopes to fault tolerant flight controllers, to prevent the impaired aircraft from LOC events?

The answer to the ***first*** question forms the basis of the whole research. Since aircraft models can be different under various categories of LOC situations, the scope of modeling is limited to only one category, which includes structural damage to actuators and airframe of an aircraft. The reason for choosing this category is that aircraft damage is closely related to the reduction of stability and control authority of the aircraft, and thereby causing the change of its flight envelope. This reason can also be regarded as a conclusion drawn from experimental data and observations from a series of wind-tunnel and computational tests conducted by other researchers, which our modeling work is based on.

The reference aircraft of damage modeling in this dissertation is a twin-jet business aircraft known as the Cessna Citation, which is the laboratory aircraft operated by TU Delft. The damaged model of the Cessna Citation is used for three purposes: 1) to extend

the current simulation environment, such that flight under damage cases can be simulated and the designed envelope prediction and protection systems can be incorporated and verified in the simulation model; 2) to provide data for system identification as well as the detection and classification of aircraft damage; 3) to enable the computation of safe flight envelopes under modeled damage cases.

The change of aerodynamic model of the damaged aircraft is very often due to the loss of aerodynamic surfaces, leading to smaller aerodynamic forces and moments than expected. In wind tunnel tests, aircraft damage is quantified by the percentage of tip loss with respect to the whole span of wing, vertical tail or horizontal stabilizers. It is observed that the influence of damage is reflected in the changed value of model parameters and additional terms to the original model structure. By studying and analyzing the aerodynamic characteristics of structurally damaged aircraft from experimental data, one can estimate the possible model structure and values of model parameters corresponding to each quantified damage cases. The estimated aerodynamic model is then incorporated in computer simulations which generate the aircraft responses in sudden damage cases. Simulation results demonstrate the expected degradation of flight performance and potential LOC risks after damage.

As the opposite direction of damage modeling, the identification of changed aerodynamic coefficients from system measurements is used to find the corresponding damage/failure case, which is the main concern of the ***second*** research question. In this dissertation, this question is regarded as a classification problem since each damage case is a discrete event that needs to be categorized. Under the framework of classification, the inputs are the identified aerodynamic coefficients and the outputs are defined damage cases with quantified damage scales (percentage of surface loss) on wings, tails as well as actuators. The classification methods used in this dissertation include neural networks and support vector machines. Both methods are implemented on the same damage cases, and their performances are evaluated by the number and rate of true positives, false negatives, true negatives and false positives in cross-validations. The evaluation results show that the method using support vector machines has better generalization ability and is more sensitive to new data in between two classes. As expected, the increased rate of false positives and false negatives of both methods is shown to increase with the noise level and external disturbances imposed on the validation data, showing that the classifier becomes less 'certain' about the results.

The occurrence of damage causes the change of aircraft dynamics, and subsequently influences the original flight envelope. Generally, the flight envelope is described as a subset of the state space within which the aircraft can be safely operated. There are different ways of defining a safe flight envelope, which results in different ways of computing it. Conventional ways consider flight envelopes as static limits, while this dissertation focuses on computing *dynamic* flight envelopes limits. Regarding the ***third*** question, reachability analysis is chosen in this research as the method to compute safe flight envelopes, since the theory can provide a set-valued insight into the safety and control design of dynamic systems. One advantage of this method is that all possible trajectories can be computed from all available control strategies and initial states, which naturally meets the safety guarantees. In this dissertation, the full aircraft model is decoupled, and safe flight envelopes for decoupled longitudinal and lateral motions are computed

using the level set method. It is shown that the shape and size of envelopes are influenced by the current flight condition. A flight envelope computed under a certain level of wing damage, for example, shows an obvious reduction in size and variation in shape as compared to the nominal flight envelope, which verifies the adverse impact of structural damage, and emphasizes the necessity of updating the shrunken envelopes during flight after damage.

To answer the ***fourth*** question, a database is designed, which contains flight envelopes encompassing a range of abnormal scenarios such as damage and failures. The index key to each envelope in the database is determined by the classification results. The number of safe flight envelopes in the database is constrained, however, by storage volume and the number of modeled abnormal cases. Hence, it may be necessary to interpolate between two envelopes to obtain safe strategies for events not included in the database. In this dissertation, flight envelopes are considered as geometric structures, and the method used for interpolation is inspired by research on surface reconstruction and image matching. The basic idea of interpolation is to construct optimal paths between two contours that share similar geometric features (e.g., shapes in two dimensions). Since the contours are composed of data points, the optimal paths are segments between two points, and the points that form the intermediate contour are found on each segment by interpolation. In this dissertation, interpolation is performed between two envelopes in two dimensions. Envelopes of higher dimensions are not discussed here, since it is assumed that high-dimensional envelopes can be decomposed into several 2D contours by fixing the values of certain dimensions.

The interpolation error is calculated by comparing the interpolated envelope with the one computed by the level set method. It is shown that the interpolation can approximate the computed envelope with high accuracy, which is very important to reducing the number of stored envelopes in the database. Compared with the level set method, the improvement in computational efficiency of the direct database retrieval and interpolation is shown to be significant, which indicates the feasibility of online flight envelope prediction using database retrieval and interpolation methods.

The answer to the ***fifth*** question finalizes the research by using the predicted flight envelope in the online implementation of flight envelope protection with fault tolerant control. Unlike currently-used envelope protection systems, where the flight envelope is an implicit set of data at the basis of the control law design, the flight envelopes defined and computed in this dissertation are explicitly referred to by the system as a separate module. By using online database retrieval, the protection system can be adaptive to a wider range of abnormal conditions. The closed-loop simulations implemented in this dissertation include previously discussed modules of system identification, damage classification and envelope database, together with the fault tolerant control to give feedback control input to the aircraft. It is shown in the simulation that after the sudden occurrence of damage, the aircraft is quickly re-stabilized by the controller, generating excitation to the identification, and subsequently providing input to the classifiers. The classification result is then used as an index to a safe flight envelope in the database, and safe boundaries of certain flight states are extracted from the retrieved envelope under the current flight condition. When new maneuvers are initiated after damage, those safe boundaries are used as constraints and limitations to the reference commands to

the control system. Simulation results show that without envelope protection, LOC accidents will happen due to excessive pilot commands, since both the controller and pilots are not aware of the shrunken flight envelope after damage. By comparison, it is shown that the incorporation of the online retrieved envelope can effectively prevent the damaged aircraft from entering the LOC condition, under the pre-condition that the aircraft is not so severely damaged and all remaining actuators are not saturated. The implementation of the whole closed-loop flight in computer simulations indicates that online flight envelope prediction and protection is feasible based on the offline-built database.

In conclusion, this dissertation proposes a database-driven method to address the challenges of online safe flight envelope prediction under LOC hazards. Simulations have shown that the proposed system is feasible for online implementation, with reduced computational effort as compared to existing methods. Research work should continue in the future to improve the proposed system and apply it to other safety-critical fields. For example, it is recommended to investigate other LOC contributors and include their influences in the modeling work and the computation of safe flight envelopes. Furthermore, experiments with real vehicles in real flight should be conducted, to verify the proposed system and explore its limitations in an environment full of uncertainties. Apart from fixed-wing aircraft, future applications may extend to autonomous systems like drones, self-driving cars and robots, where several critical safety-related issues can be potentially resolved by the techniques developed in this dissertation.

SAMENVATTING

Statistische analyse van onderzoeken naar de voorbije dodelijke ongelukken in de civiele luchtvaart laten zien dat van alle oorzaken, het verlies van controle tijdens de vlucht (LOC-I) een van de grootste groepen is. LOC-I verwijst in het algemeen naar ongevallen waar de vliegtuigbemanning niet in staat was de controle van het vliegtuig te behouden en resulteert in een onherstelbare afwijking van het geplande traject. Verschillende onderzoeken hebben in detail uitgezocht hoe zo een situatie zich ontwikkelt en wat mogelijke ontwerpen zijn van systemen die dit kunnen voorkomen.

Een belangrijk kenmerk van een situatie waar de controle over het vliegtuig verloren wordt, is dat het vliegtuig zich naar, of zelf over, de prestatie limieten beweegt. De algemene definitie van de prestatie limieten van een vliegtuig is een verzameling van toestanden waar een vliegtuig gegarandeerd veilig kan worden gebruikt en gecontroleerd. Een aantal beveiligingssystemen van deze prestatie limieten zijn tegenwoordig ontwikkeld om het veiligheidsniveau van de luchtvaart te verbeteren. Deze systemen gebruiken verschillende manieren om de prestatie limieten te bepalen en om waarschuwingen te geven.

Veelgebruikte beveiligingssystemen van de prestatie limieten werken met vaste eigenschappen: ze nemen aan dat de intrinsieke vliegtuigdynamica onder geen omstandigheden verandert. Wanneer zich abnormale situaties voordoen, zoals beschadiging van de structuur of ijsafzetting, kunnen de eigenschappen van het vliegtuig op verschillende snelheden veranderen, wat uiteindelijk betekent dat de prestatie limieten veranderen. Als de nieuwe, meestal verminderde limieten niet tijdig beschikbaar zijn voor het systeem of de piloot, bestaat er een risico dat het vliegtuig 'onbewust' de veilige regio verlaat en de controle over het vliegtuig verloren wordt. Het is daarom essentieel om een systeem te maken dat de prestatie limieten kan voorspellen tijdens de vlucht, vooral bij abrupte gebeurtenissen zoals systeemstoringen of schade.

De ontwikkeling van zo een voorspellingssysteem dat tijdens de vlucht werkt heeft verschillende uitdagingen en beperkingen. Ten eerste moeten de veilige prestatie limieten berekend worden op het globale model van het vliegtuig om veilige vliegbegeleiding te geven over alle vliegcondities. Wanneer er schade en storingen optreden, kan de data die nodig is om het systeem te identificeren alleen bekomen worden voor een beperkte regio rond de huidige vliegconditie. Dit omdat het gehavende vliegtuig misschien maar een beperkte bewegingsvrijheid heeft. Daarom kunnen de globale modellen die aan boord gebruikte worden enkel lokaal in de directe omgeving van de huidige vliegconditie ge-update worden en blijft de rest van het globale model verborgen. Zonder een model dat globaal ge-update is zullen de berekende veilige prestatie limieten onnauwkeurig zijn voor vliegcondities waar het model niet bijgewerkt is.

Ten tweede is er een zeer grote rekenkracht nodig is om de prestatie limieten te berekenen tijdens de vlucht omdat die technieken lijden onder de zogenaamde vloek van dimensionaliteit: ze schalen slecht met een groter aantal toestanden. Dit maakt de

berekening in de lucht onmogelijk, zeker en vast in noodsituaties waar zelfs één seconde vertraging kan leiden tot onherstelbare gevolgen.

Omdat de berekening van de prestatie limieten tijdens de vlucht onmogelijk is, kijkt dit proefschrift naar de berekening van de prestatie limieten voor er zich iets voordoet. Een breed scala aan schade en storingen dat kan optreden zal worden onderzocht. Voor elke geval zullen de veilige prestatie limieten berekend worden en opgeslagen in een database. Door zo een uitgebreide database op te nemen in de prestatie voorspellingssystemen, kan zelfs in het geval van schade of storingen de veilige prestatie limieten snel worden opgezocht en gebruikt om te voorkomen dat de controle over een vliegtuig verloren wordt.

Het hoofddoel van dit onderzoek is het ontwerpen van een voorspellingssysteem van de veilige vliegtuig prestatie limieten gebaseerd op een database en dit toe te passen op de controle en herstel van controle van een beschadigd vliegtuig. Om dit doel te bereiken moeten verschillende vragen beantwoord worden:

- Hoe wordt het aerodynamische model van een vliegtuig met schade/storingen bepaald?
- Hoe kan een beoordelingssysteem voor in de vlucht ontwikkeld worden om de huidige staat van het vliegtuig te bepalen met behulp van de geïdentificeerde parameters?
- Op welke manier worden de veilige prestatie limieten gedefinieerd en berekend?
- Hoe moet de database eruit zien en hoe kan er worden geïnterpoleerd tussen twee instanties van prestatie limieten in de database?
- Hoe kunnen de opgehaalde prestatie limieten worden toegepast op fouttolerante vliegtuigbesturing, om te voorkomen dat de controle verloren wordt?

Het antwoord op de eerste vraag vormt de basis van het hele onderzoek. Aangezien vliegtuigmodellen onder verschillende categorieën van LOC-situaties anders kunnen zijn, is de reikwijdte van de modellering beperkt tot slechts één categorie: schade aan actuatoren en de structuur van een vliegtuig. De reden voor het kiezen van deze categorie is dat vliegtuigschade nauw samenhangt met de vermindering van de stabiliteit en de autoriteit van de besturing van het vliegtuig. Door deze veranderingen gaan de prestatie limieten van het vliegtuig ook veranderen. Door de aerodynamische kenmerken van structureel beschadigde vliegtuigen uit experimentele gegevens te bestuderen en te analyseren, kan een schatting worden gemaakt van de mogelijke modelstructuur en waarden van modelparameters die overeenkomen met elk gekwantificeerd schadegeval. Het geschatte aerodynamische model wordt vervolgens opgenomen in computersimulaties die de reactie van het vliegtuig op plotselinge schade genereren.

Naast de modellering van schade wordt de identificatie van veranderende aerodynamische coëfficiënten uit metingen gebruikt om het corresponderende schadegeval of storing te vinden. Dit is het belangrijkste onderdeel van de tweede onderzoeksvraag. Aangezien elk schadegeval een discrete gebeurtenis is die moet die worden gecategoriseerd, wordt de deze tweede vraag in dit proefschrift beschouwd als een classificatieprobleem.

De classificatiemethoden die in dit proefschrift worden gebruikt, omvatten neurale netwerken en een vector ondersteunde beslissingsmachine. Beide methoden werden geïmplementeerd voor dezelfde schadegevallen en hun prestaties werden geëvalueerd. De resultaten tonen aan dat de methode met behulp van een vector ondersteunde beslissingsmachine een beter generalisatievermogen oplevert en meer gevoelig is voor nieuwe gegevens tussen twee klassen.

Wat de derde vraag betreft, is de analyse van bereikbaarheid van toestanden in dit onderzoek gekozen als methode voor het berekenen van veilige prestatie limieten. Dit omdat die theorie kan zorgen voor een waardevol inzicht in het veiligheids- en besturingsontwerp van dynamische systemen. Een voordeel van deze methode is dat alle mogelijke trajecten die voldoen aan de veiligheidsgaranties kunnen worden berekend op basis van alle beschikbare regelstrategieën en initiële toestanden. In dit proefschrift wordt het volledige vliegtuigmodel ontkoppeld voor longitudinale en laterale bewegingen. Voor deze ontkoppelde dimensies worden veilige vliegtuig prestatie limieten berekend met behulp van de vlakke verzameling-methode. De limieten berekend onder een bepaald niveau van vleugelbeschadiging tonen bijvoorbeeld een duidelijke vermindering in afmeting en variatie in vorm in vergelijking met de nominale limieten. Dit bevestigt de nadelige invloed van structurele schade en benadrukt de noodzaak van het bijwerken van de verminderde prestatie limieten tijdens de vlucht na schade.

Om de vierde vraag te beantwoorden is een database is ontworpen. Deze database bevat de prestatie limieten van een reeks abnormale scenario's zoals schade en storingen. De indexsleutel voor elke instantie van prestatie limieten in de database wordt bepaald door de classificatieresultaten. Het aantal instanties in de database is echter beperkt door het beschikbare opslagvolume en door het aantal gemodelleerde abnormale gevallen. Daarom kan het nodig zijn om tussen twee instanties van limieten te interpoleren om veilige strategieën te verkrijgen voor gebeurtenissen die niet in de database zijn opgenomen. Het basisidee van interpolatie is om optimale paden te construeren tussen twee contouren met vergelijkbare geometrische kenmerken (bijvoorbeeld vormen in twee dimensies). In dit proefschrift wordt interpolatie uitgevoerd tussen twee instanties van prestatie limieten in twee dimensies. Instanties met hogere afmetingen worden hier niet besproken, omdat er aangenomen wordt dat instanties met meer dimensies kunnen worden ontbonden in verschillende tweedimensionale contouren door de waarden van de andere dimensies vast te zetten.

Het antwoord op de vijfde vraag rondt het onderzoek af met de implementatie van een beveiligingssysteem dat gebruik maakt van voorspelde limieten en van fouttolerante besturing. Het beveiligingssysteem kan zich aanpassen aan een groter aantal abnormale omstandigheden door gebruik te maken van het opvragen van elementen in de database tijdens de vlucht. Simulatieresultaten tonen aan dat zonder de beveiligingssystemen LOC-ongevallen zullen gebeuren als gevolg van buitensporige piloot stuurgedrag. Dit gebeurt omdat zowel de controller als de piloten zich niet bewust zijn van de verminderde prestatie limieten na beschadiging. Er wordt ook aangetoond dat het gebruik van de opgevraagde prestatie limieten in de vlucht kan voorkomen dat het beschadigde vliegtuig in een LOC-toestand terecht komt. Dit is allemaal op voorwaarde dat het vliegtuig niet te zwaar beschadigd is. De implementatie van de hele keten aan systemen in computersimulatie toont aan dat het in de vlucht mogelijk is om de prestatie limieten te

voorspellen en te beschermen van op basis van de vooraf gebouwde database.

Meer onderzoek is nodig om het voorgestelde systeem te verbeteren en toe te passen op andere domeinen waar veiligheid kritiek is. Zo is het aanbevolen om te onderzoeken welke andere factoren ervoor kunnen zorgen dat de controle van het vliegtuig verloren wordt. Deze factoren moeten worden onderzocht en hun invloed moet meegenomen worden in het model en de berekening van veilige prestatie limieten. Verder moeten experimenten met echte vliegtuigen in echte vlucht worden uitgevoerd om het voorgestelde systeem te valideren en de beperkingen ervan te verkennen in een omgeving vol onzekerheden. Afgezien van vliegtuigen met een vaste vleugel, kunnen toekomstige toepassingen zich uitbreiden naar autonome systemen zoals drones, zelfrijdende auto's en robots. Bij deze systemen kunnen verschillende kritieke problemen voor de veiligheid mogelijks worden opgelost met behulp van de technieken die in dit proefschrift zijn ontwikkeld.

1

INTRODUCTION

"Aircraft systems technology in particular has been conscientiously evolved with safety in mind."

Aviation Accidents Report by Airbus

1.1. BACKGROUND: TOWARD A SAFER FLIGHT

1.1.1. LOSS OF CONTROL IN-FLIGHT ACCIDENTS

Loss of control In-Flight (LOC-I) is the single biggest cause of fatal accidents over the last 20 years [1]. According to the definition given by the International Association of Air Transport (IATA) [2], LOC-I refers to "*accidents in which the flight crew was unable to maintain control of the aircraft in flight, resulting in an unrecoverable deviation from the intended flight path.*"

LOC-I accidents are almost always catastrophic, and are considered to be the highest risk to aviation safety. Therefore, LOC-I is deemed to be an area for increased attention [2]. In recent years, improvements in mitigating other accident categories have resulted in LOC-I becoming the leading cause of fatal accidents in commercial air transportation worldwide. The fact that LOC-I is receiving substantial attention from industry despite the relatively low number of accidents is on account of the disturbing number of fatalities they have caused [2].

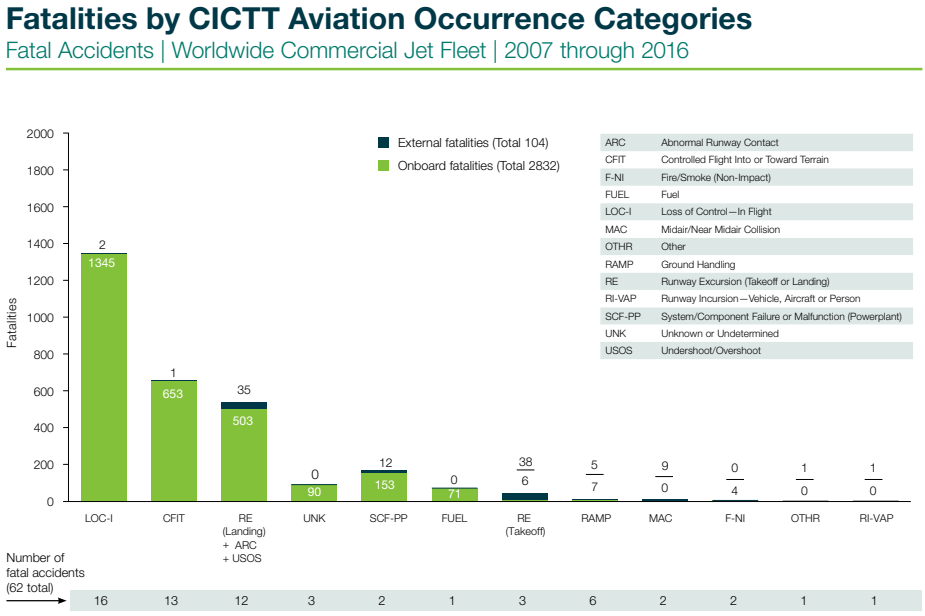

Figure 1.1: Overview of Fatal Aviation Accidents and Principal Categories (Copyright © 2017 Boeing)

In the latest statistical summary of commercial jet airplane accidents published by the Boeing company [3], a figure on worldwide fatal accidents occurring from 2007 through 2016 (Fig. 1.1) reveals that LOC-I remains the largest fatal accident category. As shown in Fig. 1.1, LOC-I resulted in 16 accidents and 1347 total fatalities [3]. It is also indicated in the report that LOC-I is a significant contributor to accidents and fatalities across all civil vehicle classes, operational categories, and phases of flight [3], exposing passengers and crew to the highest risk of a catastrophic accident with no survivors

[4]. Similar trends can be found in the statistics on aircraft accidents from 2010 to 2016 published by IATA [2, 4, 5]. In the IATA report, LOC-I is also considered as the largest contributor, accounting for 49% of total fatalities from 2010 to 2014 and 58% from 2012 to 2016.

LOC-I accidents have been shown to be significantly reduced by technologies already existing on new generation aircraft, such as flight envelope protection systems that come with fly-by-wire technology [1]. However, despite the positive impact of these developments, with low survivability ratio, LOC-I still remains the primary cause of fatalities in air transportation, and its frequency is increasing compared to other categories.

Compared with other accident occurrence categories, LOC-I is challenging to predict and prevent, since it is a highly complex event: usually resulting from multiple causal and contributing factors that can occur individually or (more often) in combination. There is no single intervention strategy that can be readily identified to prevent LOC accidents. Therefore, the analysis on causal factors of LOC-I accidents has been an extensively ongoing research topic in recent years [6]. In the LOC accident study conducted by NASA, a review of 126 LOC accidents occurring between 1979 and 2009 was performed based on accident reports and databases. Information from the reports was transcribed into a categorized set of causal factors, which were then grouped into three large categories: adverse onboard conditions, vehicle upsets, and external hazards and disturbances [7]. As shown in Table 1.1, each category includes several subcategories of precursors/hazards to enable a further statistical analysis.

Table 1.1: Categories of LOC Causal Factors

Adverse Onboard Conditions	External Hazards and Disturbances	Aircraft Upsets
system faults and failures	icing and snow	stall
airframe damage	wind gusts	abnormal attitude
engine failure	wake vortices	abnormal velocity
inappropriate crew response	poor visibility	abnormal trajectory

Of 126 accidents investigated in [7], 94.4% of accidents and 93.4% of fatalities involved adverse onboard conditions. In addition, these precursors are also used to define a LOC accident as a time sequence of connected events [7]. For example, some LOC accidents are first precipitated by an adverse onboard condition (e.g., airframe damage) and then lead to vehicle upset (e.g., stall). 54.8% of the accidents and 61.3% of the fatalities are initiated by adverse onboard conditions, which accounts for the largest proportion [8]. This dissertation focuses on airframe damage and system faults in this category.

1.1.2. FLIGHT ENVELOPE PREDICTION AND PROTECTION IN LOC PREVENTION AND RECOVERY

Research into LOC-I accidents concluded that, in spite of numerous hazards and their combinations, a key characteristic of LOC is the deviation of the aircraft from its normal flight envelope [8]. An analysis of typical LOC accident data [9], in terms of angle of attack and sideslip as compared to wind-tunnel data of normal flight, concluded that LOC

events often include flight conditions that lie far beyond the normal flight envelope. In a research jointly conducted by the Boeing Company and NASA Langley [10], a quantitative set of metrics is developed to define LOC accidents, based on five envelopes relating the aircraft flight dynamics, aerodynamics, structural integrity, and flight control. These research results revealed a strong relationship between LOC-I accidents and the excursion of a set of predefined envelopes. Generally, flying out of the envelopes has three causes: 1) pilots are not provided with enough information on the current situation and envelope restrictions, 2) a lack of anticipatory guidance and recovery to mitigate the crisis, and 3) possible changes in the flight envelope are not estimated and monitored in time. Due to these reasons, the development of *onboard* flight prediction, protection and awareness systems to improve flight safety has received significant attention from industry and research institutes.

Currently, the fly-by-wire system with flight envelope protection carried onboard modern airliners protects the aircraft within limitations of load factor, speed and angle-of-attack to prevent stall [11]. The protection was designed to be either "hard" envelope protection (as adopted by the Airbus airplanes), or "soft" envelope protection (as utilized by the Boeing airplanes) depending on different policies on pilot authority [12]. Although it is debatable which one is better, both types of envelope protection systems have reduced the pilot's workload and enhanced flight safety. According to the latest safety report issued by the Airbus Company[1], in 2016 the proportion of flights flown by aircraft equipped with flight envelope protection has risen to 48%, which is likely to contribute to a significant reduction in accident rate.

Nevertheless, research on improving and augmenting the aircraft flight control system is still ongoing due to the high frequency of LOC-I. Regarding the complexity of LOC accidents and practical challenges in conducting high-risk flight experiments (e.g., flying with structurally damaged aircraft), there is no single intervention strategy or a holistic solution to all the problems. Most research work focuses on one of five sub-topics:

1. Aircraft dynamic modeling under various LOC precursors/hazards,
2. Detection and identification of the precursors/hazards that lead to envelope change and excursion,
3. Experimental and theoretical ways of defining and computing safe flight envelopes,
4. Integrating fault tolerant control systems with flight envelope protection, to enable automatic recovery and mitigate LOC hazards, and
5. Developing interface systems that improve the situation awareness and provide anticipatory guidance to pilots under LOC hazards.

Fig. 1.2 illustrates that these topics are closely related to each other, and together they form a complete system of online LOC prevention through flight envelope prediction and protection.

1.2. PRESENT RESEARCH

Based on the five sub-topics listed above, a brief review of literature is given in this section. Some research work has inspired the ideas and studies included in this thesis.

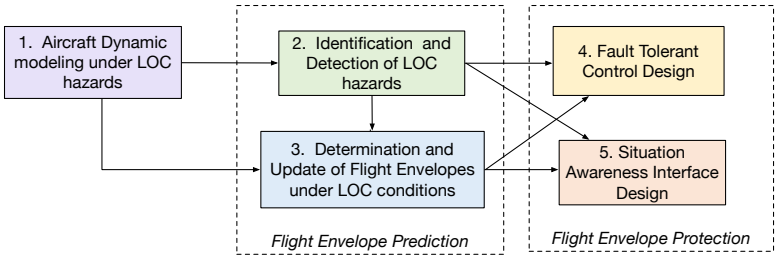

Figure 1.2: Five sub-topics relating to LOC prevention via flight envelope prediction and protection

1.2.1. MODELING OF AIRCRAFT DYNAMICS

The motivation of this subject is three-fold: 1) to understand and model the characteristics of aircraft dynamics under upset conditions, airframe damage, and external hazards, 2) to develop and evaluate technologies for the detection and identification of upset conditions and structural damage, and 3) to integrate the modeling result into high-fidelity simulation environments that enable improved pilot training and the validation of onboard LOC prevention and recovery systems under realistic LOC scenarios. In general, this is the primary phase and foundation of all LOC-related research work.

Considering the number of different hazards to be modeled, and their possible coupled effects, acquiring data and developing a representative model is challenging. Currently, the aerodynamic modeling approaches involve analytical, experimental and computational methods, which are applied to obtain data. The data are used for developing a database and math models for characterizing aerodynamic effects associated with aircraft upset conditions, structural damage and external hazards [8].

Aircraft upset conditions are often related to conditions in the stall/post stall flight regimes where the aircraft leaves the normal flight envelope at a high angle-of-attack. An extensive aerodynamic database was obtained through static and dynamic wind-tunnel testing over a wide range of angles of attack and sideslip [9, 13]. Further enhancements addressed the effects of various flap configurations in approach-to-stall, stall, and post-stall flight regimes [14]. Particular attention was also devoted to the stall region where full-scale transport aircraft have demonstrated a tendency for roll instability, and the aerodynamic model was estimated from dynamic wind-tunnel data [15]. Extensive research was also performed in advancing CFD modeling methods and software tools for aerodynamic effects under upset conditions [16].

Aircraft structural damage can be caused by incipient fatigue crack growth that may potentially reach sudden catastrophic failures and loss of components, and then lead to changes in dynamic characteristics and control capability [8]. Aerodynamic data of structurally damaged aircraft were obtained from wind-tunnel tests and CFD methods. In a wind tunnel test conducted by NASA, damage was physically modeled on a sub-scale general transport model (GTM) in the form of partial or total loss of wing area, horizontal tail, and vertical tail [13, 17, 18]. The CFD assessment of aerodynamic degradation due to airframe damage was obtained from experiments conducted on the same GTM model [19]. Not only airframe structural damage, the aerodynamic effects of airframe icing were also modeled and studied experimentally and computationally for onboard detection

and mitigation of icing conditions [8, 20].

1.2.2. LOC HAZARDS DETECTION AND IDENTIFICATION

Much of the research on this subject has mainly focused on: 1) real-time system identification of aerodynamic models, 2) failure detection, isolation and identification of flight sensors and control actuators, 3) detection of damage size and location in structures based on vibration characteristics and estimation of residual strength of the damaged structure, and 4) detection of in-flight icing conditions.

System identification is a broad field of study, which involves various methods in both the time-domain and frequency-domain applied to a variety of applications. Generally, it can be considered as the development of a mathematical model from modeling data as an abstraction of physical reality. In aerospace, the identification of aircraft models can be decomposed into two parts using the two-step method [21]: 1) estimation of system states based on the kinematics model, and 2) estimation of system parameters based on the aerodynamic model. The changed characteristics of the aircraft under LOC hazards are reflected in the change of the aerodynamic model in both structures and parameters [22, 23]. Once the change is correctly identified, the faults and failures causing the change can be detected and isolated.

Faults/Failure Detection and Isolation (FDI) represents a series of methods and systems that detect the occurrence and isolate the source/location of certain malfunctions of sensors and actuators [24]. The most commonly used FDI methods for sensors rely on hardware redundancy, which uses multiple parallel sensors for the same function and compares duplicative signals generated by different sensors. Instead, model-based analytical FDI methods do not require additional hardware, and have been developed and used for aircraft actuators [25]. By comparison, the analytical approach is more cost effective with a wider spectrum of applications covering different types of aircraft components [23, 26, 27].

The airframe structural damage can be defined in two levels. In developing structural health monitoring (SHM) systems [28], structural damage is regarded as fatigue cracks that may occur anywhere on the airframe [29]. If these incipient faults are not detected or left unattended for a long period of time, they may build up slowly and lead to abrupt break away of a certain part of the airframe, which is the second level of structural damage. Nowadays, most attention focused on the first level in order to prevent the occurrence of more severe damage like wing tip loss.

Airframe and engine icing is another important category of LOC hazards besides the aforementioned system faults and structural damage. In-flight icing can cause changes in vehicle dynamics as well as control effectiveness, and can accumulate until the aircraft suddenly enters an upset condition. To address this problem, methods and systems have been developed to detect the icing effects on aircraft and to provide pilots with an advance warning of the adverse effects [8].

1.2.3. FLIGHT ENVELOPE DEFINITION AND DETERMINATION

The term “flight envelope” is loosely applied without a strict definition, since in literature various types of envelopes are derived and computed based on different methods, flight states and metrics. In general, the flight envelope can be described as a region

where the aircraft can perform a safe flight. Normally it is a subset of the state space confined by certain flight conditions, which indicate aerodynamic limits (stall), energy limits (thrust), and structural limits (load factor), all reflected in the operational constraints on airspeed, angle-of-attack, altitude and turn rate etc.

Commonly used flight envelopes are: 1) a V-n diagram which indicates the relation between limitations on speed and load factor, 2) an Energy-Maneuverability (E-M) diagram which improves the V-n plot by adding turn rate and provides more information about dynamic maneuvers and energy state, which is also referred to as the "doghouse plot". These flight envelopes and their improved extensions indicate the flight performance and designed characteristics of an airplane. The boundaries of these envelopes are derived from dynamic equations on a certain operation condition like a coordinated turn or level flight. These flight envelopes can be correlated and combined to form a larger envelope with more state constraints in flight planning.

From the perspective of LOC prevention, conventional flight envelopes are not sufficient to show the relation between flight states and various LOC accidents. In [10], five two-dimensional flight envelopes are defined to describe LOC in a quantitative way. These envelopes are related to: 1) aircraft aerodynamics mapped in angle of attack and angle of sideslip, 2) aircraft attitude in bank angle and pitch angle, 3) structural integrity represented by airspeed and load factor, 4) dynamic pitch control, and 5) dynamic roll control. By mapping flight test data (including stall) and LOC accident data into these flight envelopes, LOC events can be characterized by excursions outside at least three of these envelopes. Therefore, these metrics of flight envelopes can be used to predict and prevent LOC accidents [8].

The aforementioned flight envelopes indicate the static hard limits of the aircraft. Sometimes it is of equal importance to look more into the safe maneuvering and recovery during flight. From this perspective, a safe flight envelope can be defined as a subset of the hard-limit-envelope, in which the aircraft can maneuver to and from trim sets, or transit between trim points. Theoretically, the determination of this kind of flight envelope is always regarded as a reachability analysis problem, which has been addressed in the literature [30–32]. Basically, the reachability analysis seeks to decide whether the trajectories of a system model can reach a certain target set from an initial set within given time horizons and input constraints [33].

The approach to the reachability problem is characterizing flight envelopes as level sets of the value function of an optimal control problem based on the aircraft dynamics and control authorities [34–38]. Given the intrinsic nonlinearity of the aircraft model and the high complexity of the numerical computation [39], most methods cannot be realized online. Methods with lower computational load and simplified aircraft models have been proposed for online application [22, 40–43]. In [44, 45], a recoverable set is defined and computed on a linearized model to guide safe transitions between trim points that have been calculated and stored offline [46]. However, in-flight computation of reachable sets of complex nonlinear aircraft models remains infeasible.

1.2.4. FLIGHT ENVELOPE PROTECTION AND RECOVERY

The flight envelope protection and recovery system is developed and used to ensure that the aircraft can stay in the safe flight envelope. As mentioned earlier, currently used on-

board envelope protection systems have enhanced flight safety, but most of them are typically designed for normal operating conditions, which leaves out much room for further improvements and extensions to abnormal situations. Given convoluted contributing factors to LOC accidents, online fault tolerant control and adaptive control are integrated into a flight envelope prediction and estimation scheme [47] to help aircraft recover from upset conditions after sudden failures. In [48, 49], a flight envelope protection scheme is developed on a command-limiting architecture based on the pre-defined LOC quantitative envelopes [10] and is augmented by an adaptive controller to reject system disturbances [50]. Other flight envelope protection systems are designed to accommodate aircraft model changes that are the result of system failures and structural damage [22, 51].

1.2.5. SITUATION AWARENESS AND ANTICIPATORY GUIDANCE

Developing human-machine interface systems, that provide anticipatory guidance and improve situational awareness under LOC hazards, is another important aspect of LOC prevention and recovery, and depends on progress in the aforementioned sub-topics. In [52], a real-time method for predicting LOC safety margins as the aircraft gets close to the edge of the safe flight envelope of operation is developed, which additionally provides flight-deck cues to the pilot [8]. The critical information of the edges of dynamic envelopes computed in [22] can be mapped to pilot displays to show adverse impact of engine degradation and icing conditions [53]. In [54], intuitive information on the flight envelope is provided to pilots through haptics, force feedback trough the control device, integrated in the existing Airbus control laws. An automation situation awareness display is proposed in [55] that provides cues about the state of automation directly in terms of pilot control actions as well as flight parameters. Asymmetric flight envelope limits are incorporated in interface design [56] to help crew plan an emergency landing trajectory. For icing conditions, real-time envelope protection cues and alerting messages are indicated on pilot displays, and the icing contamination envelope protection system has been evaluated positively by pilots in flight simulations [57].

1.3. RESEARCH GOALS AND APPROACH

1.3.1. RESEARCH CHALLENGES AND MOTIVATIONS

It can be concluded from the literature review that the research on LOC-I prevention has undoubtedly made significant progress in every aspect. Nevertheless, theoretical and technical challenges are still present, some of which have become the motivation for this thesis.

As mentioned in the previous section, most flight envelope protection systems currently applied onboard the aircraft work with fixed flight envelopes on the assumption that the intrinsic aircraft dynamics do not change under any circumstances, that is, these systems are static in nature. However, for many LOC hazards, like structural damage and icing, the aerodynamic model as well as the nominal flight envelopes of the aircraft may have changed. For example, in case of wing damage, the maximum lift coefficient decreases, which results in a higher stall speed and lower maximum load factor. Therefore, the control and guidance constraints used by fixed flight envelope protection systems

may no longer be valid. If the new, potentially shrunken envelopes are not provided to the system or pilot in time, the aircraft will be under the risk of 'unconsciously' leaving the safe flight envelope and move into a LOC event. To address this problem, an online flight envelope prediction system is required.

The development of such a system faces a number of challenges, of which two are crucial to consider. The first, called the *fundamental challenge*, states that an accurate global model of the aircraft dynamics is required to obtain a flight envelope that is globally valid. In the presence of failures and damage, however, measurement data required for online model identification can realistically only be obtained in a limited region around the current flight condition because the impaired aircraft may not be able to maneuver freely without exiting the new flight envelope, thereby causing the very problem the system is intended to prevent. Hence, the onboard global model can only be updated locally in the direct neighborhood of the current flight state, with the remainder of the global model necessarily assumed unchanged. Without a valid global model, the updated flight envelopes will be inaccurate.

The second challenge is more practical in nature, and entails the high computational costs of existing methods for obtaining flight envelopes that exploit high-dimensional nonlinear global models. Consequently, onboard use of such methods online in LOC situations is currently infeasible unless significant simplifications are made [22]. Although methods on linearized models take less computational time [41, 45], the computed flight envelopes are only valid within a limited region around the current state.

1.3.2. RESEARCH QUESTIONS AND METHODOLOGIES

Based on the aforementioned challenges, the main research goal can be formulated as:

Research Goal

To develop an online safe flight envelope prediction system for aircraft subject to in-flight faults and damage.

Since the computation of flight envelopes in flight is infeasible, we may consider to compute the envelopes in advance. The solution that is proposed in this dissertation is to retrieve the flight envelopes from an onboard database, which is constructed offline and contains precomputed flight envelopes for various representative faults and damage scenarios. To achieve this, a wide spectrum of damage and failure cases that might possibly occur to an aircraft will be considered. For each representative case, a global dynamics model and its corresponding flight envelopes are obtained offline and then stored into the database. Then, only the database retrieval is performed online, circumventing the two main challenges associated with direct online flight envelope prediction. Having a comprehensive database within the envelope protection system means that it is likely that a safe flight envelope can be quickly retrieved and used to save the aircraft from transgressing into a LOC event.

To achieve this goal, four research questions need to be answered, which together frame the objectives of this research. Figure 1.3 shows a general framework of the database-

driven system proposed in this thesis, as well as the key topic of each research question marked by four different colors. The solution to each question can be considered as one of the components of a complete flight envelope prediction and protection system developed in this thesis.

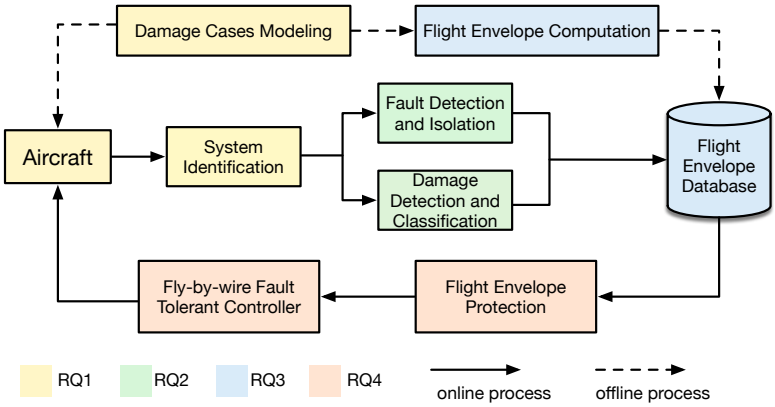

Figure 1.3: An overview of the proposed database-driven system and main research questions.

Research Question 1

How to establish the global aerodynamic model of damaged aircraft and identify the parameters of the model?

The precondition of a reliable online envelope prediction system is an accurate global model, which is composed of a set of local models under different flight conditions. Different local models may have different model structures and parameters, which are obtained by using system identification under specific flight conditions. The identification method used in this thesis is the two-step method in the time domain, where the estimation of flight states and aerodynamic coefficients are separately dealt with [21]. Since this research is aimed at aircraft structural damage, the focus is on the second step of the two-step method, in which the identification of changed aerodynamic coefficients may help to diagnose the damage to the aircraft.

The aerodynamic characteristics of the partially damaged aircraft requires data measured from damaged aircraft in a series of destructive tests. Since real-time flight data of aircraft under off-nominal conditions are hardly available, unless destructive tests are repeatedly conducted, most experiments are based on using subscale models in the wind tunnel [13, 17, 18] and CFD experiments [19]. By identifying the model parameters and model structures from experimental and simulation flight data, the aerodynamic model of partially damaged aircraft can be established.

Research Question 2

How to develop an online damage assessment system, which can diagnose the current health condition of a damaged aircraft?

From wind-tunnel data, it can be observed that each damage case, with different structural parts missing, results in unique aerodynamic effects on the aircraft as well as changes in different stability derivatives. For instance, the experiment data obtained in a situation with horizontal stabilizer damage show that the damage causes significant changes in longitudinal stability, which is indicated by the changed value of C_{m_α} and C_{m_q} [17]. Additionally, due to geometric asymmetry after one-sided damage or unequal damage to both stabilizers, a slight incremental rolling moment is observed with the increasing value of C_{l_α}. The vertical tail damage mainly results in a steady change in lateral forces and directional stability, as indicated by the values of C_{Y_β}, C_{n_β}, and C_{n_r} [58]. For wing damage experiments conducted in [17, 18], the most important observation is the reduced lift force and the incremental rolling moment induced by unequal normal force contributions from left to right wings. Also, the effective dihedral C_{l_β} is affected due to wing tip loss.

From these observations, one can imagine that the damage can be detected and isolated based on diverse aerodynamic characteristics caused by different damage parts on the aircraft. Through creating a training set by performing a number of simulation experiments based on several pre-defined damage cases, a classification problem can be formulated. One of the key steps is training the classifier offline with known damage classes to get the decision boundaries or surfaces that divide the measurement space into several regions. Based on the offline training and online identification results, the current structural integrity of the aircraft can then be accurately assessed.

Research Question 3

How to compute the safe flight envelopes of an aircraft, and build a database of various fault and damage cases?

Reachability analysis is chosen in this research as the technique to compute safe flight envelopes. One advantage of this technique is that all possible trajectories can be computed from all available control strategies and initial states, which naturally meets the safety guarantees [41]. The computed results are called reachable sets, which are defined as a set of states that reach a certain target set within a given time horizon and current control authority [33, 35, 59]. During the process of predicting the safe flight envelope, two reachable sets are needed, which are normally referred to as the backward reachable set and the forward reachable set [38, 42, 60], as shown in Fig. 1.4(a). The intersection between these two reachable sets of a given trim set is then defined as the safe flight envelope, as it indicates the region in the state space where aircraft can reach the trim set and maneuver freely within a certain time horizon. When failures or damage occurs, both the forward and backward reachable sets will shrink, as well as the trim set

due to the changed aircraft model. Therefore, some state trajectories that are part of the reachable sets during normal flight become part of the unreachable set after failures or damage, which typically results in the reduced safe flight envelope shown in Fig. 1.4(b).

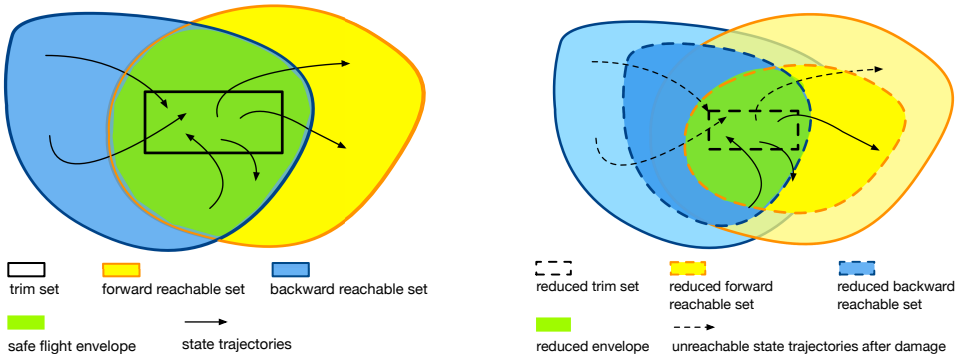

(a) normal flight (b) after failures or damage

Figure 1.4: Illustration of the safe flight envelope based on reachability analysis and its change after sudden damage and failures.

Based on the computed safe flight envelopes, a database containing offline calculated envelopes under different fault and damage scenarios can be designed and established. Each flight envelope stored in the database corresponds to one index number, that is, the database "key", which is determined by the current flight condition and the assessed health condition of the aircraft. Since the finite number of safe flight envelopes in the database is constrained by storage volume and the number of modeled abnormal cases, there are inevitably situations where the true flight envelope falls in-between two neighboring categories in the database. In this case, it is necessary to interpolate between two envelopes to obtain safer flight strategies. Since flight envelopes can be considered as a geometric structure, the method used for interpolation in this research is inspired by research on surface reconstruction and image matching using the fast marching method [61–64]. The basic idea is to compute a distance map of a set of points, based on which the optimal paths between two contours can be established and interpolation be implemented. By assuming the same trend of change of contours within certain computation bounds, extrapolation is also possible based on the distance map computed by the fast marching method.

Research Question 4

How to integrate the retrieved flight envelope with an onboard fault tolerant flight controller to develop a flight envelope protection strategy?

Note that the term "safe flight envelope" is used interchangeably with "flight envelope" throughout this dissertation because they have the same meaning and definition, and the word "safe" is only used to emphasize its importance in flight safety.

The utilization of the retrieved flight envelopes is a very important part in closed-loop flight control, especially for an impaired aircraft. Conventional flight envelope protection systems work with fixed state constraints. For damaged aircraft, however, the available control authority may have been reduced. Therefore, the new flight envelope retrieved online is used to limit/modify the reference command to the controller, in order to prevent the aircraft from flying outside the flight envelope and subsequently undergoing LOC. The flight envelope protection system is embedded in the framework of a multi-loop nonlinear controller. The main focus of this research question is on the combination of online flight envelope prediction and control-based flight envelope protection under post-damage/failure situations. As shown in Fig. 1.3, the flight envelope protection closes the loop of the proposed database-driven system which aims to maintain the damaged aircraft under control.

1.4. SCOPE AND LIMITATIONS

In flight envelope protection, it is not (yet) possible to come up with one holistic solution which considers all possible LOC precursors and causes. Hence, the scope of this thesis is inevitably limited to one of the categories. From the perspective of flight dynamics and control, the most influential contributors to LOC-I include airframe icing, structural damage, stall, sensor and actuator faults etc. And indeed, many detection and monitoring systems have been intensively developed and applied onboard for these factors. Structural damage, however, has not yet received much attention in literature. The reason is that conducting repeated destructive experiments on large-scale structures like aircraft is not feasible, and there are no sensors onboard to collect direct measurement data for analysis. Since the aerodynamic model, as well as the flight envelope of an aircraft, is largely influenced by its aerodynamic and control surfaces, it is necessary to monitor and assess the integrity of them and analyze their aerodynamic characteristics. Based on these reasons, in this thesis, flight envelope prediction and protection methods are mainly developed for structurally damaged aircraft with significant changes of its aerodynamic model. It is expected in future work that the proposed methods can be extended to the prevention of other LOC contributors.

Structural damage can be defined in two ways: 1) a small interior crack on a two-dimensional plate that leads to the reduction of load. If the crack is left undetected or unintended, it will grow to a critical size in flight and may lead to: 2) sudden damage and break away of large aerodynamic surfaces like wings, vertical tail and horizontal stabilizers. This kind of large-scale damage may quickly lead to LOC if recovery and control strategies are not readily applied. Research on the first type of structural damage mainly focuses on developing continuous health monitoring methods, based on vibration or ultrasonic wave characteristics, or strains measured at preselected simulated sensor locations [28, 29]. Such small-scale damage does not induce instant crucial effects on the stability, dynamics and control authority of the aircraft before it develops into large-scale damage. From the perspective of flight envelope estimation and fault tolerant control, this research focuses on the second type, which is large-scale damage to the aircraft, like partial loss of wings, vertical tail, horizontal stabilizers and control actuators.

The effects of such large-scale structural damage are mainly a combination of aerodynamic changes and mass property shifts [17]. However, mass properties change due to damage, though coupled with moments and forces, seem not to have a substantial effect on flight characteristics compared to the aerodynamic and control effects, according to a wind tunnel experiment [18], in which a large, asymmetric mass change (physical separation of an engine) was modeled. Besides, in actual flight when structural damage happens, there are no sensors or numerical methods to measure the changed mass properties instantly onboard. The damage detection and classification method developed in this thesis does not necessarily require the exact value of forces and moments, but only the aerodynamic effect that each damage case has on the aircraft. In a sense, we lump the effects of changed weight and inertia with that of the aerodynamic changes, and the mass and inertia properties are not modeled and assumed constant.

In this theis, the simulation environment is called "DASMAT", which is the abbreviation of "Delft University Aircraft Simulation Model and Analysis Tool" [65]. The DASMAT provides a high-fidelity simulation environment for developing and testing new methodologies in a fly-by-wire system before they are implemented in real flight [65]. The model data incorporated in the DASMAT environment is based on **Cessna 500 Citation I**, which is a generic twin-jet business aircraft.

Since our research focuses on method development and theoretical analysis, no actual wind-tunnel tests or complete computational experiments for different damage cases are conducted for the Cessna Citation. Hence, aerodynamic data for a damaged Cessna Citation aircraft are not fully available for damage modeling. Alternatively, several wind-tunnel tests of a 5.5% scale model of a commercial aircraft called the Generic Transport Model (GTM) were conducted by NASA with a number of damage cases [13, 17, 18]. The results of these tests are used as a reference for damage modeling of the Cessna Citation on the assumption that the two aircraft types have similar aerodynamic characteristics after damage. This assumption has been partially verified by computational experiments on the Cessna Citation using digital DATCOM, where different levels of vertical tail damage were modeled [58]. The ultimate goal of the research presented in this thesis is to develop a generic system of flight envelope prediction and protection.

In theory, deterministic reachable sets and flight envelopes are accurate in showing flight states that can be reached within a given time horizon. In reality, however, under the influence of (external) disturbances, the theoretical flight envelopes computed from deterministic reachability analysis may not include states that are practically unreachable. Therefore, probabilistic reachability analysis has been developed to consider the influence of uncertainties and disturbances usually modeled as a stochastic process [66]. Important as it is, the modeling of uncertain disturbances and computing probabilistic reachable sets are not within the scope of this thesis, however. The focus of our research is not the absolute accuracy of obtaining a realistic flight envelope, but to show the feasibility of an online database-driven system. In this thesis, the database is loaded with deterministic flight envelopes, while in future work the database can be augmented to cover more realistic situations.

1

1.5. OUTLINE

The main contents of Chapters 2 to 5 map one-on-one to the four research questions stated above, whereas Chapter 6 summarizes the main results and provides some recommendations for future research.

CHAPTER 2

Chapter 2 first gives the general framework of online safe flight envelope prediction system based on offline-assembled databases. The chapter discusses the study on different damage cases and their effects on the aerodynamic model of aircraft [13, 17, 18]. Based on this, the mathematical modeling of damaged aircraft is conducted, which enables the identification of the aerodynamic model of aircraft with various structural damage cases.

CHAPTER 3

Here we discuss methods to diagnose the aircraft health by categorizing the current states into one of the predefined damage cases. Three methods, based on fuzzy logic, neural networks and support vector machines, respectively, are used for in-flight damage detection and classification. The proposed methods are compared and their relative merits discussed based on their performance in simulation experiments with three damage cases.

CHAPTER 4

In this chapter, the database is built containing different flight conditions for which the flight envelopes are computed. Both longitudinal and lateral envelopes are computed with the level set method, which shows obvious shrinkage between damaged and undamaged aircraft. It is found that by interpolating between two retrieved envelopes in the database, more accurate results can be achieved, and the size of the database can be reduced. Complexity analysis shows that compared to other computational methods, the database approach, with its high efficiency and flexibility, is indeed feasible for online safe flight envelope prediction.

CHAPTER 5

This chapter mainly focuses on the implementation of the whole flight envelope prediction system by connecting all the separate modules discussed in previous chapters together. The retrieved flight envelopes are utilized by a fault-tolerant controller, to form a complete flight envelope prediction and protection system. Simulation results indicate that the proposed system can help prevent the damaged aircraft from transgressing into loss-of-control conditions.

CHAPTER 6

This chapter finalizes the dissertation with conclusions and recommendations, as well as a short discussion about new developments and the way ahead for future research.

REFERENCES

[1] *A Statistical Analysis of Commercial Aviation Accidents 1958-2016*, Tech. Rep. (Airbus, 2017).

[2] *Loss of Control In-Flight Accident Analysis Report 2010-2014*, Tech. Rep. (International Air Transport Association, 2015).

[3] *Statistical Summary of Commercial Jet Airplane Accidents, 1959-2016*, Tech. Rep. (Boeing Commercial Airplanes, 2017).

[4] *IATA Safety Report 2016*, Tech. Rep. (International Air Transport Association, 2017).

[5] B. Kavai, *Loss of Control Inflight Accident Data 2012-2016*, Tech. Rep. (International Air Transport Association, 2017).

[6] S. R. Jacobson, *Aircraft Loss of Control Causal Factors and Mitigation Challenges,* in *AIAA Guidance, Navigation, and Control Conference* (2010).

[7] C. M. Belcastro and J. V. Foster, *Aircraft Loss-of-Control Accident Analysis,* in *AIAA Guidance, Naviation, and Control Conference* (2010).

[8] C. M. Belcastro, J. V. Foster, G. H. Shah, I. M. Gregory, D. E. Cox, D. A. Crider, L. Groff, R. L. Newman, and D. H. Klyde, *Aircraft Loss of Control Problem Analysis and Research Toward a Holistic Solution,* Journal of Guidance, Control, and Dynamics **40**, 733 (2017).

[9] J. V. Foster, K. Cunningham, C. M. Fremaux, G. H. Shah, E. C. Stewart, R. A. Rivers, J. E. Wilborn, and W. Gato, *Dynamics Modeling and Simulation of Large Transport Airplanes in Upset Conditions,* in *AIAA Guidance, Navigation, and Control Conference and Exhibit* (2005).

[10] J. E. Wilborn and J. V. Foster, *Defining Commercial Transport Loss-of-control: A Quantitative Approach,* in *AIAA Atmospheric Flight Mechanics Conference* (2004).

[11] D. Briere and P. Traverse, *AIRBUS A320/A330/A340 Electrical Flight Controls - A Family of Fault-tolerant Systems,* FTCS-23 The Twenty-Third International Symposium on Fault-Tolerant Computing , 616 (1993).

[12] A. A. Lambregts, *Flight Envelope Protection for Automatic and Augmented Manual Control,* in *Proceedings of the EuroGNC 2013, 2nd CEAS Specialist Conference on Guidance, Navigation & Control* (Delft, 2013) pp. 1364–1383.

[13] G. H. Shah, J. V. Foster, and K. Cunningham, *Simulation Modeling for Off-Norminal Conditions-Where Are We Now?* in *AIAA Modeling and Simulation Technologies Conference* (2010).

[14] K. Cunningham and J. V. Foster, *Simulation Study of Flap Effects on a Commercial Transport Airplane in Upset Conditions,* in *AIAA Atmospheric Flight Mechanics Conference* (2005).

[15] P. C. Murphy, V. Klein, and N. T. Frink, *Unsteady Aerodynamic Modeling in Roll for the NASA Generic Transport Model,* in *AIAA Atmospheric Flight Mechanics Conference* (2012).

[16] N. T. Frink, P. C. Murphy, H. L. Atkins, S. A. Viken, J. L. Petrilli, A. Gopalarathnam, and R. C. Paul, *Computational Aerodynamic Modeling Tools for Aircraft Loss of Control,* Journal of Guidance, Control, and Dynamics **40**, 789 (2017).

[17] G. H. Shah, *Aerodynamic Effects and Modeling of Damage to Transport Aircraft,* AIAA Guidance, Navigation and Control Conference (2008).

[18] G. H. Shah and M. A. Hill, *Flight Dynamics Modeling and Simulation of a Damaged Transport Aircraft,* AIAA Modeling and Simulation Technologies (2012).

[19] N. T. Frink, S. Z. Pirzadeh, and H. L. Atkins, *CFD Assessment of Aerodynamic Degradation of a Subsonic Transport Due to Airframe Damage,* in *48th AIAA Aerospace Sciences Meeting* (2010).

[20] A. P. Broeren, S. Lee, G. H. Shah, and P. C. Murphy, *Aerodynamic Effects of Simulated Ice Accretion on a Generic Transport Model,* in *International Conference on Aircraft and Engine Icing and Ground Deicing* (2012).

[21] J. A. Mulder, J. K. Sridhar, and J. H. Breeman., *Identification of Dynamic Systems-Applications to Aircraft Part 2: Nonlinear Analysis and Manoeuvre Design.*, Vol. 3 (North Atlantic Treaty Organization, Advisory Group for Aerospace Research and Development., 1995).

[22] S. Schuet, T. J. J. Lombaerts, D. Acosta, J. Kaneshige, K. Wheeler, and K. Shish, *Autonomous Flight Envelope Estimation for Loss-of-Control Prevention,* Journal of Guidance, Control, and Dynamics **40**, 847 (2017).

[23] T. J. J. Lombaerts, H. Huisman, Q. P. Chu, J. A. Mulder, and D. Joosten, *Nonlinear Reconfiguring Flight Control Based on Online Physical Model Identification,* Journal of Guidance, Control, and Dynamics **32**, 727 (2009).

[24] H. Alwi, C. Edwards, and C. Pin Tan, *Fault Detection and Fault-Tolerant Control Using Sliding Modes* (Springer, 2011) pp. 7–27.

[25] I. Hwang, S. Kim, Y. Kim, and C. E. Seah, *A Survey of Fault Detection, Isolation, and Reconfiguration Methods,* IEEE Transactions on Control Systems Technology **18**, 636 (2010).

[26] P. Lu, *Fault Diagnosis and Fault-Tolerant Control for Aircraft Subjected to Sensor and Actuator Faults*, Ph.D. thesis, Delft University of Technology (2016).

[27] T. E. Menke and P. S. Maybeck, *Sensor / Actuator Failure Detection in the Vista F-16 by Multiple Model Adaptive Estimation,* IEEE Transactions on Aerospace and Electronic Systems **31** (1995).

[28] I. Lopez and N. Sarigul-Klijn, *A Review of Uncertainty in Flight Vehicle Structural Damage Monitoring, Diagnosis and Control: Challenges and Opportunities,* Progress in Aerospace Sciences **46**, 247 (2010).

[29] B. R. Seshadri and T. Krishnamurthy, *Damage Diagnosis and Prognosis Methodology to Estimate Safe Load for Aircraft Structure,* Journal of Aircraft **54**, 694 (2017).

[30] A. B. Kurzhanski and P. Varaiya, *Dynamic Optimization for Reachability Problems,* Journal of Optimization Theory and Applications **108**, 227 (2001).

[31] A. M. Bayen, I. M. Mitchell, M. Oishi, and C. J. Tomlin, *Aircraft Autolander Safety Analysis Through Optimal Control-Based Reach Set Computation,* Journal of Guidance, Control, and Dynamics **30**, 68 (2007).

[32] U. Topcu, A. K. Packard, P. Seiler, and G. J. Balas, *Robust Region of Attraction Estimation,* IEEE Transactions on Automatic Control **55**, 137 (2010).

[33] J. H. Gillula, G. M. Hoffmann, Haomiao Huang, M. P. Vitus, and C. J. Tomlin, *Applications of Hybrid Reachability Analysis to Robotic Aerial Vehicles,* The International Journal of Robotics Research **30**, 335 (2011).

[34] J. Lygeros, C. J. Tomlin, and S. Sastry, *Controllers for Reachability Specifications for Hybrid Systems,* Automatica **35**, 349 (1999).

[35] J. Lygeros, *On Reachability and Minimum Cost Optimal Control,* Automatica **40**, 917 (2004).

[36] I. M. Mitchell, A. M. Bayen, and C. J. Tomlin, *A time-dependent Hamilton-Jacobi Formulation of Reachable Sets for Continuous Dynamic Games,* IEEE Transactions on Automatic Control **50**, 947 (2005).

[37] C. J. Tomlin, J. Lygeros, and S. Sastry, *A Game Theoretic Approach to Controller Design for Hybrid Systems,* Proceedings of the IEEE **88** (2000), 10.1109/5.871303.

[38] E. R. Van Oort, *Adaptive Backstepping Control And Safety Analysis For Modern Fighter Aircraft,* Ph.D. thesis, Delft University of Technology (2011).

[39] R. Fedkiw and S. Osher, *Level Set Methods and Dynamic Implicit Surfaces* (Springer, 2003).

[40] D. M. Stipanovic, I. Hwang, and C. J. Tomlin, *Computation of An Over-approximation of The Backward Reachable Set Using Subsystem Level Set Functions,* Dynamic of Continuous, Discrete and Impulsive Systems **11**, 399 (2004).

[41] S. Kaynama, I. M. Mitchell, M. Oishi, and G. A. Dumont, *Scalable Safety-preserving Robust Control Synthesis for Continuous-time Linear Systems,* IEEE Transactions on Automatic Control **60**, 3065 (2015).

[42] T. J. J. Lombaerts, S. Schuet, D. Acosta, and J. Kaneshige, *On-Line Safe Flight Envelope Determination for Impaired Aircraft,* in *Advances in Aerospace Guidance, Navigation and Control* (Springer, 2015) 1st ed., pp. 263–282.

[43] L. Tang, M. Roemer, J. Ge, J. Prasad, and C. M. Belcastro, *Methodologies for Adaptive Flight Envelope Estimation and Protection,* in *AIAA Guidance, Navigation and Control Conference* (2009).

[44] K. Mcdonough, I. Kolmanovsky, and E. M. Atkins, *Recoverable Sets of Initial Conditions and Their Use for Aircraft Flight Planning After a Loss of Control Event,* in *AIAA Guidance Navigation and Control Conference* (2014).

[45] K. McDonough and I. Kolmanovsky, *Fast Computable Recoverable Sets and Their Use for Aircraft Loss-of-Control Handling,* Journal of Guidance, Control, and Dynamics **40**, 934 (2017).

[46] G. Yi, J. Zhong, E. M. Atkins, and C. Wang, *Trim State Discovery with Physical Constraints,* Journal of Aircraft **52**, 90 (2015).

[47] W. Falkena, C. Borst, Q. P. Chu, and J. A. Mulder, *Investigation of Practical Flight Envelope Protection Systems for Small Aircraft,* Journal of Guidance, Control, and Dynamics **34**, 976 (2011).

[48] N. Tekles, J. Chongvisal, E. Xargay, R. Choe, D. A. Talleur, N. Hovakimyan, and C. M. Belcastro, *Design of a Flight Envelope Protection System for NASA's Transport Class Model,* Journal of Guidance, Control, and Dynamics **40**, 863 (2017).

[49] N. Tekles, E. Xargay, and R. Choe, *Flight Envelope Protection for NASA's Transport Class Model,* in *AIAA Guidance Navigation and Control Conference* (2014).

[50] H. Lee, S. Snyder, and N. Hovakimyan, *L1 Adaptive Control Within a Flight Envelope Protection System,* Journal of Guidance, Control, and Dynamics **40**, 1013 (2017).

[51] P. F. A. Di Donato, S. Balachandran, K. McDonough, E. M. Atkins, and I. Kolmanovsky, *Envelope-Aware Flight Management for Loss of Control Prevention Given Rudder Jam,* Journal of Guidance, Control, and Dynamics **40**, 1027 (2017).

[52] V. Stepanyan, K. Krishnakumar, G. Dorais, S. Reardon, J. Barlow, A. Lampton, and G. Hardy, *Loss-of-Control Mitigation via Predictive Cuing,* Journal of Guidance, Control, and Dynamics **40**, 831 (2017).

[53] T. J. J. Lombaerts, S. Schuet, D. Acosta, J. Kaneshige, K. Shish, and L. Martin, *Piloted Simulator Evaluation of Safe Flight Envelope Display Indicators for Loss of Control Avoidance,* Journal of Guidance, Control, and Dynamics **40**, 948 (2016).

[54] D. Van Baelen, J. Ellerbroek, M. M. van Paassen, and M. Mulder, *Design of a Haptic Feedback System for Flight Envelope Protection,* in *AIAA Modeling and Simulation Technologies Conference* (2018).

[55] K. A. Ackerman, D. A. Talleur, R. S. Carbonari, E. Xargay, B. D. Seefeldt, A. Kirlik, N. Hovakimyan, and A. C. Trujillo, *Automation Situation Awareness Display for a Flight Envelope Protection System,* Journal of Guidance, Control, and Dynamics **40**, 964 (2017).

[56] A. D. T. Rijndorp, C. Borst, C. C. de Visser, O. Stroosma, M. Mulder, and M. M. Van Paassen, *Aviate, Navigate: Functional Visualizations of Asymmetric Flight Envelope Limits,* in *AIAA Information Systems* (2017).

[57] R. Ranaudo, B. Martos, and B. Norton, *Piloted Simulation to Evaluate the Utility of a Real Time Envelope Protection System for Mitigating In-Flight Icing Hazards,* in *AIAA Atmospheric and Space Environments Conference* (2010).

[58] H. N. Nabi, T. J. J. Lombaerts, Y. Zhang, E. van Kampen, Q. P. Chu, and C. C. de Visser, *Effects of Structural Failure on the Safe Flight Envelope of Aircraft,* Journal of Guidance, Control, and Dynamics **41**, 1257 (2018).

[59] M. Althoff and B. H. Krogh, *Reachability analysis of nonlinear differential-algebraic systems,* IEEE Transactions on Automatic Control **59**, 371 (2014).

[60] I. M. Mitchell, *Comparing Forward and Backward Reachability as Tools for Safety Analysis,* in *Hybrid systems: computation and control*, edited by A. Bemporad, A. Bicchi, and G. Buttazzo (Springer Berlin Heidelberg, 2007) pp. 428–443.

[61] H. Zhao and R. Fedkiw, *Fast Surface Reconstruction Using the Level Set Method,* Proceedings IEEE Workshop on Variational and Level Set Methods in Computer Vision , 194 (2001).

[62] J. A. Sethian, *Evolution, Implementation, and Application of Level Set and Fast Marching Methods for Advancing Fronts,* Journal of Computational Physics **169**, 503 (2001).

[63] J. A. Sethian, *A Fast Marching Level Set Method for Monotonically Advancing Fronts,* Proceedings of the National Academy of Sciences of the United States of America **93**, 1591 (1996).

[64] D. Adalsteinsson and J. A. Sethian, *The Fast Construction of Extension Velocities in Level Set Methods,* Journal of Computational Physics **148**, 2 (1999).

[65] C. A. A. M. Van Der Linden, *DASMAT-Delft University Aircraft Simulation Model and Analysis Tool: A Matlab/Simulink Environment for Flight Dynamics and Control Analysis.* (Delft University of Technology, 1996).

[66] R. van den Brandt, *Safe Flight Envelope Uncertainty Quantification using Probabilistic Reachability Analysis*, Master's thesis, Delft University of Technology (2017).

2

MODELING AND SIMULATION OF DAMAGED AIRCRAFT

In this chapter, the adverse impact of damage/failures on the stability and control authority of the aircraft is thoroughly discussed. Damage cases are transformed into mathematical models based on data from wind tunnel tests, where the aerodynamic influences of damage are reflected in the changed values of model parameters. The flight of damaged aircraft is simulated based on the damage modeling, and the model parameters are identified online, which in turn reveals the modeled aerodynamic effects of typical damage cases. The study on aircraft damage and failures lays the foundation of the whole research.

This chapter is based on:
Y. Zhang, C. C. de Visser, and Q. P. Chu, *Aircraft Damage Identification and Classification for Database-Driven Online Flight-Envelope Prediction*, Journal of Guidance, Control, and Dynamics, Vol. 41, No. 2 (2018), pp. 449-460.

2.1. INTRODUCTION

As discussed in Chapter 1, the prediction and protection of safe flight envelope (SFE) is essential for preventing aircraft loss of control. The SFE is characterized by aerodynamic and kinematic models of the aircraft as well as its control authority, and represents the region in the state-space in which the aircraft can be safely operated. Different definitions of the flight envelope are proposed in literature [1–6]. Widely used to prevent stall and potential structural damage, the conventional maneuvering envelope defines hard constraints on speed and load factor.

In addition to these static limitations, dynamic envelope bounds can be established by determining the controllable, or reachable states given the control authority of the pilot or autopilot [2, 3]. Reachability analysis provides a rigorous approach to actually calculate the dynamic envelope bounds [2, 3]. In principle, reachability analysis determines the complete set of states that can be reached from a target set within a given time horizon while subject to the system dynamics and input constraints. As introduced in Chapter 1, the SFE is defined as the intersection between a forward reachable set and a backward reachable set. This intersection indicates the region in the state-space inside which the aircraft is guaranteed to be capable of maneuvering from as well as returning to a trim set within a certain time horizon [4–6].

In normal situations, flight envelopes can be stored as a fixed part of a loss-of-control (LOC) prevention system [1]. However, they may no longer be valid after sudden failures or structural damage, since the aerodynamic properties of the impaired aircraft would change, often significantly. For example, under the situation of wing damage, the maximum lift coefficient decreases, which results in higher stall speed and lower maximum load factor. Therefore the overall maneuvering envelope will shrink due to the change in the aerodynamic coefficients. Under such abnormal conditions, the pilots need to acquire the reduced SFE as quickly as possible, implying that the onboard computer must recalculate the solution in near real-time.

Considering the challenges of implementing such an online system, a possible solution is proposed, which is retrieving the SFEs from an onboard database. For each representative damage case, a global dynamics model and its corresponding SFE are computed offline and then stored in the database. The process of predicting the flight envelopes online based on the pre-built databases is indicated as a “Database-driven onlinE Flight ENvelope preDiction system (DEFEND)”.

2.2. SYSTEM OVERVIEW

The general process of the DEFEND system is illustrated in Fig. 2.1, where the onboard system is supported by offline databases. It is clearly shown that the realization of online SFE prediction is strongly connected to the database retrieval system, and a reliable online identification process is essential for successful retrieval from the database. As displayed in Fig. 2.1, the FDI module is used to monitor the health conditions of the actuators. If any failure happens (e.g., hardover, jam), it will soon be detected by abnormal residuals between the actual outputs of actuators and the expected values calculated from their mathematical models [7]. Meanwhile, onboard sensors are also being monitored by advanced FDI techniques such that any sensor faults can be quickly detected

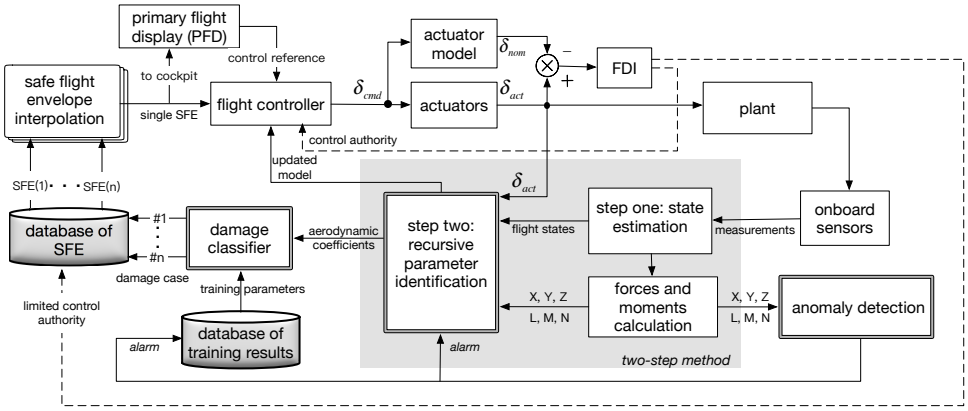

Figure 2.1: The general framework of DEFEND: a database-driven safe flight envelope prediction system

and compensated for [8]. New measurements of flight states and responses are sent to the system identification module which uses the two-step method [9] to update the aircraft model. At the first step, the aircraft states and sensor bias are estimated by a Kalman filter or other advanced state estimators based on aircraft kinematic models [8].

Next, the nondimensional forces and moments along each axis are calculated using the estimated states and sensor information, which provides the input to the second step of the two-step method, i.e. the estimation of stability derivatives using a recursive least squares method. For damaged aircraft, it is likely that the conventional model structure has changed, so a model structure selection scheme is used [10]. According to a series of experiments and reports [11–14], the aerodynamic model is directly related to the integrity of airplane's components and structures. Hence, the calculated dimensionless forces and moments are used to initiate an online aerodynamic anomaly detection process, which works by comparing the output of nominal flight models with the current output measurements. If there are any abnormal changes to the forces and moments, control inputs will be given in an effort to counteract the induced motion, creating sufficient input excitation needed for the identification of the changed local model. Meanwhile, an alarm will be generated that triggers the damage classification to determine the position and scale of the possible damage based on the newly-identified stability derivatives and the training knowledge of the current flight condition. Once the damage case is estimated, this information will be provided to the database as an index to retrieve a set of candidate SFEs. By applying database retrieval schemes and interpolation algorithms, a unique SFE is obtained that is closest to the current damage situation. The obtained SFE can then be presented to the pilots and utilized by the fault tolerant controller to generate new control laws.

As mentioned in Chapter 1, the ultimate goal of my research is to implement the DEFEND system and integrate the predicted flight envelopes with online flight controller to finally form a complete loop of controlled flight. Each following chapter will discuss one part of the DEFEND system, and they will be combined together in Chapter 5. This

chapter mainly focuses on the system identification, damage modeling and detection of the aircraft.

2.3. AIRCRAFT MODEL IDENTIFICATION

2.3.1. STEP 1: FLIGHT STATE ESTIMATION

The identification of a high-fidelity mathematical model of aircraft is essential. The general state space model set of nonlinear system equations describing the kinematics of the aircraft is given by:

$$\begin{aligned} \dot{\mathbf{x}}(t) &= \boldsymbol{f}(\mathbf{x}(t), \mathbf{u}_m(t), \boldsymbol{\lambda}, t) + \boldsymbol{G}(\mathbf{x}(t))\mathbf{w}(t), \\ \dot{\boldsymbol{\lambda}} &= 0 \\ \mathbf{y}_m(t) &= \boldsymbol{h}(\mathbf{x}(t), \mathbf{u}_m(t), \boldsymbol{\lambda}, t) + \mathbf{v}(t) \end{aligned} \tag{2.1}$$

where $\mathbf{x} = [V, \alpha, \beta, \phi, \theta, \psi]^T$ represents the system states. $\mathbf{u}_m$ is the vector of inputs measurements $\mathbf{u}$ from the inertial navigation system (INS), which includes specific forces (A_x, A_y, A_z) and angular rates (roll rate p, pitch rate q, and yaw rate r). $\mathbf{y}_m = [V_m, \alpha_m, \beta_m, \phi_m, \theta_m, \psi_m]$ is the vector of outputs measured from air-data sensors and INS. These measurements from onboard sensors are usually perturbed by sensor noise and biases. The input noise vector and output noise vector are $\mathbf{w}$ and $\mathbf{v}$ respectively. $\boldsymbol{G}$ is the noise distribution matrix. In general cases, the input noise vector $\mathbf{w}(t)$ is assumed to be a continuous white noise process and the output noise vector $\mathbf{v}(t)$ a discrete time white noise process. $\mathbf{w}(t)$ and $\mathbf{v}(t)$ are uncorrelated. The standard deviation of noise model can be estimated based on the known characteristics of onboard measurement equipment specified by the manufactures. The sensor biases $\boldsymbol{\lambda}$ are modeled as constant states, and $\mathbf{u}_m = \mathbf{u} + \boldsymbol{\lambda} + \mathbf{w}$ [10]. The estimation of true aircraft states from the biases and noise-contaminated states can be done by the iterated extended Kalman filter (IEKF), which has been successfully applied on aircraft [15].

Having caused many fatal accidents, faults in air-data sensors should also be considered as part of the system for detection and diagnosis. Besides, external disturbances like wind shear and gusts can severely degrade the performance of state estimation and sensor-fault detection if not carefully addressed and modeled in the system. Researches focusing on these challenging issues can be found in [8, 16].

2.3.2. STEP 2: AERODYNAMIC MODEL ESTIMATION

As the first step of the tow-step method, state estimation provides accurate values of states and inputs without the perturbation of sensor noise, biases and faults. This step is essential for the second step, which ensures that the identification of aerodynamic coefficient is not subjected to uncertainties from sensors.

By deducing estimated biases from filtered measurements, the dimensionless aero-

dynamic forces and moments of the aircraft are calculated by [10]:

$$\begin{bmatrix} C_L \\ C_D \\ C_Y \end{bmatrix} = \begin{bmatrix} \sin\alpha & 0 & -\cos\alpha \\ -\cos\alpha & 0 & -\sin\alpha \\ 0 & 1 & 0 \end{bmatrix} \begin{bmatrix} \dfrac{mA_x}{1/2\rho V^2 S} \\ \dfrac{mA_y}{1/2\rho V^2 S} \\ \dfrac{mA_z}{1/2\rho V^2 S} \end{bmatrix} \tag{2.2}$$

$$\begin{aligned} C_l &= \frac{\dot{p}I_{xx} + qr\left(I_{zz} - I_{yy}\right) - \left(pq + \dot{r}\right)I_{xz}}{\frac{1}{2}\rho V^2 Sb} \\ C_m &= \frac{\dot{q}I_{yy} + rp\left(I_{xx} - I_{zz}\right) + \left(p^2 - r^2\right)I_{xz}}{\frac{1}{2}\rho V^2 S\bar{c}} \\ C_n &= \frac{\dot{r}I_{zz} + pq\left(I_{yy} - I_{xx}\right) + \left(qr - \dot{p}\right)I_{xz}}{\frac{1}{2}\rho V^2 Sb} \end{aligned} \tag{2.3}$$

The calculated dimensionless coefficients in Eq. 2.2 and 2.3 are used to identify the aerodynamic model parameters. The model structure needed for identification depends on the type and condition of the aircraft, which is usually selected offline via flight test data. In this chapter, the model structure in Eq. (2.4) is used for identifying the aerodynamic model of the Cessna Citation aircraft from simulation data, where each model parameter corresponds to one of the control and stability derivatives. The values of these parameters contain important information about the physical health condition of the aircraft.

$$\begin{aligned} C_L &= C_{L_0} + C_{L_\alpha}\alpha + C_{L_q}\frac{q\bar{c}}{2V} + C_{L_{\delta_e}}\delta_e \\ C_D &= C_{D_0} + C_{D_\alpha}\alpha + C_{D_{\alpha^2}}\alpha^2 + C_{D_q}\frac{q\bar{c}}{2V} + C_{D_{\delta_e}}\delta_e \\ C_Y &= C_{Y_0} + C_{Y_\beta}\beta + C_{Y_p}\frac{pb}{2V} + C_{Y_r}\frac{rb}{2V} + C_{Y_{\delta_a}}\delta_a + C_{Y_{\delta_r}}\delta_r \\ C_l &= C_{l_0} + C_{l_\beta}\beta + C_{l_p}\frac{pb}{2V} + C_{l_r}\frac{rb}{2V} + C_{l_{\delta_a}}\delta_a + C_{l_{\delta_r}}\delta_r + C_{l_\alpha}\alpha \\ C_m &= C_{m_0} + C_{m_\alpha}\alpha + C_{m_q}\frac{q\bar{c}}{2V} + C_{m_{\delta_e}}\delta_e \\ C_n &= C_{n_0} + C_{n_\beta}\beta + C_{n_p}\frac{pb}{2V} + C_{n_r}\frac{rb}{2V} + C_{n_{\delta_a}}\delta_a + C_{n_{\delta_r}}\delta_r \end{aligned} \tag{2.4}$$

The flight data for identification is generated from DASMAT environment introduced in Chapter 1, which incorporates the nonlinear aircraft model with aerodynamic look-up tables identified from real flight tests [17]. DASMAT is used in our research to simulate, analyze and compare the dynamic behavior of damaged and undamaged aircraft given different control inputs and strategies [18]. The whole process of two-step identification with DASMAT model is illustrated in Fig. 2.2.

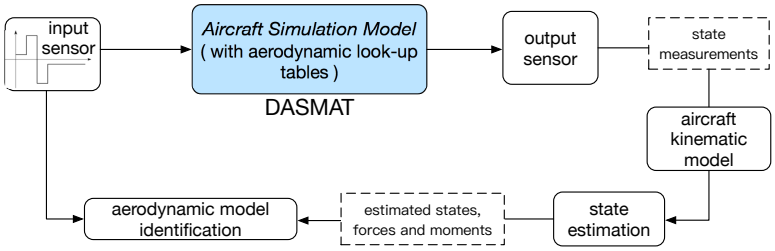

Figure 2.2: System identification based on the input/output data generated from DASMAT simulation environment

2.3.3. ONLINE RE-IDENTIFICATION OF CHANGED MODEL PARAMETERS

Given a certain model structure, a recursive least squares method can be used to estimate the aerodynamic model parameters. During normal flight, these parameters barely changes under the same flight condition. After the occurrence of faults and damage, however, the aerodynamic model parameters change and need to be re-identified online, which requires sufficient excitation input to the system. The re-identification is triggered by an alarm, which is generated when anomalies in aerodynamic forces and moments are detected. The detection is based on the residual $r(t)$ of estimated aerodynamic model. The mean of the residual $E[r(t)]$ should be zero in the normal situation, otherwise it will deviate from zero. In reality, however, the residuals are corrupted by noise, unknown disturbances (e.g. wind shear/gusts), and uncertainties in the system model [7]. Therefore, the distribution of the residual is used as the criterion for anomaly detection because the output residual during normal flight can be expected to have statistics determined by the noise present in the system [19].

As illustrated in Fig. 2.3, the distribution of the residual is calculated using data from a series of flight tests under nominal condition. Each training data point is the absolute value of the residual, which is used to fit in a certain distribution (e.g., Gaussian) by calculating the parameters of its probability density function (PDF). The trained PDF is then utilized to evaluate the probability density of newly measured data and decide whether it contains anomalies or not. Take Gaussian distribution for example, the probability density of each incoming new data point $p(r_{new})$ is computed according to:

$$p(r_{new} \mid \mu, \sigma) = \frac{1}{\sqrt{2\pi\sigma^2}} \exp\left(-\frac{(r_{new}-\mu)^2}{2\sigma^2}\right) \tag{2.5}$$

where μ and σ are the trained parameters of the Gaussian distribution of the undamaged aircraft. When damage occurs, the sudden change of forces and moments will result in a residual that has a very low probability in the distribution of normal data. Anomalies can then be detected using a threshold, where $y = 1$ signifies the potential existence of an anomaly:

$$y = \begin{cases} 1 & \text{if } p(r_{new}) < \varepsilon \text{ (anomaly)} \\ 0 & \text{if } p(r_{new}) > \varepsilon \text{ (normal)} \end{cases} \tag{2.6}$$

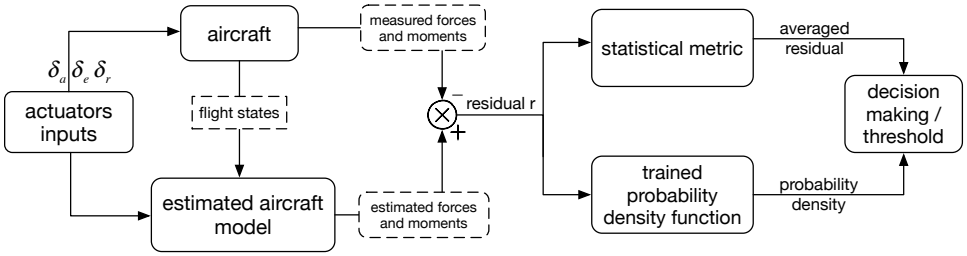

Figure 2.3: Online anomaly detection and re-identification trigger

The threshold ε is determined based on a cross validation set of labeled examples including both normal and abnormal data points [20].

Alternatively, a statistical metric of residuals can be used for anomaly detection, which calculates the averaged residuals over a period of time [19]:

$$\bar{r}(t) = \frac{1}{n_s} \sum_{i=0}^{n_s} r(t-i) \tag{2.7}$$

where n_s is the number of samples over which the average is taken to prevent false-alarms. For each channel, a threshold is chosen based on the simulation data or real flight test data. A trigger alarm is generated if $\bar{r}(t)$ exceeds the threshold.

Once the re-identification process is triggered by the detection alarm, apart from sufficient excitation input, the covariance matrix of the estimation also needs to be reset to a higher value in order to enhance the influence of new incoming data. The resetting of the covariance matrix can also be done via a forgetting factor, which varies with the estimation residual [21].

Sudden occurrence of wind shear/gusts often causes abrupt change of wind speed and direction, thus leading to unexpected responses of aircraft. Like other abnormal cases, this will also generate excessive residuals and trigger the re-identification of parameters in Eq. 2.4. Hence, the detection alarm defined above cannot effectively distinguish among faults, damage and wind shear/gusts, but only indicates the possibility of model change and necessity of re-identification.

One of the differences between system failures (e.g., faults and damage) and external wind shear/gusts is the duration of impact. Therefore, it is important to examine the value of the steady state each parameter converges to, given sufficient excitation. If the converged steady state is close to its original value after a period of deviation and fluctuation, it is more likely due to external disturbances, compared to the situation where the converged steady state is quite different from its original value. The discrepancy between the new steady state and its original value can be used to evaluate the extent of model change and thus diagnosis the health condition of the aircraft, which will be further discussed in Chapter 3

2.4. AERODYNAMIC EFFECTS MODELING OF STRUCTURAL DAMAGE

A high-fidelity model of a structurally damaged aircraft is the basis for flight simulation and data generation, which is essential to damage case estimation, flight envelope computation and controller design etc. In the "ideal" case, the modeling of aerodynamic effects of structural damage requires data from systematically conducted flight experiments with damaged aircraft, which for obvious reasons is problematic to obtain. Most experiments are therefore based on subscale models in the wind tunnel [14] and CFD experiments [22]. In recent years, the Generic Transport Model (GTM), a 5.5% scale model of a commercial aircraft has been the subject of a series of extensive wind tunnel tests undertaken by NASA [11, 12] for the exploration of loss-of-control events [13]. In these experiments, the damage was modeled in the form of partial or complete tip loss of the three major parts that provide the aerodynamic forces and moments: the horizontal stabilizers, the vertical tail, and the wings.

Figure 2.4 shows the geometrical configuration of a damaged Cessna Citation aircraft. The damage is located on horizontal stabilizers, vertical tail and wings respectively. It should be noted that the aforementioned wind tunnel experiments are based on GTM, which is not the subject aircraft of my PhD research. However, preliminary work on damage modeling has also been performed using digital DATCOM, where the aerodynamic characteristic of a Cessna Citation aircraft with various levels of vetical tail damage was modeled [23]. Compared with the GTM model, the results of Cessna Citation show similar patterns and trends of aerodynamic changes after vertical tail damage. The similarity can be explained by the similar geometrical configurations of these aircraft types. Therefore, it is reasonable to assume similar aerodynamic characteristics between these two models in the other two damage cases, which are horizontal stabilizer damage and wing damage.

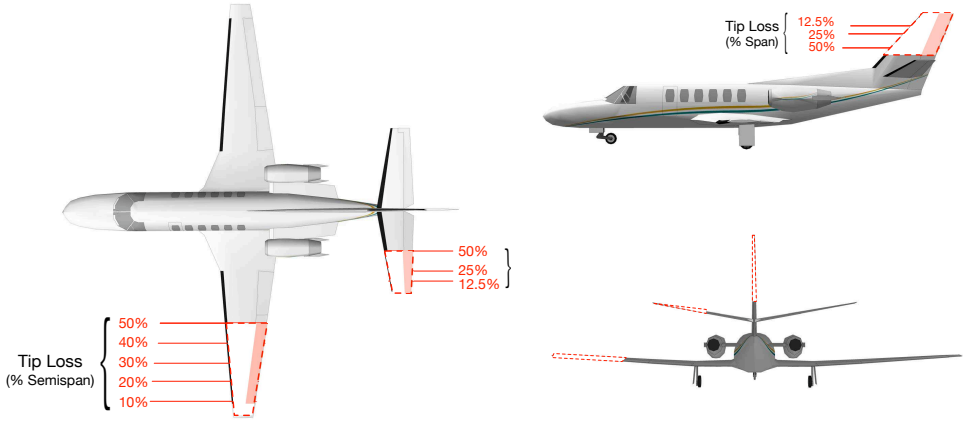

Figure 2.4

It can be concluded from wind-tunnel experiments [11–13] that each damage case results in unique aerodynamic effects on the aircraft, which are indicated by changes in

different stability derivatives. The experimental results of horizontal stabilizer damage [11] shows that the damage causes significant changes to longitudinal stability, which is indicated by the changed value of C_{m_α} and C_{m_q}. Additionally, due to geometric asymmetry, a slight incremental rolling moment is observed. The vertical tail damage mainly results in a steady change in lateral forces and directional stability indicated by the values of C_{Y_β}, C_{n_β}, and C_{n_r}. In wing damage experiments, the most important observation is the incremental rolling moment ΔC_linduced by unequal normal force contributions from left to right wings. Also, the effective dihedral C_{l_β} and roll damping C_{l_p} are affected due to wing tip loss. The change scale of aerodynamic coefficients is calculated by:

$$\text{change scale}\,\Delta C = \frac{C_{damaged} - C_{undamaged}}{|C_{undamaged}|} \cdot 100\% \tag{2.8}$$

Fig. 2.5 shows the calculated change scales on different percentages of tip loss of three different parts [11–13, 23]. By adding the change scales of GTM to DASMAT's original aerodynamic look-up tables, the model of a damaged Cessna Citation aircraft can be established in the simulation.

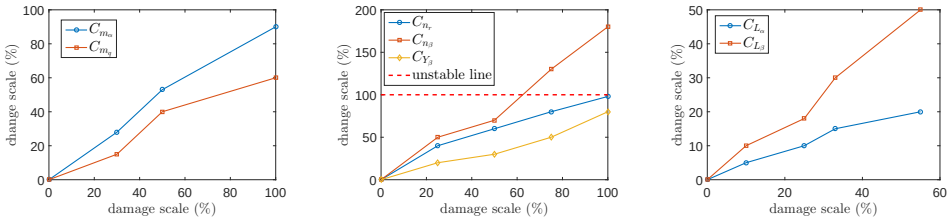

(a) horizontal stabilizer (b) vertical tail (c) wing

Figure 2.5: the change scales of aerodynamic coefficients from wind-tunnel and computation experiments [11, 23]

Another challenge in the modeling process is due to the physical limitations of making aircraft models and conducting wind tunnel tests. These limitations result in limited damage cases and experiment data, which may not be enough to cover all the possible situations. For example, damage to horizontal stabilizers is modeled with 12.5%, 25% and 50% tip loss respectively, while information on other scales, like 40% tip loss, is still missing. To deal with this problem, interpolation is used by treating the available experiment data points as "knots" and estimate the values in between. It can be observed from Fig. 2.5 that the relation between the change scale of each aerodynamic coefficient and the percentage of tip loss can be approximated by linear functions. The calculated and interpolated ΔC together form the damage scale matrix $\mathbf{D}_m \in \Re^{n\times n}$, which is used for the modeling of control and stability derivatives via:

$$\mathbf{C}_{dmg} = (\mathbf{I} - \mathbf{D}_m)\mathbf{C}_{nom} + \mathbf{B}_m \tag{2.9}$$

where $\mathbf{I}$ is an $n \times n$ identity matrix, $\mathbf{C}_{nom} \in \Re^{n\times 1}$ and $\mathbf{C}_{dmg} \in \Re^{n\times 1}$ are the vectors of aerodynamic coefficients (see Eq 2.4) before and after damage. For instance, the vector of

rolling moment is $\mathbf{C}_l = \left[C_{l_0}, C_{l_\beta}\beta, C_{l_p}\frac{pb}{2V}, C_{l_r}\frac{rb}{2V}, C_{l_{\delta_a}}\delta_a, C_{l_{\delta_r}}\delta_r\right]^T$. $\mathbf{B}_m \in \Re^{n\times 1}$ denotes the incremental forces and moments induced by the damage, which are determined based on experimental data [11–13]. By using Eq. 2.9, five damage levels ranging from 10% to 50% tip loss of wings and tails are modeled in the DASMAT simulation environment, where the original aerodynamic model is stored in the form of look-up tables.

2.5. SIMULATION FLIGHT

To simulate an onboard identification process, aircraft responses are generated by the open-loop DASMAT simulation model. Given doublet maneuvers of ±5° on elevators, ailerons and rudder triggered at different times, where the data is contaminated by measurement noise (SNR = 25). It is important to note that when damage happens in reality, the actuator inputs required for excitation of the system for online system identification may not be specified as doublets but generated automatically by the onboard fault tolerant controller to compensate for damage-induced excursions from the reference trajectory. In that sense, the fault tolerant controller indirectly excites the system by making efforts to stabilize it. The incorporation of a fault tolerant controller is discussed later in Chapter 5.

The first two subplots of Figs. 2.6, 2.7, and 2.8 show the time histories of dimensionless forces and moments obtained by applying a doublet maneuver of ±5° on the actuators of the DASMAT simulation model. The measurements and identified values of the damaged aircraft are denoted by solid lines and dashed lines respectively, which are compared with measurements from the undamaged aircraft in solid-dashed lines. It is observed that the identification algorithm succeeds in tracking the measured value of dimensionless forces and moments of the damaged aircraft and results in satisfactory low identification errors during the entire time span. The identification results of the stability derivatives along with their real values are displayed in the (c)(d)(e) subplots of Figs. 2.6, 2.7, and 2.8 for each of the damage cases accordingly. It is noted that the real values are extracted from the look-up table from the simulation model, but in real flight these cannot be directly read or measured from the aircraft. The estimated values are expected to converge to the real values during the identification process.

The ratio between the converged coefficients of the damaged and undamaged aircraft indicates the change induced by structural damage. It is clearly shown that the identified stability derivatives quickly converge to the changed values, capturing the aerodynamic characteristics accurately and providing essential information for damage classification, which is immediately triggered once the anomaly detection block gives a positive alarm. The last three subplots of Figs. 2.6, 2.7, and 2.8 shows the anomaly detection results of three damage cases based on the residuals between the responses of damaged and undamaged models. The upper plots of (f)(g) in Figs. 2.6, 2.7, and 2.8 depict the absolute value of residuals between measured outputs and estimated outputs with respect to time, and the probability density of the residuals computed from Eq. 2.5 is displayed in the lower plots. The increase of the estimation error and the corresponding decrease of its probability density are observed soon after the damage is triggered. A threshold is used to capture the anomaly observed in the data. Each channel has a separate detection threshold and different re-identification time, so the anomaly alarms are

triggered individually, which are displayed in Figs. 2.6(h), 2.7(h), and 2.8(h). It is important to note that in the open-loop simulation, the time of change detection and anomaly alarms are closely related to the time of maneuver execution of the aircraft. Hence, an updated model identified from sufficient input excitation is a key factor for a successful anomaly detection, which again leads to the work of Chapter 5.

REFERENCES

[1] J. Chongvisal and D. Talleur, *Loss-of-control Prediction and Prevention for NASA's Transport Class Model,* in *AIAA Guidance, Navigation, and Control Conference*, AIAA Paper 2014-0784 (2014).

[2] J. Lygeros, *On Reachability and Minimum Cost Optimal Control,* Automatica **40**, 917 (2004).

[3] I. M. Mitchell, *A Toolbox of Level Set Methods (Version 1.1)* (2007).

[4] T. J. J. Lombaerts, S. Schuet, and K. Wheeler, *Safe Maneuvering Envelope Estimation Based on A Physical Approach,* in *AIAA Guidance, Naviation, and Control Conference*, AIAA Paper 2013-4618 (2013).

[5] E. R. Van Oort, *Adaptive Backstepping Control And Safety Analysis For Modern Fighter Aircraft*, Ph.D. thesis, Delft University of Technology (2011).

[6] Y. Zhang, C. C. de Visser, and Q. P. Chu, *Online Safe Flight Envelope Prediction for Damaged Aircraft: A Database-driven Approach,* in *AIAA Modeling and Simulation Technologies Conference*, AIAA Paper 2016-1189 (2016).

[7] I. Hwang, S. Kim, Y. Kim, and C. E. Seah, *A Survey of Fault Detection, Isolation, and Reconfiguration Methods,* IEEE Transactions on Control Systems Technology **18**, 636 (2010).

[8] P. Lu, *Fault Diagnosis and Fault-Tolerant Control for Aircraft Subjected to Sensor and Actuator Faults*, Ph.D. thesis, Delft University of Technology (2016).

[9] J. A. Mulder, J. K. Sridhar, and J. H. Breeman., *Identification of Dynamic Systems-Applications to Aircraft Part 2: Nonlinear Analysis and Manoeuvre Design.*, Vol. 3 (North Atlantic Treaty Organization, Advisory Group for Aerospace Research and Development., 1995).

[10] T. J. J. Lombaerts, *Fault Tolerant Flight Control: A Physical Model Approach*, Ph.D. thesis, Delft University of Technology (2010).

[11] G. Shah, *Aerodynamic Effects and Modeling of Damage to Transport Aircraft,* in *AIAA Atmospheric Flight Mechanics Conference and Exhibit*, AIAA Paper 2008-6203 (2008).

[12] G. Shah and M. Hill, *Flight Dynamics Modeling and Simulation of a Damaged Transport Aircraft,* in *AIAA Modeling and Simulation Technologies Conference*, AIAA Paper 2012-4632 (2012).

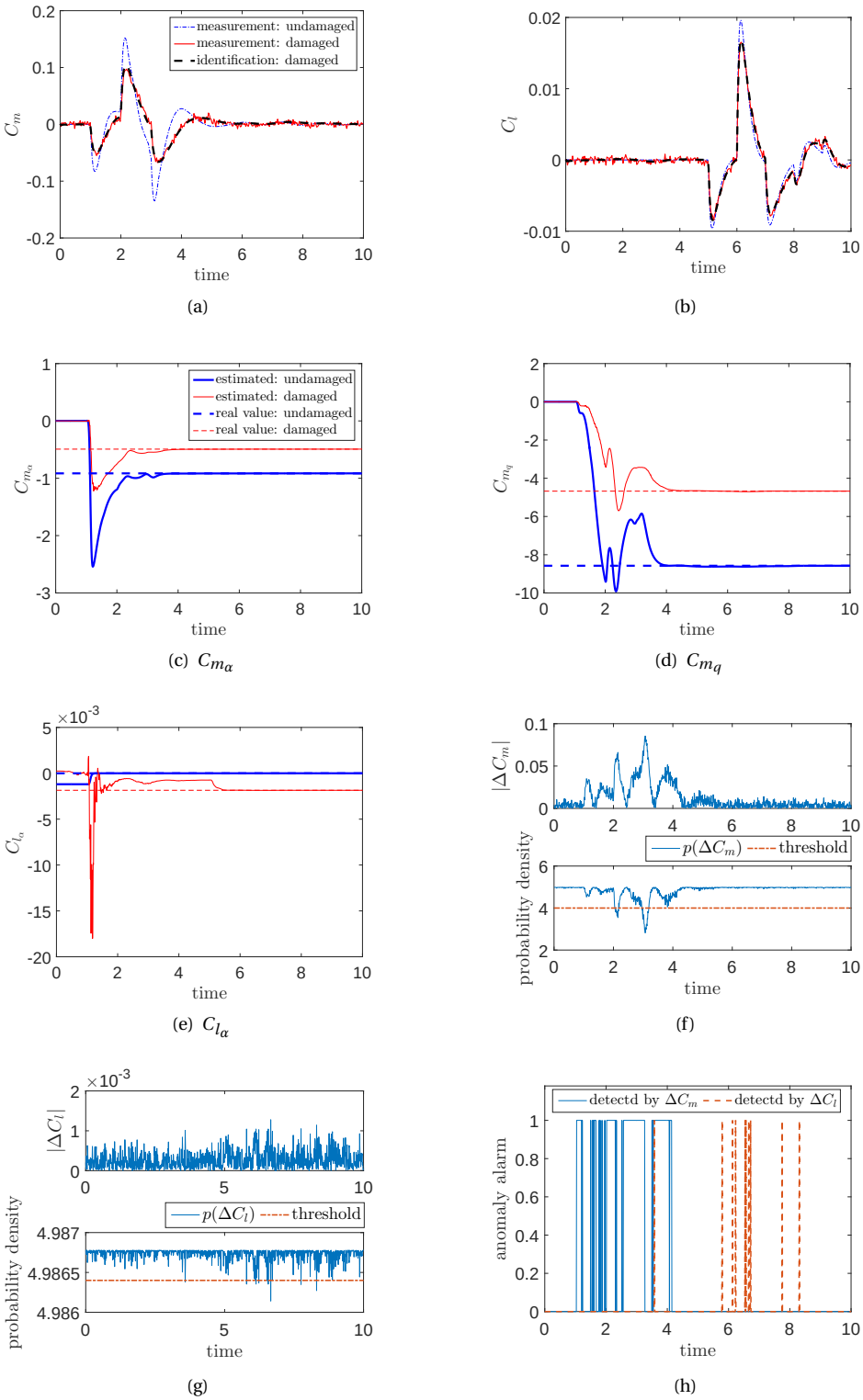

Figure 2.6: Identification and anomaly detection results of 30% tip loss of left horizontal stabilizer. The damage is triggered after 1 second

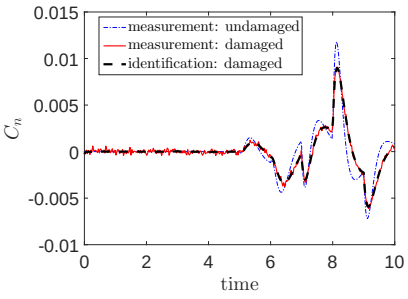

(a)

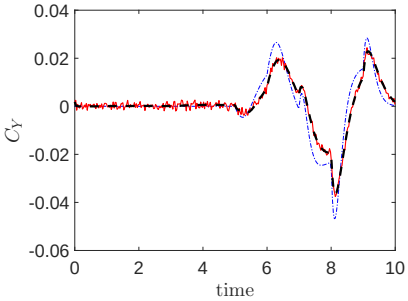

(b)

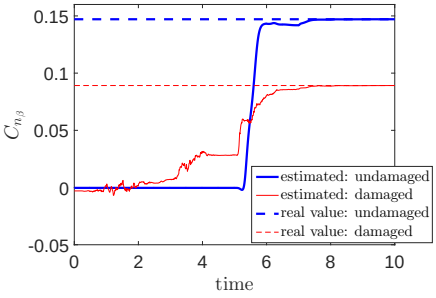

(c) C_{n_β}

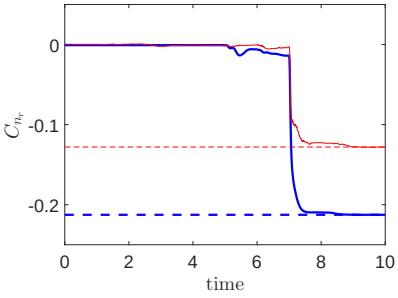

(d) C_{n_r}

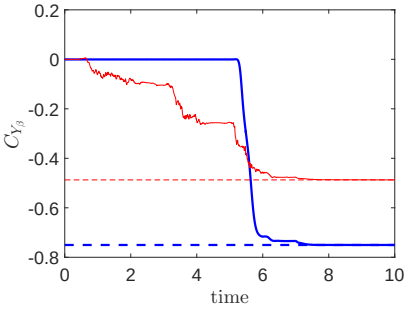

(e) C_{Y_β}

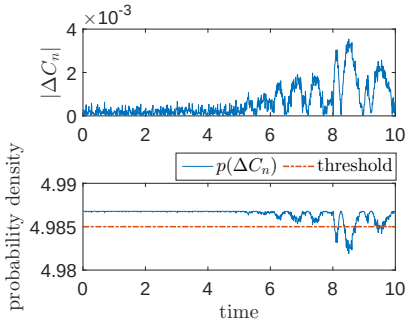

(f)

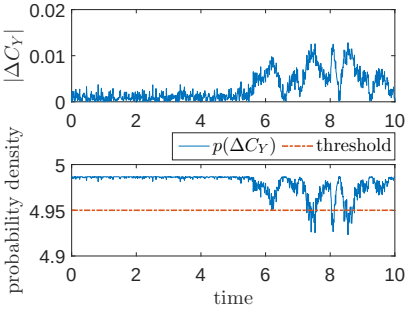

(g)

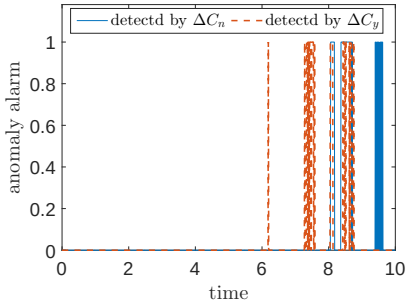

(h)

Figure 2.7: Identification and anomaly detection results of 20% tip loss of vertical tail. The damage is triggered after 4 seconds

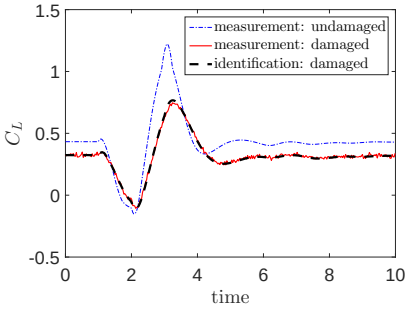

(a)

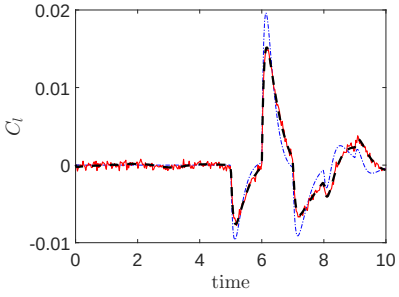

(b)

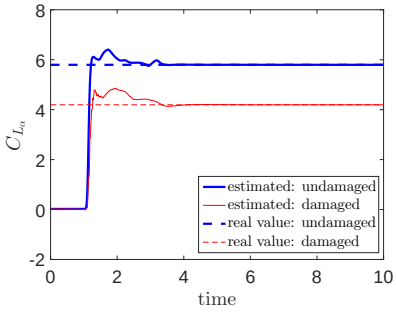

(c) C_{L_α}

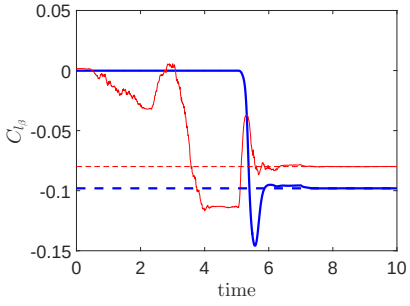

(d) C_{l_β}

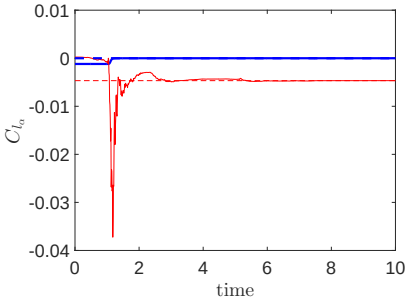

(e) C_{l_α}

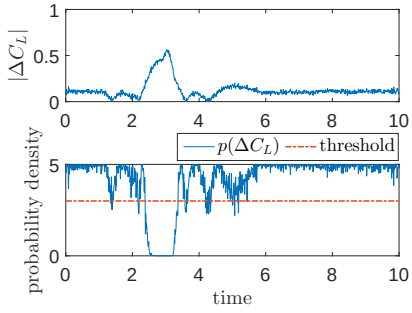

(f)

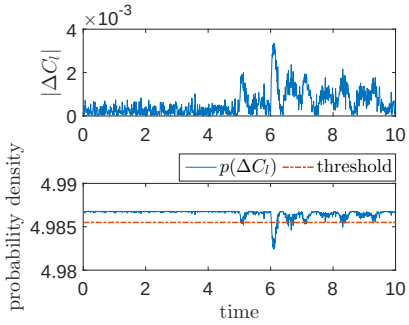

(g)

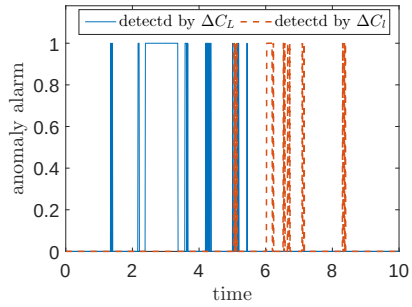

(h)

Figure 2.8: Identification and anomaly detection results of 40% tip loss of left wing. The damage is triggered after 1 second

[13] G. Shah, J. Foster, and K. Cunningham, *Simulation Modeling for Off-Norminal Conditions-Where Are We Now?* in *AIAA Modeling and Simulation Technologies Conference*, AIAA Paper 2010-7792 (2010).

[14] C. Hayes, *Effects of Simulated Wing Damage on The Aerodynamic Characteristics of a Swept-wing Airplane Model*, Tech. Rep. (NASA TM X-1550, 1968).

[15] C. C. de Visser, *Global Nonlinear Model Identification with Multivariate Splines*, Ph.D. thesis, Delft University of Technology (2011).

[16] L. Rodriguez, J. A. Cobano, and A. Ollero, *Wind Field Estimation and Identification having Shear Wind and Discrete Gusts Features with a Small UAS,* in *2016 IEEE/RSJ International Conference on Intelligent Robots and Systems (IROS)* (IEEE, 2016) pp. 5638–5644.

[17] A. N. M. Baarspul, J.A. Mulder and J. Breeman, *Mathematical Model Indentification for Flight Simulation, Based on Flight and Taxi Tests*, Tech. Rep. LR-550 (Delft University of Technology, 1988).

[18] C. A. A. M. Van Der Linden, *DASMAT-Delft University Aircraft Simulation Model and Analysis Tool: A Matlab/Simulink Environment for Flight Dynamics and Control Analysis.*, Series 03: Control and Simulation 03 (Delft University of Technology, 1996).

[19] T. J. J. Lombaerts, H. Huisman, Q. P. Chu, J. Mulder, and D. Joosten, *Nonlinear Reconfiguring Flight Control Based on Online Physical Model Identification,* Journal of Guidance, Control, and Dynamics **32**, 727 (2009).

[20] A. Ng, *Machine Learning Lecture Notes*, Tech. Rep. (Stanford Univeristy, 2014).

[21] H. J. Tol, C. C. D. Visser, L. G. Sun, E. V. Kampen, and Q. P. Chu, *Multivariate Spline-Based Adaptive Control of High-Performance Aircraft with Aerodynamic Uncertainties,* Journal of Guidance, Control, and Dynamics **39**, 781 (2016).

[22] N. Frink, S. Pirzadeh, and H. Atkins, *CFD Assessment of Aerodynamic Degradation of a Subsonic Transport Due to Airframe Damage,* in *48th AIAA Aerospace Sciences Meeting*, AIAA Paper 2010-500 (2010).

[23] H. N. Nabi, T. J. J. Lombaerts, Y. Zhang, E. van Kampen, Q. P. Chu, and C. C. de Visser, *Effects of Structural Failure on the Safe Flight Envelope of Aircraft,* Journal of Guidance, Control, and Dynamics **41**, 1257 (2018).

3

CLASSIFICATION AND ASSESSMENT OF AIRCRAFT DAMAGE

In the damage assessment system discussed in this chapter, the identification results from Chapter 2 are used as input data to diagnose the current health condition of the damaged aircraft. Inspired by the application of machine learning in health monitoring, two classification methods are investigated and used to diagnose the aircraft by categorizing the current states into one of the pre-defined damage cases. The damage cases are modeled and defined by the location (e.g., wing) and the percentage of surface loss based on the discussion in Chapter 2. The results given by the damage assessment system will be used as the key index to the database of safe flight envelopes introduced in the following chapters. In addition, fuzzy logic is also used to assess the damage severity in order to enhance the situational awareness of pilots.

This chapter is based on:
Y. Zhang, C. C. de Visser, and Q. P. Chu, *Aircraft Damage Identification and Classification for Database-Driven Online Flight-Envelope Prediction*, Journal of Guidance, Control, and Dynamics, Vol. 41, No. 2 (2018), pp. 449-460.
Y. Zhang, C. C. de Visser, and Q. P. Chu et al, *Aircraft Damage Pattern Recognition Using Aerodynamic Coefficients and Fuzzy Logic*, Advances in Aerospace Guidance, Navigation and Control, Springer, pp. 335-348

3.1. DAMAGE ESTIMATION FOR DATABASE RETRIEVAL

In general, faults on aircraft can be categorized into three types: actuator faults, sensor faults and component faults [1]. The first two types of faults, i.e. actuator and sensors faults, are commonly modeled as *additive faults*, while component faults are typically modeled as *multiplicative faults* [1]. The reason is that faults in actuators (e.g. aileron stuck) and sensors are modeled as additive term to the states and measurement model of the system, which does not change the parameters of the model. On the other hand, component faults, or structural failures (e.g. wing damage) always lead to changes in the parameters of the system dynamics, which contributes to multiplicative factors to the system states.

A system or process that performs the Fault Detection, Isolation or Diagnosis is generally referred to as an FDI system [1]. In aerospace engineering, FDI methods are intensively used in monitoring and diagnosing the health of aircraft structures, sensors and actuators, as well as providing updated information for control systems [2]. Hence, having a reliable FDI system onboard is crucial for safe flight.

The FDI methods are based on either hardware redundancy or analytical redundancy [1]. The hardware redundancy is utilized when there are redundant hardware (e.g. sensors) to generate duplicative signals. As a more cost-effective approach, the analytical redundancy methods rely on the mathematical models of the system, which require no additional hardware but suffer from model uncertainties and noise [1]. In practice, the installation of redundant hardware is not easily implemented on aircraft, thus my research mainly focus on model-based analytical redundancy FDI methods.

Residual generation is the key step of model-based FDI, which calculates the discrepancies between the output of the mathematical model and the actual output of the system [1, 3]. The mean of residuals is expected to be zero when no fault occurs, and deviate from zero when any fault occurs [1]. In most cases, the residuals are inevitably corrupted by model uncertainties and noise. Therefore, in order to generate robust residuals for additive faults, Kalman filter is used to filter out the noise and estimate the system states and measurement as well as system faults [3, 4]. For fault isolation, several filters are operated in parallel, each of which corresponds to one of the fault scenarios [4, 5]. Decisions can be made on which type of fault has occurred based on the residuals. For additive faults that normally occur in sensors and actuators, the advantage of using Kalman filter is that both detection and estimation can be achieved.

For multiplicative faults like structural damage, the detection and estimation is separately dealt with. As explained in the previous Chapter 2, the detection part can be achieved in a similar way to the detection of additive faults. Under the framework of the two-step identification method, measurement noise is filtered in the first step by the Kalman filter [4], so that anomalies in aircraft components can be detected by calculating the residuals between measured and modeled aerodynamic forces and moments in the second step.

Unlike actuator and sensor faults, the isolation and estimation of structural damage is not based on filtered model states but on identified model parameters [6]. The identification-based FDI [1] of such component faults is mostly used for structural health monitoring (SHM) and diagnosis systems [7]. In SHM, component faults are classified by machine learning and pattern recognition algorithms [8] like neural networks and sup-

port vector machines, which are applied to observation data acquired from large arrays of sensors.

In accordance with the discussions on damage modeling in Chapter 2, the main focus of this chapter is to find out the location and severity of the damage to one of the three major aerodynamic surfaces (horizontal stabilizers, wings, vertical tail) and their affiliated actuators. Inspired by the techniques and methods used in SHM [7], this chapter proposes a novel way of using pattern classification techniques, where 'patterns', or 'classes' specifically indicate the damage situation of the aircraft represented by discrete values with a chosen interval (e.g., 10%, 20%, 30%, ...). In this way, damage severity can be approximated by these discrete values. The mapping from locally identified aerodynamic coefficients to the damage conditions can be trained offline from a supervised learning process [9], thus the current damage condition can be diagnosed by pattern classification. The proposed method can be regarded as a combination of system identification and data-based learning approach.

The advantage of using this approach is that it has "black box" characteristics and the ability to "learn" from training examples, which requires much less a priori information and knowledge. Besides, class labels can be used as retrieval index to the database. More importantly, the use of classification can tolerate a certain level of inaccuracy of re-identification when sufficient excitation is unavailable in risky situations.

The essential part of any pattern classification method is the training of the mapping from a data set $\mathscr{X}$ to its assigned class label set $\mathscr{Y}$:

$$f : \mathscr{X} \rightarrow \mathscr{Y} \tag{3.1}$$

The class label set $\mathscr{Y}$, or target set, contains k vectors corresponding to k pre-defined damage cases (e.g. 20% tip loss of left wing). The data set $\mathscr{X}$ consists of m vectors denoted by $\mathbf{x}$, which are collected from m experiments, each $n-$dimensional vector $\mathbf{x}^{(m)}$ contains n extracted features, which are specifically defined in this research as the stability derivatives (e.g., C_{m_α}, C_{m_q}) identified from each of the k damage cases. Many methods are well developed for classification [9, 10], and each method has different ways of computing decision boundaries. This chapter implements and compares two commonly used classifiers for damage diagnosis, which are neural networks (NN) and support vector machines (SVM).

Once the damage case is estimated, this information will be provided to the database as an index to the flight envelope that corresponds to the current damage situation. The obtained flight envelope can be used by the fault-tolerant controller to generate new control laws. This topic will be discussed later in the following chapters.

3.2. CLASSIFICATION BY NEURAL NETWORKS

3.2.1. BASIC THEORY

In this section, a multilayer neural network is used for classification. One major difference of the neural network from other classifiers is that it can deal with multiclass classification problems by a single network structure [11, 12], where each input unit represents one of the features in the vector $\mathbf{x}$, and each output label defined as $\mathbf{y} \in \Re^k$ represents one of the k classes. As illustrated by Fia. 3.1, a multilayer neural network [9] consists of one

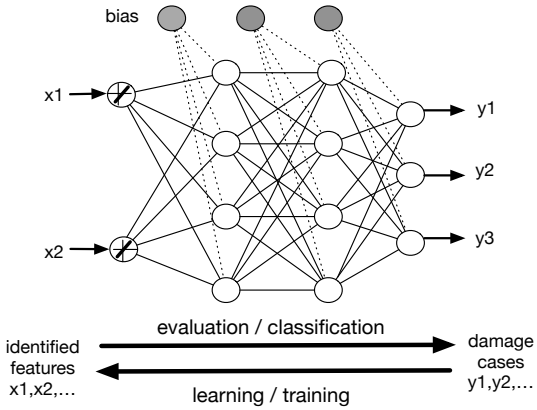

Figure 3.1: A basic structure of a neural network for classification

input layer, several hidden layers and an output layer, all interconnected by modifiable weights, and a single bias unit that is connected to each unit other than the input units.

Nonlinear multilayer networks have great approximation power and can implement arbitrary decision boundaries. The decision regions need not be convex, nor simply connected. The neural networks have two primary modes of operation: evaluation and learning. For evaluation operation, the input is simply passed through the network to the output layer and the information flow forward in the network. During the learning process of the network, the network parameters (i.e. weights) are modified until the network output converges towards the target output and the training error is reduced to meet certain stopping criteria. Various function approximation methods can be used [9] for training the weights of the multilayer networks, which will not be detailed in this thesis.

When structural damage occurs, some representative stability derivatives need to be extracted from the identified models as features for damage classification. The identified parameters in every simulated flight test form a training set for each typical damage case, which is used to generate decision boundaries during the training process. The richness of the training set is one of the key factors that determine the accuracy of the classification results. If the number of classes is too small, the estimation of the actual situation can be coarse and inaccurate, while too many classes may lead to the problem of ambiguity and complex implementations. Hence, the designed number of classes in the training set is a trade off between desired numerical accuracy and physical restrictions.

For each new feature vector $\mathbf{x}_{new} \in \mathscr{X}$ extracted from an unknown damage case, the classification can be performed by finding out its class label $\mathbf{y}_{new} \in \mathscr{Y}$ based on the trained mapping:

$$\mathbf{y}_{new} = f(\mathbf{x}_{new}) \tag{3.2}$$

In this way the current damage severity can be classified and estimated based on the identified aerodynamic parameters. In the next section, it will be shown how the whole

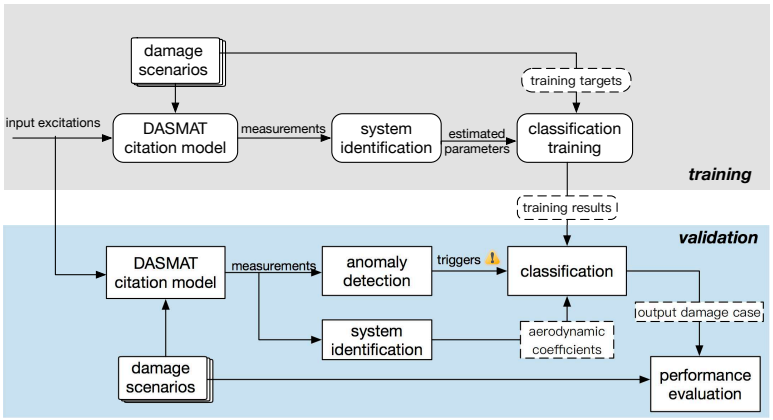

Figure 3.2: The training and validation process for damage classification

process is implemented via well-trained neural networks in a high-fidelity simulation environment.

3.2.2. TRAINING AND VALIDATION VIA SIMULATION DATA

It is illustrated in Fig. 3.2 how the training data is generated and utilized in the simulation of damage classification. As in the previous chapter, the output data for system identification and anomaly detection is generated by the DASMAT citation model given certain input excitation. For each damage case, the stability derivatives that have the most dominant and discernible effects are picked as classification features as listed in Table 3.1. These features are used for the training and validation of damage classifiers.

In this research, a realistic number needs to be chosen for the interval of damage severity to verify the applicability of the proposed approach. If the damage interval is too small, the aerodynamic effects will be obscured by the presence of noise and disturbances, and what is left will be a set of data that is not well suited for identification and classification. On the other hand, by using small intervals, coarse results can be avoided during classification and safety can be guaranteed by a more comprehensive database. By referring to the setting of wind tunnel tests [13, 14], where the damage interval ranges from 7% to 25% tip loss for different locations, a number of 10% is chosen for damage interval to achieve the balance between feasibility and accuracy.

To generate a classification data set of 300 examples for each damage part and damage level, 5400 simulations were repeatedly run with the same input and noise level. The data set is divided into a training set and a validation set with the proportion of 2 : 1. Table 3.1 lists all the classification features, where in this chapter only two of them are shown in Fig. 3.3.

A base architecture of one hidden layer neural network with sigmoid functions as the activation function is used for training. The output layer has six outputs with the softmax function as the output transfer function. Various numbers of hidden nodes ranging from 3 to 30 were experimented with and the performances were evaluated based on the

Table 3.1: Damage parts and the corresponding stability derivatives used as features

Damage part	Features for classification
horizontal stabilizers	$C_{m_\alpha}, C_{m_q}, C_{m_{\delta_e}}$
vertical tail	$C_{n_\beta}, C_{n_r}, C_{n_{\delta_r}}$
wings	$C_{L_\alpha}, C_{l_\alpha}, C_{l_{\delta_a}}, C_{l_p}$

validation data. In this simulation, the best performance is given by a neural network with 10 hidden nodes. Based on this structure, the training results of the features based on this structure are displayed in the left column of Fig. 3.3, where six damage levels on three different parts of the aircraft are defined as class labels. The black markers represent the training data of different classes, and the region of each class is demonstrated by different colors. The accuracy of the training results rely on the richness of the training data.

To evaluate the performance of the trained classifier, validation experiments are conducted on different damage scales for a single damage location. The right column of Fig. 3.3 shows three examples of validation tests on three different locations, which are 30% tip loss of the left horizontal stabilizer, 20% tip loss of the vertical tail, and 40% tip loss of the left wing.

If data assigned to the correct class are defined as positive and the rest as negative, the validation results can be represented by four measures, which are the number of correctly classified positive data (true positive), correctly classified negative data (true negative), misclassified positive data (false positive), and misclassified negative data (false negative) respectively. Widely used criteria to evaluate classifier performance for classification problems are precision and recall, which are defined as [10]:

$$\begin{aligned} \text{Recall} &= \frac{\text{number of true positives}}{\text{number of true positives} + \text{number of false negatives}} \\ \text{Precision} &= \frac{\text{number of true positives}}{\text{number of true positives} + \text{number of false positives}} \end{aligned} \tag{3.3}$$

The evaluation results of the classifiers for each of the damage case are listed in Table. 3.2, which shows that the damage to any of the three main parts of the Cessna Citation aircraft can be successfully detected and classified under a moderate noise level (SNR = 25).

3.3. CLASSIFICATION BY SUPPORT VECTOR MACHINES

3.3.1. CLASSIFICATION WITH SAFETY CONSIDERATIONS

As mentioned in Sec. 2.4, there exist physical limitations of modeling damage cases on a sub-scale model and conducting wind-tunnel tests with it. These limitations and the presence of external noise constraint the size of intervals between two damage levels, which influences the number of damage cases for training the classifiers. If the training data is not sufficient to cover all possible situations, it may cause safety problems in real flight.

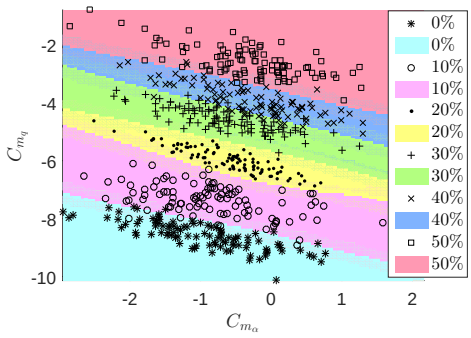

(a) left horizontal stabilizer tip loss

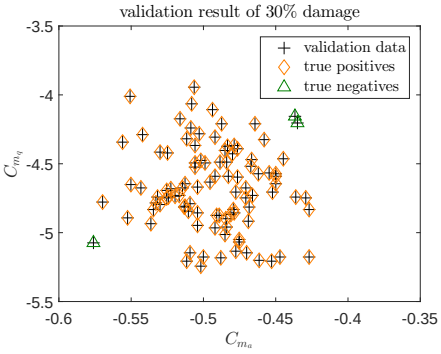

(b)

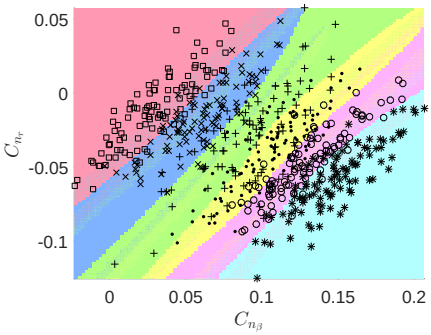

(c) vertical tail tip loss

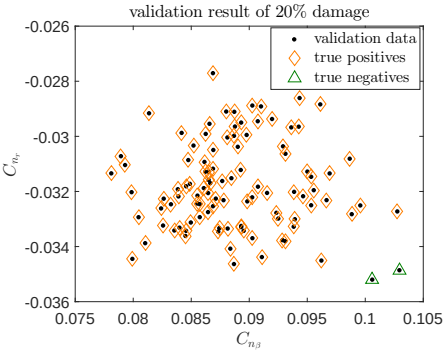

(d)

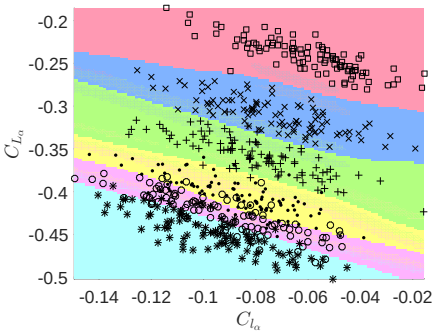

(e) left wing tip loss

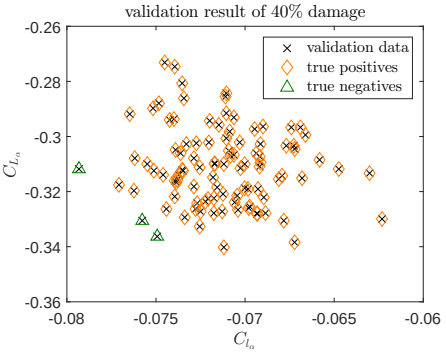

(f)

Figure 3.3: Training and validation results of damage severity classification in three different parts

For example, when the damage interval is relatively large, the actual damage level is in between two damage classes. If it is classified into the less severe one and the classification result is directly used as the index to the corresponding flight envelope in the

Table 3.2: Validation results of classification (SNR = 25)

	horizontal stabilizer		vertical tail		wing	
Damage Severity	recall	precision	recall	precision	recall	precision
10%	95.15%	98.98%	96.57%	98.78%	98.98%	97.76%
20%	98.94%	98.51%	98.65%	99.88%	98.61%	97.89%
30%	99.00%	99.50%	97.86%	98.96%	99.50%	95.89%
40%	98.02%	98.50%	97.58%	98.66%	99.50%	96.98%
50%	99.05%	99.00%	99.76%	98.56%	99.00%	99.75%

database, it may lead to potential risks. This issue reflects the gap between damage modeling and real aircraft damage, which can be circumvented by simply choosing the more severe case. However, it may also result in imprecise and over-conservative problems.

Another approach considers generating new training data in between two available classes, which requires apriori knowledge and assumptions. If the newly generated training data and class labels can not be guaranteed to reflect the real situation, the classification result may still lead to risks.

Instead of generating new training classes, classification score of new incoming data can be used, since it represents the relationship between data from real situation and existing training sets. For example, it may happen that the new incoming data is close to neither of the two neighboring classes but lies near the boundary. This situation is reflected in the values of classification scores, which suggests a new condition: *in between*. The suggested results can be used for further decision-making process. In damage cases for instance, if the classification score suggests a label in between 10% and 30% tip loss, it is reasonable to conclude that the current damage situation is closer to 20% tip loss.

Therefore, the classifier is required to give not only the chosen class label, but also classification scores for all class labels. Together with a decision-making strategy, *new* possible classes could be found in between the trained classes, and a larger safety margin can be guaranteed with more accurate prediction results.

It has been shown in the previous section that multilayer neural networks give satisfactory cross-validation results on multiclass problems for damaged aircraft. In this section, support vector machines are expected to give better results in finding a new class in between the two training classes, which may lead to more accurate estimation of damage severity. The results of SVM classifier is compared with that of neural networks under different levels of external noises in binary and multi-class classification problems. The training data for both classifiers is obtained from flight simulations specified in Sec. 3.2.2.

3.3.2. BINARY CLASSIFICATION

The SVM classifier is developed to enhance the ability of classifying unknown data while keeping the accuracy of the training in both linear-separable and linear-inseparable situations. In order to find a trade-off between over-fitting and generalization, the SVM approaches the classification problem through the concept of *margin*, which, from a

geometrical view, is defined as the perpendicular distance between the separating hyperplane and the closest of the data points. A large margin represents a confident and a correct prediction, so the optimal separating hyperplane to be found is the one which gives the maximum margin to guarantee the generalization ability of the classifier.

Given a set of $m-$dimensional training data $\mathbf{x}$, a hyperplane/decision function is defined as [10, 15]:

$$f(x) = \mathbf{w}^T \phi(\mathbf{x}) + b = c \tag{3.4}$$

where $\mathbf{w}$ is an $m-$dimensional vector, and b a bias parameter. $\phi(\mathbf{x})$ denotes a fixed feature-space transformation. When $c = 0$, a separating hyperplane is defined in the middle of the two hyperplanes with $c = 1$ and $c = -1$. The parameters of the separating hyperplane $(\mathbf{w}, b)$ are determined by finding out the support vectors during the process of maximizing the margin. The resulting value of the decision function $f(\mathbf{x})$ is the classification/decision score of $\mathbf{x}$. The new data $\mathbf{x}_{new}$ is thus classified by its decision score via:

$$\begin{cases} \text{class 1} & \text{if } f(\mathbf{x}_{new}) > 0 \\ \text{class 2} & \text{if } f(\mathbf{x}_{new}) < 0 \end{cases} \tag{3.5}$$

If the training data is not linearly separable, the obtained classifier may not have high generalization ability although the hyperplane is determined optimally. One of the advantages of SVM is that the generalization performance of the classification can be improved by using kernel tricks and soft margins [10, 15]. Through properly selected kernel functions and soft margin parameters, the trade-off between the maximization of the margin and the minimization of the classification error can be achieved.

The region $\{\mathbf{x}| -1 \leq f(\mathbf{x}) \leq 1\}$ is the generalization region for the decision function. As indicated by Eq. 3.5, new data that fall into the generalization region will normally be categorized into either class as long as they are not on the decision boundary [10, 15]. In our application of damage level classification, new data around the decision boundary in the generalization region will be categorized as a "middle-class". The new middle-class is generated by new incoming data if their classification scores are within the generalization region:

$$\begin{cases} \text{class 1} & \text{if } f(\mathbf{x}_{new}) \geq 1 \\ \text{middle class} & \text{if } f(\mathbf{x}_{new}) \in (-1, 1) \\ \text{class 2} & \text{if } f(\mathbf{x}_{new}) \leq -1 \end{cases} \tag{3.6}$$

Figure 3.4(a) shows the training result given by a binary SVM classifier, where the data points are identified from a stabilizer damage simulation. Data points in the two training sets are indicated by + and $\triangle$ symbol respectively, and data points to be classified as the middle class, which are not in the training set, are denoted by $\bigcirc$. When the two classes are linearly separable and the noise level is low, a clear generalization region can be recognized between the two training classes, which covers most of the data points from the middle class. As for the classification results on the same training set by the neural networks shown in Fig. 3.4(b), the classification score changes sharply, leaving a

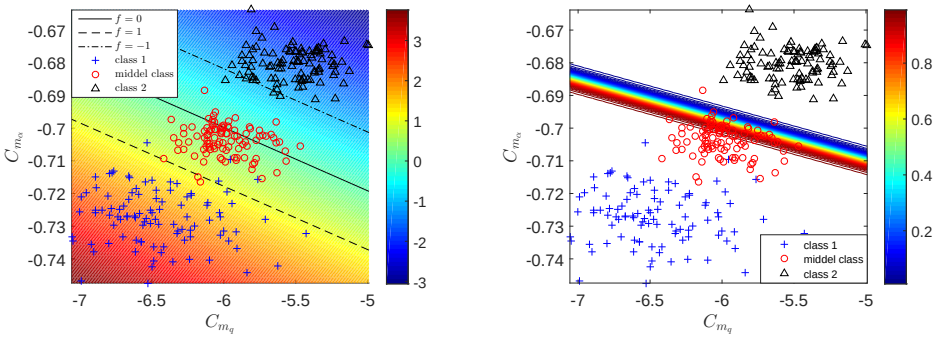

(a) support vector machines (b) multilayer neural networks

Figure 3.4: Binary classification results under low noise level with two different classification methods

much narrower band in between. By comparison, SVMs are more capable of identifying new data points in the middle class.

When the external noise imposed on the training data increases, the two separable classes may become inseparable with a much smaller margin in between. In order to keep the capability of generalization, a soft-margin SVM is used to allow some of the training points to be misclassified. The goal is still maximizing the margin, but at the same time "softly" penalizing points on the wrong side of the margin boundary. This method controls the trade-off between model complexity and minimizing training errors [10, 15]. It can be observed in Fig. 3.5 that despite the adverse affect of high noise level that may blur the boundary of different classes, the SVM can still identify more points in the middle class than neural networks as well as keeping the accuracy of the classification.

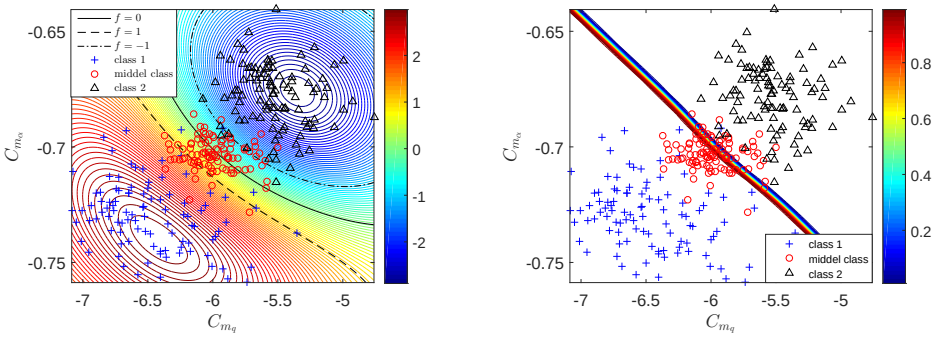

(a) support vector machines (b) multilayer neural networks

Figure 3.5: Binary classification results under high noise level with two different classification methods

3.3.3. MULTICLASS CLASSIFICATION

In practice, what will be tackled in damage classification problem may involve more than two classes even though SVM is inherently a two-class classifier. Various methods have been developed to decompose the multiclass problem into several two-class SVMs. Reviews on these proposed methods can be found in [11], which shows that the "one-against-one" SVM [16] and directed acyclic graph SVM (DAGSVM) [17] are more suitable for practical use than other methods, according to the results in experiments from [11]. In this chapter, the "one-against-one" SVM is used and compared with neural networks adopted in [18] to estimate the damage severity under different noise levels. For a K-class problem, $K(K-1)/2$ decision functions are trained and the same number of decision scores will be generated for new test data in the order: $(1,2),(1,3),...,(1,j);(2,3),...$ $(2,j);...(j-1,j)$. Instead of using max vote strategy [11], we propose a new method to find possible middle classes.

For a new data point x_{new}, the minimum absolute value of all the $K(K-1)/2$ classification scores are computed, which is:

$$f_{min} = \min_{i=1,2,...,K(K-1)/2} \left(|f_i(x_{new})| \right) \tag{3.7}$$

If f_{min} is the score of two neighboring classes (e.g. $(1,2),(2,3),...,(j-1,j)$), x_{new} will be classified according to the rules in Eq. 3.6, which may lead to a new middle class in between. If f_{min} is not the score of two neighboring classes, it means that there is no potential middle class in between existing classes. In this situation, x_{new} will be classified in the normal way, which is based on the signs of decision scores and the maximum number of votes[19].

To evaluate and compare the performance of the SVMs and neural networks, identified feature data from three damage levels form the training set, which are 30%, 40% and 50% tip loss respectively. The new data points to be classified are identified parameters from 35% and 45% tip loss cases, which are used to test the generalization of the two classifiers. The classification results under low-level and high-level noise are shown in Figs. 3.6 and 3.7 respectively.

By comparison, it is observed that the training results of neural networks (NN) show little change under two different noise levels, and the generalization region is not wide enough to cover most of the points from the middle classes. The SVMs, on the other hand, show obvious change in training results with the increase of noise level. As with binary classification, the SVM classifier shows better balance between generalization and accuracy.

3.3.4. MULTI-DAMAGE DIAGNOSIS VIA SVM

In real flight accidents, structural damage may happen simultaneously to more than one locations on the aircraft. As discussed in Sec. 2.4, the aerodynamic effects of damage to different parts of the aircraft are relatively independent from each other and the couplings, though exist, are of little impact [13]. Hence, the combined forms of damage can be detected and classified by using separate training features listed in Table 3.1.

For example, if one side of horizontal stabilizers and wings are damaged at the same time, the changed dimensionless moment coefficients caused by this multi-damage are

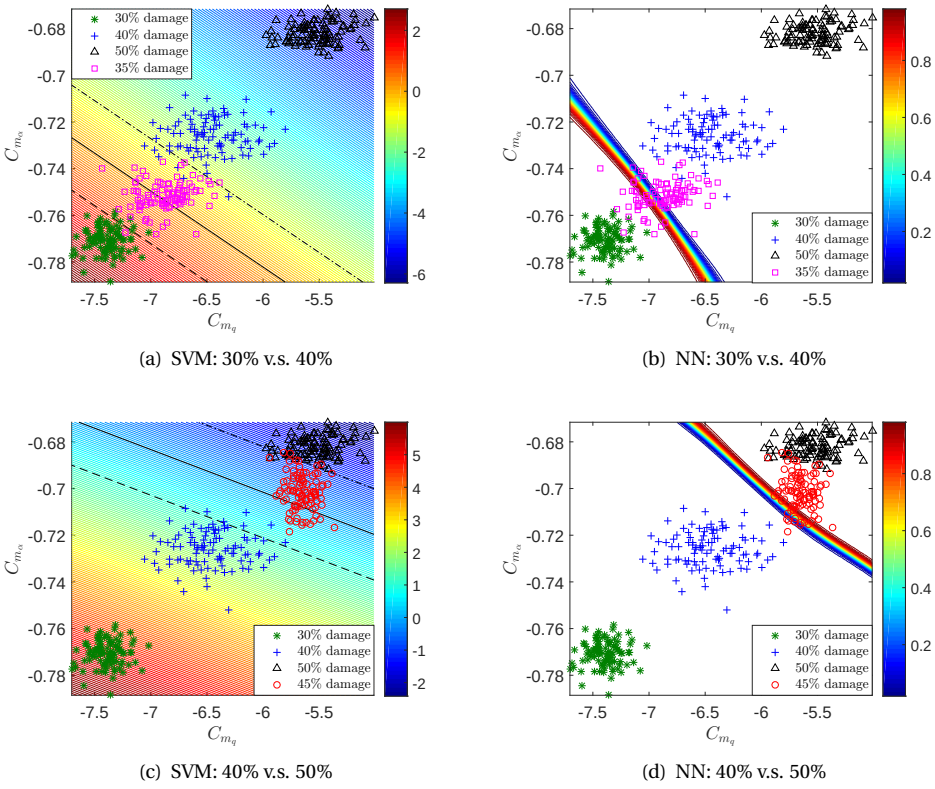

(a) SVM: 30% v.s. 40%

(b) NN: 30% v.s. 40%

(c) SVM: 40% v.s. 50%

(d) NN: 40% v.s. 50%

Figure 3.6: Multi-class classification results under low noise level with two different classification methods

C_m and C_l. Hence, alarms of re-identification in these two channels will be triggered individually by the anomaly detection system. Two separate sets of classifiers are initiated based on the training results displayed in Fig. 3.3. In this sense, the diagnosis of a multi-damage case can be reduced to several simultaneous single-damage detection and classification problems.

In this section, structural damage to two locations is triggered simultaneously at 20s in the DASMAT simulation model. The first damage case is 45% tip loss of one horizontal tail with 25% tip loss of the affiliated elevator on the same side, and the second damage case is 25% tip loss of one wing with 50% tip loss of the affiliated aileron on the same side. The damage modeling in the DASMAT simulation is based on the discussion in Chapter 2.

Fig. 3.8 shows the time series of identified results of aerodynamic parameters that are influenced by the triggered damage. These identified parameters are used as test data to find the location and severity of the unknown damage in the diagnosis system based on the decision rules proposed in this thesis. The time series of the classification result and the number of data points classified in each damage case label are displayed in Fig. 3.9.

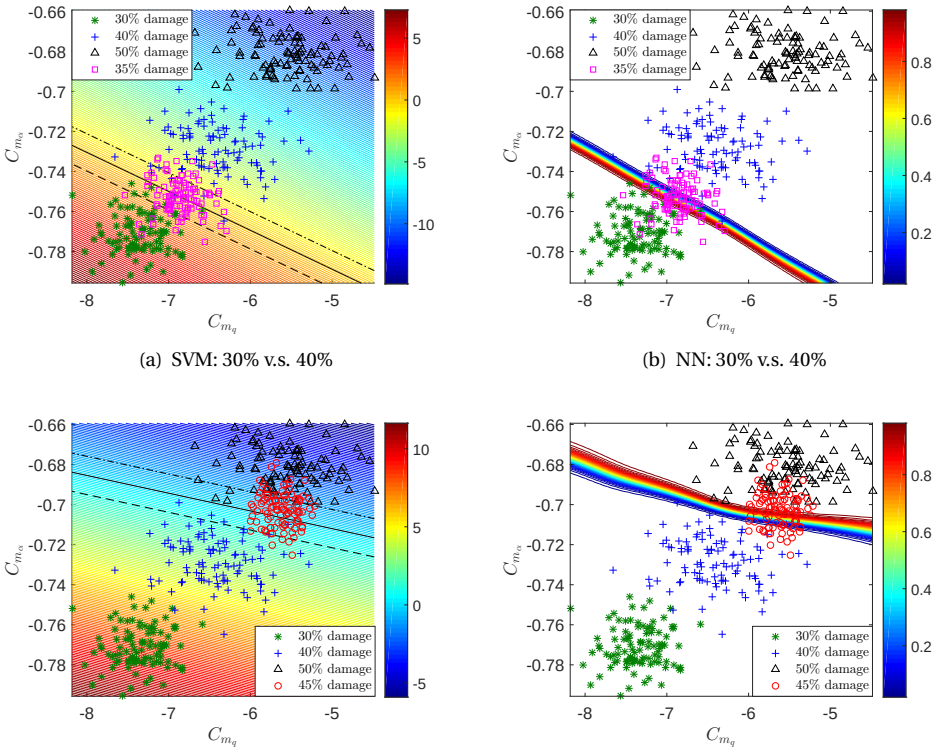

(a) SVM: 30% v.s. 40%

(b) NN: 30% v.s. 40%

(c) SVM: 40% v.s. 50%

(d) NN: 40% v.s. 50%

Figure 3.7: Multi-class classification results under high noise level with two different classification methods

It can be concluded that by using the training results of the SVM classifier, the damage diagnosis system can be applied to the multi-damage case with satisfactory outcomes.

3.4. DAMAGE ASSESSMENT FOR SITUATION AWARENESS

In section 3.1, structural damage is classified into one of the predefined cases for database retrieval of flight envelopes, which are then used in the flight controller. For human pilot, a fuzzy logic system can sometimes provide more illustrative information than numerical results. As a combination of numerical and symbolic knowledge of the system, the fuzzy logic is designed to achieve a balance between the vague, uncertain world and its precise, deterministic estimation. As illustrated in Fig. 3.10, the severity of damage can be either be defined as a percentage of tip loss, or be described by linguistic words such as “moderate damage” or “severe damage”. By using linguistic variables, fuzzy logic is a marvelous tool that provides a possible way of dealing with vagueness and imprecision of information from limited experiments.

In this section, a fuzzy logic system (FLS) is designed and integrated in the problem of damage assessment of the aircraft using aerodynamic coefficients as damage indicators.

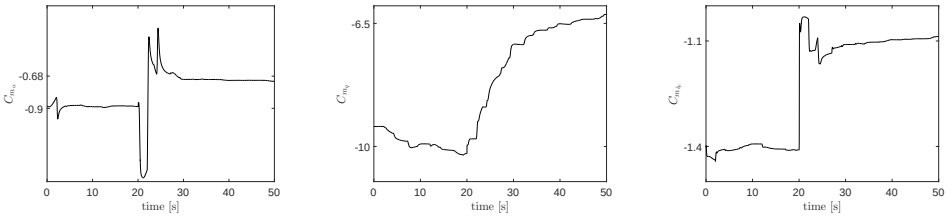

(a) C_{m_α} (b) C_{m_q} (c) $C_{m_{\delta_e}}$

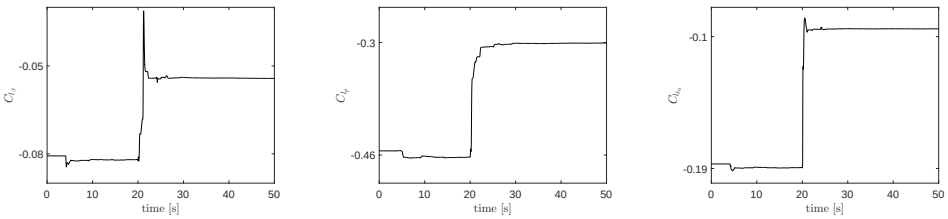

(d) C_{l_β} (e) C_{l_p} (f) $C_{l_{\delta_a}}$

Figure 3.8: Online identified aerodynamic parameters used as features for multi-damage assessment

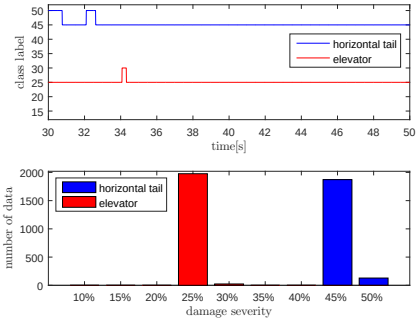

(a) 25% elevator damage and 45% horizontal tail damage

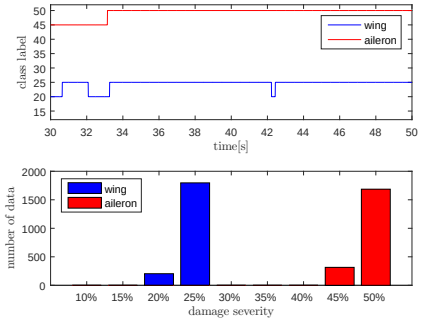

(b) 50% aileron damage and 25% wing damage

Figure 3.9: Multi-damage severity assessment result of wing and horizontal tail

By using fuzzy logic, aircraft structural damage is assessed in a more qualitative manner rather than a quantitative way, in order to enhance the situation awareness of the human pilot. This can be used as an auxiliary part in LOC prevention systems, where the pilot is warned of the current situation by the damage assessment system.

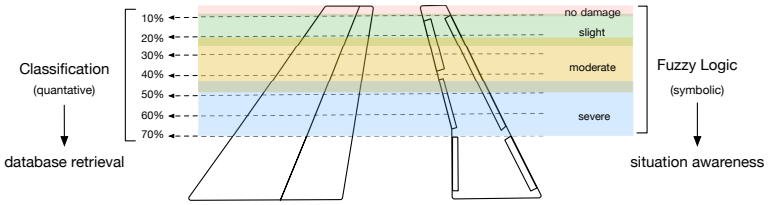

Figure 3.10: Two different ways of describing the damage condition of aircraft wings and tails

3.4.1. INPUT AND OUTPUT OF A FUZZY LOGIC SYSTEM

Mathematically, an FLS performs a mapping from crisp inputs x to the outputs y [20, 21]:

$$y = F(x) \tag{3.8}$$

In this case, the mapping reflects the relationship between the change of aerodynamic coefficients (x) and the damage condition of aerodynamic surfaces (y). The output is described by a set of linguistic variables:

$$y = \{\text{undamaged, slight damage, moderate damage, severe damage}\} \tag{3.9}$$

The inputs x to the FLS in Fig. 3.11 are the change scale of identified aerodynamic coefficients:

$$x = \frac{C_{dmg} - C_0}{C_0} \cdot 100\% \tag{3.10}$$

where C_{dmg} denotes the changed value of a certain aerodynamic coefficient (e.g., C_{n_r}) under one single damage case (e.g., vertical tail loss), and C_0 represents its original value before the damage. By using the change scale as input x, different values of identified aerodynamic coefficients can be unified between 0 and 1. Therefore, only one set of membership functions is needed for all the coefficients, which saves a lot of computation load and memory.

As shown in Fig. 3.11, the knowledge base of an FLS is basically composed of a number of fuzzy if-then rules and membership functions, which are generated offline. The fuzzification process transforms the crisp inputs into degrees of match with linguistic variables using membership functions, and a fuzzy inference engine is then used to perform the inference operations on the rules [20, 21]. The process of determining membership functions and generating fuzzy rules are illustrated in Fig. 3.11, which will be discussed in the following subsections.

3.4.2. MEMBERSHIP FUNCTIONS

The determination of membership functions is based on experimental data of different damage cases. The damage cases to be inserted in the flight simulation are defined in accordance with the output of the FLS. As shown in Fig. 3.10, each linguistic output in y corresponds to a range of damage scales in %, which is used for determining the damage scale matrix in Eq. 2.9 based on wind-tunnel tests. Five main aerodynamic surfaces are

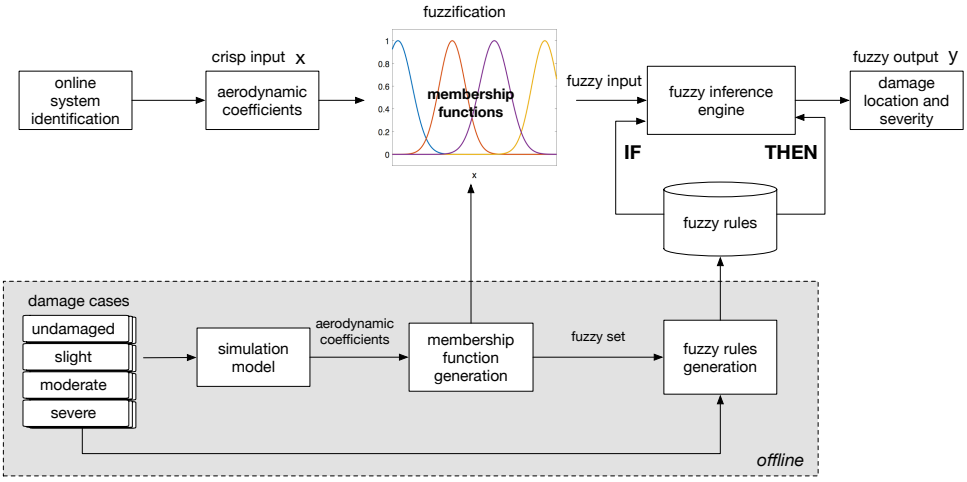

Figure 3.11: Schematic representation of a fuzzy logic system (FLS)

considered in this section, which are two horizontal tails (HT), vertical tail (VT) and two wing spans. In total there are 20 damage cases to be modeled and simulated.

The identified aerodynamic coefficients are first transformed into crisp values based on Eq. 3.10, which are then categorized into several groups. Each group corresponds to one membership function, covering a range of crisp inputs. The membership function is used to describe the degree of match of each input, which takes on the value between 0 and 1 [20, 21]. As shown in Fig. 3.12, four membership functions from F_1 to F_4 are determined based on the Gaussian combination membership function: where m is the midpoint of the fuzzy set and σ is the standard deviation.

$$\mu(x;m_1,\sigma_1,m_2,\sigma_2) = \begin{cases} e^{-0.5((x-m_1)/\sigma_1)^2} & x < m_1 \\ 1 & m_1 < x < m_2 \\ e^{-0.5((x-m_2)/\sigma_2)^2} & x > m_2 \end{cases} \tag{3.11}$$

where m_1 and σ_1 determines the shape of the left-most curve and m_2 and σ_2 determined the shape of the right-most curve. In this case, the parameters of the membership functions are chosen heuristically based on the features of identified coefficients, and the resulting functions are plotted in Fig. 3.12 based on Eq. 3.11.

3.4.3. RULE GENERATION

Rules for the fuzzy system can be expressed as[20, 21]:

$$\begin{aligned} R_i : \textbf{IF} \quad & x_1 \; is \; F_{j_1} \; \text{AND} \; x_2 \; is \; F_{j_2} \; \text{AND} \ldots x_m \; is \; F_{j_m} \\ & \textbf{THEN} \; y = K_i \end{aligned} \tag{3.12}$$

Each rule R_i corresponds to one pre-defined damage class K_i, specifying the damage location and severity in linguistic variables. Given a certain damage class, the main purpose of rule generation is to determine the **IF** part, which is also called the *antecedent* in

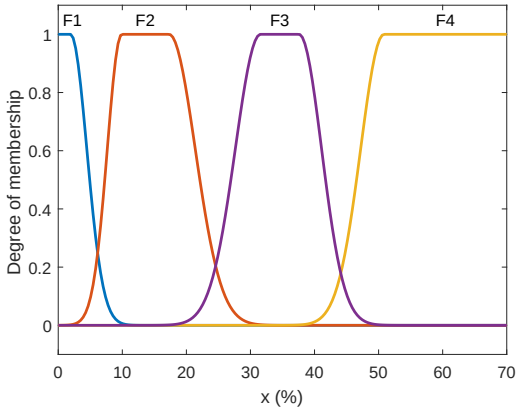

Figure 3.12: Four defined membership functions of the FLS (F1: undamaged, F2: slight damage, F3: moderate damage, F4: severe damage)

fuzzy logic theory. For each input x_m in the antecedent, it is required to find its corresponding membership function $F_{j_m} \in \{F_1, F_2, F_3, F_4\}$. As illustrated in Fig. 3.11, the generation of one fuzzy rule R_i can be followed by the precedure explained below [20, 21]:

1. Given a damage case K_i simulated in the aircraft model, the corresponding change scale of aerodynamic coefficients $(x_1, x_2, ..., x_m)$ are identified. The damage case is repeatedly simulated N times with noise and uncertainties, resulting in N samples for each input x_m.

2. For each sample of a certain input x_m, its fuzzy set is calculated, from which the membership function that has the largest value of the fuzzy set $\max_{i=1}^{4}\{\mu_{F_i}(x_m)\}$ earns one vote.

3. Maximum vote is used to determine the membership function F_{j_m} for the input x_m that has the maximum number of votes from all the N samples.

4. Step 2 and 3 are repeated for all the inputs $(x_1, x_2, ..., x_m)$ until each part of the antecedent is determined for R_i.

Based on the above procedures, part of the trained rules from simulation data are displayed in Table 3.3.

3.4.4. ONLINE UTILIZATION OF THE FUZZY LOGIC SYSTEM

After the membership functions and fuzzy rules are determined, they can be used as part of the online FLS. As shown in Fig. 3.11, the crisp inputs calculated from online system identification are evaluated by the pre-defined membership functions to produce fuzzy inputs. By applying fuzzy rules, the fuzzy inference engine transforms the fuzzy inputs into fuzzy outputs. During the inference process, a fuzzy operator (**AND**) is applied to

Table 3.3: Rules of the fuzzy logic system

IF											THEN
C_{m_α}	C_{m_q}	$C_{m_{\delta_e}}$	C_{n_β}	C_{n_r}	$C_{n_{\delta_r}}$	C_{Y_β}	C_{L_α}	C_{l_α}	C_{l_p}	$C_{l_{\delta_a}}$	fuzzy output
F_1	F_1	F_1	F_1	F_1	F_1	F_1	F_1	F_1	F_1	F_1	undamaged
F_2	F_2	F_2	F_1	F_1	F_1	F_1	F_1	F_1	F_1	F_1	HT: slight damage
F_3	F_4	F_3	F_1	F_1	F_1	F_1	F_1	F_1	F_1	F_1	HT: moderate damage
F_4	F_4	F_4	F_1	F_1	F_1	F_1	F_1	F_1	F_1	F_1	HT: severe damage
F_1	F_1	F_1	F_2	F_2	F_2	F_2	F_1	F_1	F_1	F_1	VT: slight damage
F_1	F_1	F_1	F_3	F_3	F_3	F_3	F_1	F_1	F_1	F_1	VT: moderate damage
F_1	F_1	F_1	F_4	F_4	F_4	F_4	F_1	F_1	F_1	F_1	VT: severe damage
F_1	F_1	F_1	F_1	F_1	F_1	F_1	F_2	F_2	F_2	F_2	wing: slight damage
F_1	F_1	F_1	F_1	F_1	F_1	F_1	F_3	F_3	F_3	F_3	wing: moderate damage
F_1	F_1	F_1	F_1	F_1	F_1	F_1	F_4	F_4	F_4	F_4	wing: severe damage

obtain the fuzzy result of each rule μ_{R_i} by combining the fuzzy set of each input x_m of the antecedent:

$$\mu_{R_i}(x) = \mu_F(x_1) \cdot \mu_F(x_2) \cdot \cdots \mu_F(x_m) \tag{3.13}$$

Since each damage case corresponds to one fuzzy rule, the highest value of $\mu_{R_i}(x)$ corresponds to the fuzzy output of the system, which indicates the damage location and severity.

To validate the FLS proposed in this section, validation data are generated from the DASMAT simulation model on which four levels of damage severity for different parts of the aircraft are applied. In order to test how well the FLS deal with noise, four different signal-to-noise ratios (SNR) are added to the experimental measurements. For each case, 1000 data points are generated. The performances is evaluated by success rate (in %), which is the ratio of the damage cases that are correctly recognized by the FLS. Fig. 3.13 shows the results for increasing noise levels for damage in left horizontal stabilizer, vertical tail and left wing respectively. It can be observed that the success rate increases when larger SNR, i.e, less noises are applied. It is also observed that the success rate of undamaged case is higher than other cases. This can be explained by the fact that identification performs better when damage cases are not inserted.

REFERENCES

[1] I. Hwang, S. Kim, Y. Kim, and C. E. Seah, *A Survey of Fault Detection, Isolation, and Reconfiguration Methods,* IEEE Transactions on Control Systems Technology **18**, 636 (2010).

[2] B. Bacon, A. J. Ostroff, and S. Joshi, *Reconfigurable NDI Controller Using Inertial Sensor Failure Detection & Isolation,* Aerospace and Electronic Systems, IEEE Transactions on **37**, 1373 (2001).

[3] B. Jiang and F. N. Chowdhury, *Fault Estimation and Accommodation for Linear*

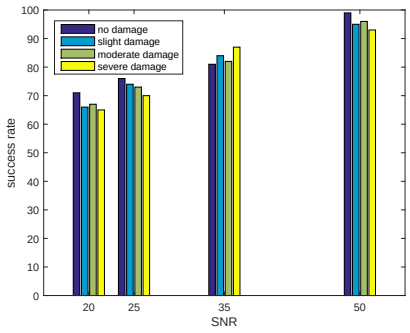

(a) Horizontal stabilizer

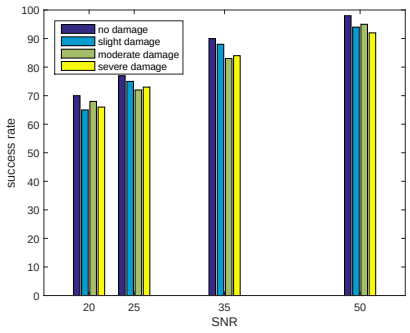

(b) Vertical tail

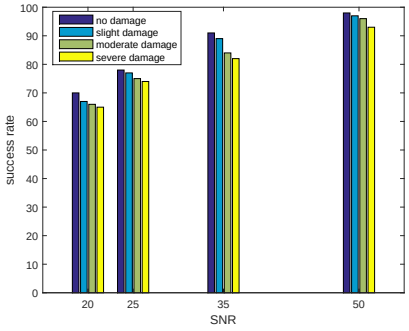

(c) Wing

Figure 3.13: The success rate of damage pattern recognition at different locations and noise levels

MIMO Discrete-Time Systems, IEEE Transactions on Control Systems Technology **13**, 493 (2005).

[4] P. Lu, *Fault Diagnosis and Fault-Tolerant Control for Aircraft Subjected to Sensor and Actuator Faults*, Ph.D. thesis, Delft University of Technology (2016).

[5] T. E.Menke and P. S.Maybeck, *Sensor / Actuator Failure Detection in the Vista F-16 by Multiple Model Adaptive Estimation,* IEEE Transactions on Aerospace and Electronic Systems **31** (1995).

[6] H. Alwi, C. Edwards, and C. Pin Tan, *Fault Detection and Fault-Tolerant Control Using Sliding Modes* (Springer, 2011) pp. 7–27.

[7] I. Lopez and N. Sarigul-Klijn, *A Review of Uncertainty in Flight Vehicle Structural Damage Monitoring, Diagnosis and Control: Challenges and Opportunities,* Progress in Aerospace Sciences **46**, 247 (2010).

[8] Gang Niu, J.-D. Son, a. Widodo, B.-S. Yang, D.-H. Hwang, and D.-S. Kang, *A Compar-*

ison of Classifier Performance for Fault Diagnosis of Induction Motor using Multi-type Signals, Structural Health Monitoring **6**, 215 (2007).

[9] R. O. Duda, P. E. Hart, and S. Analysis, *Pattern Classification*, 2nd ed. (Wiley, 2000).

[10] S. Abe, *Support Vector Machines for Pattern Classification*, edited by S. Singh (Springer, 2010).

[11] C.-w. Hsu and C.-j. Lin, *A Comparison of Methods for Multiclass Support Vector Machines,* IEEE Transactions on Neural Networks **13**, 415 (2002).

[12] G. Ou and Y. L. Murphey, *Multi-class Pattern Classification Using Neural Networks,* Pattern Recognition **40**, 4 (2007).

[13] G. Shah, *Aerodynamic Effects and Modeling of Damage to Transport Aircraft,* in *AIAA Atmospheric Flight Mechanics Conference and Exhibit*, AIAA Paper 2008-6203 (2008).

[14] G. Shah and M. Hill, *Flight Dynamics Modeling and Simulation of a Damaged Transport Aircraft,* in *AIAA Modeling and Simulation Technologies Conference*, AIAA Paper 2012-4632 (2012).

[15] C. M. Bishop, *Pattern Recognition and Machine Learning* (Springer, 2006).

[16] J. Fürnkranz, *Round Robin Classification,* Journal of Machine Learning Research **2**, 721 (2002).

[17] J. Platt, N. Cristianini, and J. Shawe-Taylor, *Large Margin DAGs for Multiclass Classification,* in *International Conference on Neural Information Processing Systems* (2000) pp. 547–553.

[18] Y. Zhang, C. C. de Visser, and Q. P. Chu, *Aircraft Damage Identification and Classification for Database-Driven Online Flight-Envelope Prediction,* Journal of Guidance, Control, and Dynamics **41 (2)**, 449 (2018).

[19] C.-C. Chang and C.-J. Lin, *LIBSVM: A Library for Support Vector Machines,* ACM Transactions on Intelligent Systems and Technology **2**, 27:1 (2011), software available at `http://www.csie.ntu.edu.tw/~cjlin/libsvm`.

[20] M. Chandrashekhar and R. Ganguli, *Damage Assessment of Structures with Uncertainty by Using Mode-shape Curvatures and Fuzzy Logic,* Journal of Sound and Vibration **326**, 939 (2009).

[21] R. Ganguli, *A Fuzzy Logic System for Ground Based Structural Health Monitoring of a Helicopter Rotor Using Modal Data,* Journal of Intelligent Material Systems and Structures **12**, 397 (2001).

4

DATABASE BUILDING AND INTERPOLATION

This chapter is focused on the building and interpolation of the database. The flight envelopes stored in the database are computed based on the dynamics model of the aircraft under various abnormal conditions. Using damage assessment results in Chapter 3, the safe flight envelopes can be retrieved from the database. Furthermore, the necessity of flight envelope interpolation is discussed and implemented. Finally, the computational complexity of the database approach is analyzed to show its feasibility of online application.

This chapter is based on:
Y. Zhang, C. C. de Visser, and Q. P. Chu, *Database Building and Interpolation for an Online Safe Flight Envelope Prediction System*, Journal of Guidance, Control, and Dynamics, 2018, published.
Y. Zhang, C. C. de Visser, and Q. P. Chu, *Online Safe Flight Envelope Prediction for Damaged Aircraft: A Database-driven Approach*, AIAA Modeling and Simulation Technologies Conference, 2016.

4.1. INTRODUCTION

Defined as the region in state space where the aircraft can be safely operated, flight envelope is vital to aircraft safety and the prevention of loss-of-control (LOC) accidents. Generally, A safe flight envelope is determined by the aerodynamic and kinematic model of the aircraft as well as its control authority. As introduced in Chapter 1, there are different ways of describing and computing a safe flight envelope [1–7], depending on the aircraft model and states that are of highest concern in terms of safety.

Among these methods, reachability analysis computes the safe flight envelope of a nonlinear aircraft model in a set-valued fashion, which defines a set of states that will reach a target set within a certain time horizon given the current control authority [8–10], and its numerical solution is given by the level set method [11, 12].

Currently, most flight envelopes are considered to be fixed and stored onboard in a static flight envelope protection system to indicate performance and structural limits of the aircraft during flight [13]. Under abnormal conditions, however, the stability margins and control authority might suddenly change due to abrupt system failures and structural damage, which leads to a changed flight envelope. In such situations, a LOC accident might follow if the (unknown) shrunken envelope is not protected and the aircraft moves outside the new safe boundary. Therefore, it is essential to obtain the changed flight envelope online as fast as possible to allow for effective upset recovery and emergency flight planning [14].

Considering the research challenges stated in Chapter 1, the online determination of changed flight envelopes without any offline support is not practical. In the presence of sudden in-flight adverse conditions, there is not enough time to acquire the global model from limited measurements and handle intensive computational load for the recomputation of unknown flight envelopes.

The crux of this research is to provide a database as an offline support to the online prediction of flight envelopes. The integration of offline database building and online data retrieval, which constitutes the DEFEND system (Fig. 2.1) introduced in Chapter 1 and 2, can compensate for the shortage of time and information during abnormal flight. As a continuation of previous chapters, this chapter mainly focus on the building and retrieval of the database.

4.2. DATABASE OF ABNORMAL CASES

The design of database is one of the most crucial and complex parts of the DEFEND system, involving a whole process of transforming high-level application requirements into lower-level application programs of database. The primary phase of database design is to investigate different abnormal cases.

In NASA's design of safety-critical systems for aircraft LOC prevention and recovery [3, 15], a preliminary set of LOC test scenarios was developed based on past accidents analysis and potential future LOC risks [16]. As listed in Table 4.1, the set contains scenarios involving four LOC precursor categories [15]. Among these four categories, structural damage and icing fundamentally change the dynamics and control abilities of the aircraft and thus may induce LOC accidents that cannot be prevented with static flight envelope protection systems. Therefore, this chapter focuses on the flight envelopes

with aerodynamic changes.

Table 4.1: LOC Accidents Causal and Contributing Factors

System Faults and Failures	**Strucutral Damage**	External Hazards	Aircraft Upsets
jammed/ stuck control effector	wing tip loss	icing and snow	stall
actuator run away	engine loss	wind gusts	abnormal attitude
loss of control effectiveness	control surfaces damage	wake vortices	abnormal trajectory
engine failure	horizontal stabilizer tip loss	poor visibility	abnormal velocity
sensor faults	vertical tail tip loss	bird strike	

Simulated flight data of structural damaged aircraft can be generated by CFD/wind tunnel experiments [17] and be used by advanced system identification methods to determine their mathematical models. These models are used to compute the safe flight envelopes for different flight situations.

4.3. COMPUTATION OF SAFE FLIGHT ENVELOPES

The guarantee of safety has always been an important consideration when synthesizing controllers of complex safety-critical systems like civil aircraft. Despite the existence of conventional flight envelope protection systems, physical constraints may not be sufficient for control design, and simulations (e.g., Monte Carlo method) may also be inadequate to help predict the unanticipated problems with all possible initial conditions.

Alternatively, reachability analysis can provide a new set-valued insight into the safety and control design of dynamic systems. On one hand, the theory can mathematically observe the system's behaviour by synthesizing states and control input constraints. On the other hand, with reachability analysis, all points belonging to all possible trajectories can be computed at once from all possible initial states, which differs itself from what simulation can achieve at one time and perfectly conform with the meaning of safety guarantee[18].

4.3.1. SAFETY-RELATED SETS

Origins from system verification, the reachability analysis seeks to decide whether the trajectories of a system model can reach a certain target set from an initial set within given time horizons and input constraints[19, 20]. To put it in a mathematical and more strict way, we first consider a continuous dynamic system[8],

$$\dot{x} = f(x, u) \tag{4.1}$$

with $x \in \mathbb{R}^n$, $u \in U \subseteq \mathbb{R}^m$. $f(\cdot,\cdot) : \mathbb{R}^n \times U \to \mathbb{R}^n$ is a bounded and Lipschitz continuous function. Given an arbitrary time horizon T, let $\mathscr{U}_{[t,T]}$ denote the set of Lebesgue

measurable functions from the interval $[t,T]$ to U, then for every $x \in \mathbb{R}^n$, $\tau \in [t,T]$ and $u \in \mathscr{U}_{[t,T]}$, the system admits a unique solution or trajectory $\xi(\tau;t,x,u(\cdot)) = x$.

Given a target set $\mathscr{K} \subseteq \mathbb{R}^n$, four reachable sets can be naturally formulated based on the relation between the target set and the state trajectories over the time horizon T [18, 21]:

In some literatures on differential game theory[11, 21, 22], two counter inputs with opposing influences are considered, which usually come from controllers and disturbances respectively. To simplify the situation, we only focus on one positive input, and assumes that it will always endeavor to steer the system into the safe area.

- The maximal reachable set is the set of initial states for which there exists at least *one* input such that the trajectories emanating from those states reach $\mathscr{K}$ at *some* time $\tau \in [t,T]$:

$$Reach_{max}(t,\mathscr{K}) := \left\{x \in \mathbb{R}^n | \exists u \in \mathscr{U}_{[t,T]}, \exists \tau \in [t,T], \xi(\tau;t,x,u(\cdot)) \in \mathscr{K}\right\} \tag{4.2}$$

- The minimal reachable set is the set of initial states such that for *every* input the trajectories emanating from those states reach $\mathscr{K}$ at *some* time $\tau \in [t,T]$:

$$Reach_{min}(t,\mathscr{K}) := \left\{x \in \mathbb{R}^n | \forall u \in \mathscr{U}_{[t,T]}, \exists \tau \in [t,T], \xi(\tau;t,x,u(\cdot)) \in \mathscr{K}\right\} \tag{4.3}$$

- The viability set is the set of all initial states *in* $\mathscr{K}$ for which there exists at least *one* input such that the trajectories emanating from those states remain within $\mathscr{K}$ for *all* time $\tau \in [t,T]$:

$$Via(t,\mathscr{K}) := \left\{x \in \mathbb{R}^n | \exists u \in \mathscr{U}_{[t,T]}, \forall \tau \in [t,T], \xi(\tau;t,x,u(\cdot)) \in \mathscr{K}\right\} \tag{4.4}$$

- The invariance set is the set of all initial states *in* $\mathscr{K}$ such that for *every* input the trajectories emanating from those states remain within $\mathscr{K}$ for *all* time $\tau \in [t,T]$:

$$Inv(t,\mathscr{K}) := \left\{x \in \mathbb{R}^n | \forall u \in \mathscr{U}_{[t,T]}, \forall \tau \in [t,T], \xi(\tau;t,x,u(\cdot)) \in \mathscr{K}\right\} \tag{4.5}$$

With $\mathscr{K}^c$ representing the complement of $\mathscr{K}$, we can clearly show that:

$$Reach_{max}(t,\mathscr{K}) \supseteq Reach_{min}(t,\mathscr{K}) \supseteq \mathscr{K} \supseteq Via(t,\mathscr{K}) \supseteq Inv(t,\mathscr{K}) \tag{4.6}$$

and more importantly,

$$Reach_{max}(t,\mathscr{K}) = (Inv\left(t,\mathscr{K}^c\right))^c \tag{4.7}$$

$$Reach_{min}(t,\mathscr{K}) = (Via\left(t,\mathscr{K}^c\right))^c \tag{4.8}$$

For viability set and invariance set, the computed trajectories are required to reach the target set for all time including the initial time, implying that these two sets must be

subsets of the target set. The minimum and maximum reachable sets, on the contrary, include the target set as a subset, since the trajectories can be initially outside the target set and reach it at a certain time point. These sets are used in different applications. Based on the definitions of target sets, we can establish a connection between these sets with practical safety problems.

For example, when the target set $\mathscr{K}$ is defined as the safe set where the system is expected to stay, the viability set is computed for "safety-preserving" controllers that keep the trajectories of system within the safe region for all time [18, 23]. In other cases, the target set $\mathscr{K}$ is specified as "unsafe", and we want to find out the states that may give rise to dangerous situations and we should avoid when designing control strategies[19]. Thus the minimal reachable set should be computed that includes all the states that may reach the unsafe set no matter what the controller does within a certain time interval[11].

Past researches on flight envelopes using reachability analysis [9, 10, 24] define the target set as the trim set. Therefore, for aircraft outside the trim set, reachable sets are needed. It is preferable to compute the maximum reachable set, since the requirement on control input of the minimum reachable set is too strict. If the current state is in the reachable set, it is still possible to get back to the target set within the given time horizon. If not, it may require longer time horizons than expected to reach the target set.

The maximum reachable set is also referred to as *backward* reachable set in some papers[9, 10], to distinguish it from the forward reachable set. For backward reachable set, the unknown trajectories start at initial time t and passes into or through a known target set by a certain time horizon. In this sense, the set to be computed is an initial set so that the computation should in some way go backward in time [11, 25]. For a forward reachable set, the initial set is known as the target set, and the set to be computed is the end of the trajectories by a certain time horizon. In order to unify both forward and backward reachable set in one timeline, the initial time of a backward reachable set is defined as $t = -T$ with its terminal time $t = 0$. Correspondingly, the initial and terminal time of a forward reachable set is $t = 0$ and $t = T$.

In our research, both backward reachable set and forward reachable set are needed. The backward reachable set include trajectories that may guide the aircraft back to new trim sets under appropriate control allocations. Nevertheless, the aircraft cannot stay in the trim set forever, it still needs to maneuver to other flight conditions like landing [26]. The trajectories of states that emanate from the trim set are computed to form a forward reachable set, given a time horizon and control inputs.

In general, the intersection of forward and backward reachable set of a given trim set is the safe flight envelope we are looking for[9, 10]. As illustrated in Fig. 4.1, the intersection indicates the region in the state space where aircraft can reach the trim set and maneuver freely within a certain time horizon. When failures or damage occur, both forward and reachable sets will shrink as well as the trim set [27] due to the changed aircraft model, as shown in Fig. 4.1. Therefore, some state trajectories that are part of the reachable sets during normal flight become unreachable after failures or damage, which results in the reduced safe flight envelope.

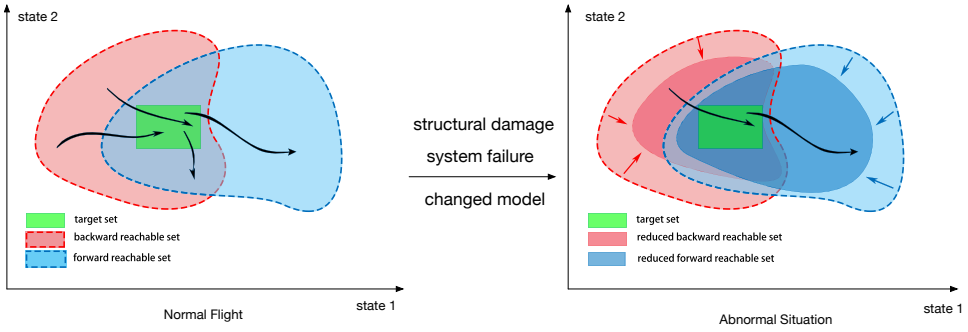

Figure 4.1: Safe flight envelope and its change after sudden damage and failures

4.3.2. CONNECTION TO OPTIMAL CONTROL

It has been clearly stated and proved in [11], that the reachable set can be determined by solving for the viscosity soluation of a time dependent Hamilton-Jacobi-Issac (HJI) partial differential equation.

Let $V : \mathbb{R}^n \times [-T, 0] \rightarrow \mathbb{R}$ be the viscosity solution of the terminal value HJI PDE:

$$\begin{aligned} &\frac{\partial \varphi(x,t)}{\partial t} + \min\left\{0, H\left(x, \frac{\partial \varphi}{\partial x}(x,t)\right)\right\} = 0, \\ &H\left(x, \frac{\partial \varphi}{\partial x}(x,t)\right) = \min_{u \in \mathscr{U}}\left\{\frac{\partial \varphi}{\partial x}(x,t) f(x,u)\right\}, \\ &\varphi(x,0) = k(x), \end{aligned} \tag{4.9}$$

where the target set $\mathscr{K}$ is closed and can be represented as the zero level set of a bounded and Lipschitz continuous function $k : \mathbb{R}^n \rightarrow \mathbb{R}$

$$\mathscr{K} = \{x \in \mathbb{R}^n | k(x) \leq 0\} \tag{4.10}$$

Then the zero level set of φ: $\varphi(x,t) = 0$ describes the boundary of a backward reachable set. Solving for a forward and a backward reachable set can be regarded as an initial and a terminal optimal control problem respectively [28]. Thus the function H of the forward reachable set is:

$$H\left(x, \frac{\partial \varphi}{\partial x}(x,t)\right) = \min_{u \in \mathscr{U}}\left\{-\frac{\partial \varphi}{\partial x}(x,t) f(x,u)\right\} \tag{4.11}$$

where the sign of spatial derivative $\frac{\partial \varphi}{\partial x}$ indicates the direction of information flows.

The minimization term with zero in the equation is to guarantee that the subset enclosed by the zero level set of the value function cannot decrease as time marches backward. This is to prevent some states that have already entered the target from leaving it before time horizon by "freezing" the evolution of the trajectory[19, 29]. More specifically, if the target set is defined as the undesired region, then the restriction is to make sure that some unsafe states will be tagged as "unwanted" once it enters the unsafe area and tries to leave. Similarly, if the target set is defined as a safe set, the restriction will include all the potential safe sets correctly.

4.3.3. LEVEL SET METHOD

The concept of level set and implicit surfaces proposed by Osher and Sethian [12] and the level set method developed by Mitchell [30], have been successfully applied to the reachability analysis of many systems including aircraft [10]. The level set method is one of the subclasses of Euler method, which discretizes the state space into grids and calculates in a dimension-by-dimension manner. One of the key process of the numerical scheme is the approximation of the spatial gradient $\partial\varphi(x,t)/\partial x$ defined on grids, especially for discontinuity points. Upwinding differencing is usually used to choose the approximation of spacial derivatives from forward and backward differencing by looking at the flow direction of $\varphi(x,u)$ indicated by the sign of dx/dt. By each grid, the minimum or maximum value of $\frac{\partial\varphi}{\partial x}(x,t)\cdot f(x,u)$ is calculated by choosing optimal control inputs. After evaluating the analytical optimal value of the Hamiltonian function, a Lax-Friedrichs approximation of the Hamiltonian is often used to ensure stability of the numerical scheme by adding an artificial viscosity term to the Hamiltonian. In the end, based on the equation:

$$\frac{\partial\varphi(x,t)}{\partial t} = -\min\left\{0, \min_{u\in\mathscr{U}} \frac{\partial\varphi}{\partial x}(x,t)\, f(x,u)\right\} \tag{4.12}$$

the value of φ for each grid node can be evaluated via time integration performed by second or higher order total variation diminishing (TVD) explicit Runge-Kutta schemes.

4.3.4. AIRCRAFT MODEL AND FLIGHT ENVELOPES

The computational load of calculating reachable sets using the level set method becomes higher with the increase of model complexity and dimensions. So it is necessary to decompose the dynamic system to alleviate the curse of dimensionality without sacrificing optimality [31]. In [8, 32–34], the full model of the aircraft is decoupled into equations of longitudinal and lateral dynamics .

Along each decoupled direction, lower-dimensional safe flight envelopes are computed. Different combinations of states lead to different shapes of safe flight envelopes, which can be stored and selected by pilots. It is important to note that aerodynamic stall is out of scope of this thesis, since the aerodynamic model of high angle of attack regime is highly nonlinear, which requires further experimental and modeling work. For the primary phase of the research, we first compute safe flight envelopes in-flight structural damage and failures, and it is assumed that the structural damage discussed in this thesis is not immediately catastrophic and is still recoverable.

Considering the infinite number of potential damage locations on an aircraft, this chapter only focuses on damage with significant controllability effects, like tip loss of wings and tails [17]. As discussed in Chapter 2 and 3, the intrinsic impact of structural damage is the change of aerodynamic characteristics of the aircraft [17, 35], which is directly reflected in the altered mathematical aerodynamic model both in its structure and parameters [36].

The model that is used in envelope computation is based on the flat-earth kinematic and moment equations in body axes and the flat-earth force equations in wind axes. The kinematic equations, which do not depend on the aerodynamic model of the aircraft, are

not influenced by structural damage [37]:

$$\begin{aligned}\dot{\phi} &= p + \tan\theta(q\sin\phi + r\cos\phi)\\ \dot{\theta} &= q\cos\phi - r\sin\phi\\ \dot{\psi} &= \frac{q\sin\phi + r\cos\phi}{\cos\theta}\end{aligned} \tag{4.13}$$

The equations of motion, on the other hand, are significantly affected by structural damage due to the change of moments and mass properties [37]:

$$\begin{aligned}\dot{p} &= (c_1 r + c_2 p)q + c_3(\frac{1}{2}\rho V^2 SbC_l) + c_4(\frac{1}{2}\rho V^2 SbC_n)\\ \dot{q} &= c_5 pr - c_6(p^2 - r^2) + c_7(\frac{1}{2}\rho V^2 S\bar{c}C_m)\\ \dot{r} &= (c_8 p + c_2 r)q + c_4(\frac{1}{2}\rho V^2 SbC_l) + c_9(\frac{1}{2}\rho V^2 SbC_n)\end{aligned} \tag{4.14}$$

where $c_1 - c_9$ are combinations of moments and cross-productions of inertia derived from the inverse of the inertia matrix [37]. The effects of structural damage on mass properties have been investigated in wind tunnel experiments [38], and it is concluded that the effects of mass property changes are not significant compared with that of aerodynamic changes induced by aerodynamic surface lose. Therefore, properties like aircraft mass, center of gravity and inertia matrix are assumed unchanged after structural damage. The wind-axis force equations transformed from body axes are [37]:

$$\begin{aligned}\dot{V} &= \frac{1}{m}\left(T\cos\alpha\cos\beta - \frac{1}{2}\rho V^2 SC_D + mg_1\right)\\ \dot{\beta} &= \frac{1}{mV}\left(-T\cos\alpha\sin\beta + \frac{1}{2}\rho V^2 SC_Y - mVr_w + mg_2\right)\\ \dot{\alpha} &= \frac{1}{mV\cos\beta}\left(-T\sin\alpha\cos\beta - \frac{1}{2}\rho V^2 SC_L + mVq_w + mg_3\right)\end{aligned} \tag{4.15}$$

where r_w and q_w are two components of rotational rates $[p_w, q_w, r_w]$ along the wind axes, which are transformed from rotational rates in body axes $[p, q, r]$ by [37]:

$$\begin{bmatrix} p_w\\ q_w\\ r_w\end{bmatrix} = \begin{bmatrix}\cos\alpha\cos\beta & \sin\beta & \sin\alpha\cos\beta\\ -\cos\alpha\sin\beta & \cos\beta & -\sin\alpha\sin\beta\\ -\sin\alpha & 0 & \cos\alpha\end{bmatrix}\begin{bmatrix} p\\ q\\ r\end{bmatrix} \tag{4.16}$$

and the components of the gravity vector are given by [37]:

$$\begin{aligned} g_1 &= g(-\cos\alpha\cos\beta\sin\theta + \sin\beta\sin\phi\cos\theta + \sin\alpha\cos\beta\cos\phi\cos\theta)\\ g_2 &= g(\cos\alpha\sin\beta\sin\theta + \cos\beta\sin\phi\cos\theta - \sin\alpha\sin\beta\cos\phi\cos\theta)\\ g_3 &= g(\sin\alpha\sin\theta + \cos\alpha\cos\phi\cos\theta)\end{aligned} \tag{4.17}$$

The aerodynamic model of the undamaged Cessna Citation aircraft is [39]:

$$
\begin{aligned}
C_D &= C_{D_0} + C_{D_\alpha}\alpha + C_{D_{\alpha^2}}\alpha^2 + C_{D_q}\frac{q\bar{c}}{2V} + C_{D_{\delta_e}}\delta_e \\
C_Y &= C_{Y_0} + C_{Y_\beta}\beta + C_{Y_p}\frac{pb}{2V} + C_{Y_r}\frac{rb}{2V} + C_{Y_{\delta_a}}\delta_a + C_{Y_{\delta_r}}\delta_r \\
C_L &= C_{L_0} + C_{L_\alpha}\alpha + C_{L_q}\frac{q\bar{c}}{2V} + C_{L_{\delta_e}}\delta_e \\
C_l &= C_{l_0} + C_{l_\beta}\beta + C_{l_p}\frac{pb}{2V} + C_{l_r}\frac{rb}{2V} + C_{l_{\delta_a}}\delta_a + C_{l_{\delta_r}}\delta_r \\
C_m &= C_{m_0} + C_{m_\alpha}\alpha + C_{m_q}\frac{q\bar{c}}{2V} + C_{m_{\delta_e}}\delta_e \\
C_n &= C_{n_0} + C_{n_\beta}\beta + C_{n_p}\frac{pb}{2V} + C_{n_r}\frac{rb}{2V} + C_{n_{\delta_a}}\delta_a + C_{n_{\delta_r}}\delta_r
\end{aligned}
\tag{4.18}
$$

The aerodynamic characteristics of a structurally damaged aircraft have been investigated through a series of flight tests [40], wind-tunnel and computational experiments [17, 35, 38, 41] conducted by NASA. In these experiments, the damage was modeled in the form of partial or complete tip loss of major aerodynamic surfaces like horizontal stabilizers, vertical tail, and wings. The experiments are conducted on a 5.5% geometrically and dynamically scaled model of a generic transport airplane, which is referred to as the Generic Transport Model (GTM) [40]. The resulting aerodynamic model of the damaged aircraft in the form of look-up tables can be found in an open-source simulation software [42]. Also, preliminary work on damage modeling of a Cessna Citation aircraft was performed in our group using digital DATCOM with various levels of vertical tail damage [24]. By analyzing these experimental data, it is observed that damage to different aerodynamic surfaces results in unique aerodynamic effects, which is reflected in the changes of different stability and control derivatives. More importantly, the changed aerodynamic coefficients can be modeled by multiplying the original value with a scaling factor. In some cases like wing damage, an incremental term as a function of flight states is added to the original model due to the induced asymmetry. Similar ways of damage modeling can be found in [43, 44], where the models of aircraft with wing damage is incorporated in the flight control design. The model of a structurally damaged Cessna Citation aircraft is built on the data and observations of aforementioned experiments.

LONGITUDINAL ENVELOPES

Under the condition of trimmed yaw and roll motion with states (p, r, ϕ, ψ, β) and their derivatives to be zero, the dynamics equation of the longitudinal motion can be written as [37]:

$$
\begin{aligned}
\dot{V} &= \frac{1}{m}\left[T\cos\alpha - \frac{1}{2}\rho V^2 S C_D - mg\sin(\theta-\alpha)\right] \\
\dot{\alpha} &= -\frac{1}{mV}\left[T\sin\alpha + \frac{1}{2}\rho V^2 S C_L - mg\cos(\theta-\alpha)\right] + q \\
\dot{\theta} &= q\cos\phi \\
\dot{q} &= \frac{1}{2}\rho V^2 S\bar{c}\frac{C_m}{I_{yy}}
\end{aligned}
\tag{4.19}
$$

By assuming constant velocity, a three-dimensional pitch envelope of (α, θ, q) can be computed based on the simplified model. Figure 4.2(a) and (b) show the safe flight envelopes computed from Eq. (4.19) under the condition of true airspeed $V_{TAS} = 100 m/s$ and load factor $n = 1$ with time horizon T = 1s. Air density ρ is assumed to be constant ρ_0 at sea level. The control inputs are thrust and elevator deflections, which are within the bounds: $T \in [4448.2, 22241]$ N, $\delta_e \in [-25, 25]$ deg. Figure 4.2(a) shows both forward and backward reachable sets, which form the safe flight envelope displayed in Fig. 4.2(b) by taking the intersection between them. When one of the horizontal tails is damaged, the dominant effect is on the longitudinal stability. If the integrity of the attached elevators are also affected, the pitch control power, i.e., the control effectiveness may reduce, and the total pitching moment coefficient after damage is modeled as:

$$C_{m_{dmg}} = (\mathbf{I} - \mathbf{D}_m)\mathbf{C}_m \tag{4.20}$$

where $\mathbf{D}_m \in \Re^{n\times n}$ is a diagonal matrix, referred to as the damage scale matrix and $\mathbf{C}_m \in \Re^{n\times 1}$ is composed of polynomial terms of the dimensionless pitching moment model. The changed values of aerodynamic coefficients under a pre-defined damage case are determined based on data from a series of wind tunnel tests [17, 38] as well as computational simulations [24]. The tests are conducted on sub-scale aircraft models with partial or total loss of wings, horizontal stabilizers, and vertical tail. The values of stability derivatives under different damage cases are recorded during the tests. By analyzing these test data, the damage scale matrix $\mathbf{D}$ can be determined, which quantifies the effects of damage on aerodynamic characteristics. Therefore, different values of $\mathbf{D}$ can be used to represent different damage/failure combinations. More details on the modeling work can be found in Chapter 2.

According to the Cessna Citation model in [39], $\mathbf{C}_m = \left[C_{m_0}, C_{m_\alpha}\alpha, C_{m_q}\frac{q\bar{c}}{2V}, C_{m_{\delta_e}}\delta_e\right]^T$, and the damage scale matrix $\mathbf{D}_m = diag(d_{m_1}, d_{m_2}, d_{m_3}, d_{m_4})$ can be identified from experimental data. Figure 4.2(c) and (d) show how the envelopes reduce with 30% tip loss of one horizontal stabilizer ($\mathbf{D}_m = diag(0.3, 0.3, 0.3, 0.2)$).

The decoupled longitudinal equation is valid under the condition of trimmed yaw and roll motion. In case of asymmetric stabilizer and elevator damage, however, an incremental rolling moment is generated. Therefore, it is assumed that rudder and ailerons are capable of re-trimming the aircraft. The continuous re-trimming process is assumed to be automatically accomplished by the onboard fault tolerant controller so that a large amount of time spent on manual control can be saved.

The 2D contours in Fig. 4.3 are "slices" taken from 3D figures in Fig. 4.2 by setting the third state as fixed value. The main purpose of showing these 2D figures is to clearly demonstrate how each state changes after damage, and the values of envelope boundaries. Among all the values within the range of each state, some values result in empty contours, which indicate conditions that are not part of the whole envelope. The values of non-empty contours are selected as conditions for clarity of presentation.

Some envelopes are not completely represented, because part of the computed reachable sets exceed the computation range, which is defined by the physical limits of the aircraft. Data points beyond this range no longer have physical meanings in protecting the aircraft. Hence, the incomplete envelopes shown in Figs. 4.3 and 4.5 are results of intersection between the computed reachable sets and the computation range.

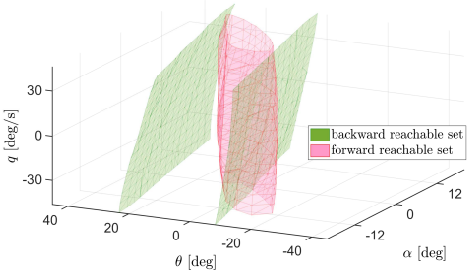

(a) Forward and backward reachable sets without damage

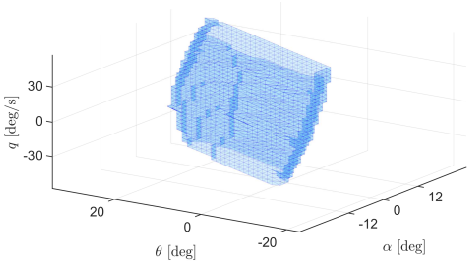

(b) Safe flight envelope without damage

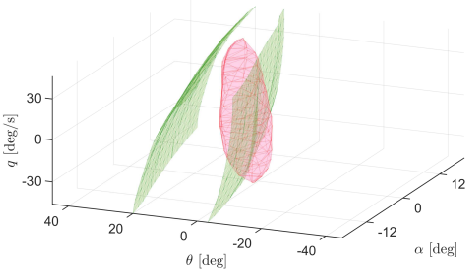

(c) Forward and backward reachable sets with damage

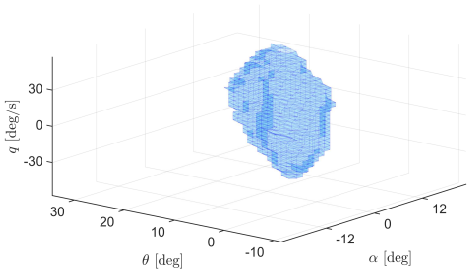

(d) Safe flight envelope with damage

Figure 4.2: Comparison of (α, θ, q) envelopes under 30% horizontal stabilizer damage

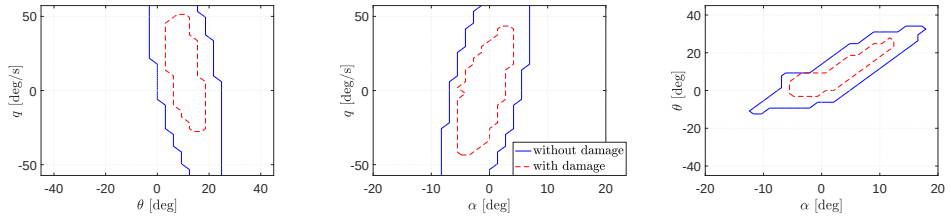

(a) (b) (c)

Figure 4.3: 2D-projected (α, θ, q) envelopes with and without 30% horizontal stabilizer damage ((a) $\alpha = 5°$, (b) $\theta = 2°$, (c) $q = 2°/s$)

LATERAL ENVELOPES

The lateral/directional motion of aircraft with zero pitch rate $q = 0$ is defined as [37]:

$$\begin{aligned}
\dot{\beta} &= p\sin\alpha - r\cos\alpha + \frac{1}{mV}\left(-T\cos\alpha\sin\beta + \frac{1}{2}\rho V^2 S C_Y + mg\sin\phi\right) \\
\dot{r} &= \frac{1}{2(J_{xx}J_{zz} - J_{zx}^2)}\rho V^2 Sb(J_{zx}C_l + J_{xx}C_n) \\
\dot{p} &= \frac{1}{2(J_{xx}J_{zz} - J_{zx}^2)}\rho V^2 Sb(J_{zz}C_l + J_{zx}C_n) \\
\dot{\phi} &= p + r\tan\theta\cos\phi
\end{aligned} \tag{4.21}$$

The rolling envelopes are mostly influenced by the integrity of wings and the attached ailerons. To compute a rolling envelope with states (β, p, ϕ) on the assumption of zero yaw rate ($\dot{r} = r = 0$), the rudder is assumed to function as normal within the bound of $\delta_r \in [-22, 22]$ deg, in order to maintain a steady heading sideslip maneuver. The deflections of aileron are set within the bound: $\delta_a \in [-33, 33]$ deg. The two reachable sets and the resulting safe flight envelope in normal condition are illustrated in Fig. 4.4(a) and (b) respectively. If one side of the wing is damaged, unequal lift forces are induced, generating an incremental rolling moment ΔC_l that increases with α in the angle of attack range in which the aerodynamic characteristics are linear. The corresponding rolling moment increases with α, assuming constant dynamic pressure.

Besides, available roll control power is reduced due to structural damage of ailerons as well as the fact that part of the aileron control is used to compensate for roll asymmetry. Therefore, the non-dimensional coefficient of rolling moment $C_{l_{dmg}}$ after damage is composed of two parts: one is formed by the original vector of lateral aerodynamic terms $\mathbf{C}_l$ scaled by the rolling damage scale matrix $\mathbf{D}_l$; and the other one is the incremental term, which is:

$$C_{l_{dmg}} = (\mathbf{I} - \mathbf{D}_l)\,\mathbf{C}_l + \Delta C_{l_\alpha}\,\alpha \tag{4.22}$$

where $\Delta C_{l_\alpha}\,\alpha$ denotes the incremental rolling moment non dimensional coefficient due to asymmetric wing damage. According to the Cessna Citation model used in [39], the vector of the lateral aerodynamic terms is $\mathbf{C}_l = \left[C_{l_0}, C_{l_\beta}\beta, C_{l_p}\frac{pb}{2V}, C_{l_r}\frac{rb}{2V}, C_{l_{\delta_a}}\delta_a, C_{l_{\delta_r}}\delta_r\right]^T$. Under 20% wing tip loss, the diagonal damage scale matrix for rolling moment is $\mathbf{D}_l = diag(0.1, 0.1, 0.1, 0.1, 0.4, 0)$ and the incremental coefficient $\Delta C_{l_\alpha} = 0.02\,\text{rad}^{-1}$, which are derived from wind tunnel tests [17].

4.4. INFORMATION RETRIEVAL AND INTERPOLATION

4.4.1. DATA STORAGE AND RETRIEVAL

Based on the computed safe flight envelopes, a database containing offline calculated envelopes under different fault and damage scenarios can be designed and established. Table 4.2 shows the main attributes that should be included in the database as well as in the right side of the ER diagram. The table shows how much information needs to be specified in order to retrieve an envelope. It should be noted that for each attribute, only a few example values are listed in Table 4.2 as an indication. The first three columns in Table 4.2 describe the damage cases defined by the damage modeling experiments,

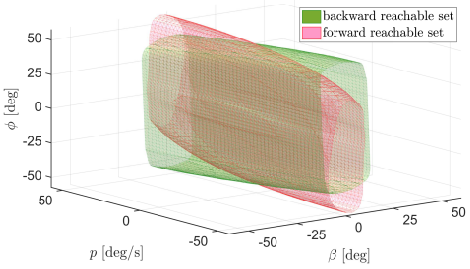

(a) Forward and backward reachable sets without damage

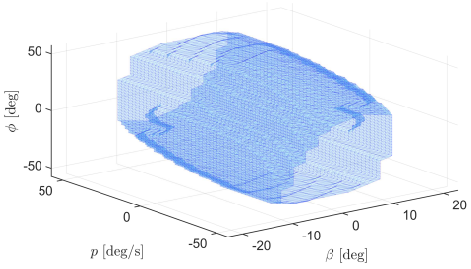

(b) Safe flight envelope without damage

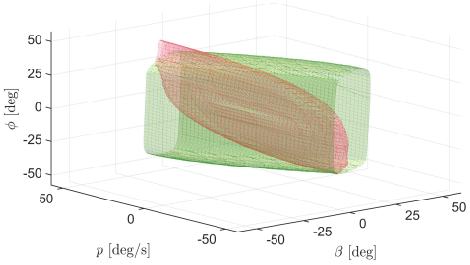

(c) Forward and backward reachable sets with damage

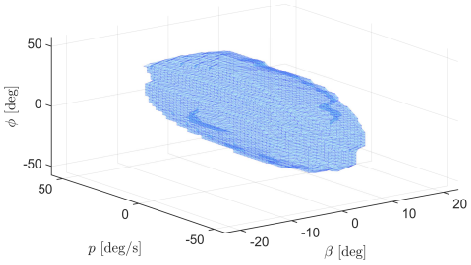

(d) Safe flight envelope with damage

Figure 4.4: Comparison of (β, p, ϕ) envelopes with and without 20% wing damage

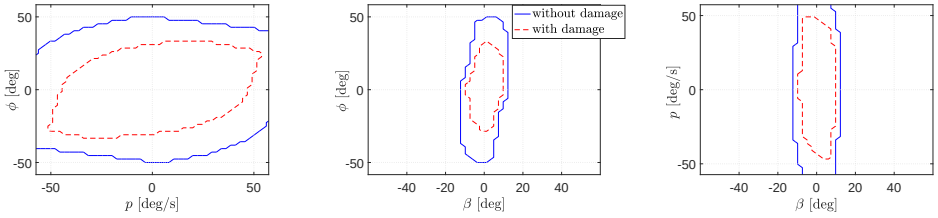

(a) (b) (c)

Figure 4.5: 2D projected (β, p, ϕ) envelopes with and without 20% wing damage ((a) $\beta = 0°$, (b) $p = 6°/s$, (c) $\phi = 0°$)

and the corresponding aircraft models are used to compute the safe flight envelopes. The following four columns indicate the time span and flight states under which the retrieved flight envelope is valid.

An unique flight envelope $E_{(e_1,e_2,...,e_r)}$ in the last column is determined by attributes in the database, where $(e_1, e_2, ..., e_r)$ denote the variables of attributes in the database. For example, e_1, e_2, e_3 describe the current fault and damage by its location, type and severity. Based on this, several flight envelopes can be retrieved under different flight conditions (e.g., time horizon, pressure altitude) defined by $e_4, e_5, ..., e_r$, among which

only one envelope will be retrieved if values of these attributes can be determined.

Table 4.2: Preliminary Design of Safe Flight Envelope Database

Location	Type	Severity	Time [s]	Model	True Air-speed [m/s]	Pressure Altitude [m]	Envelope
right horizontal stabilizer	tip loss	30%	1	(α, q, θ)	80	sea level	$E_{(e_1,\dots e_r)}$
	tip loss	50%	2	(α, q, θ)	90	5000	$E_{(e_1,\dots e_r)}$
right elevator	stuck	15°	1	(α, q, θ)	100	10000	$E_{(e_1,\dots e_r)}$
	tip loss	30%	2	(α, q, θ)	110	5000	$E_{(e_1,\dots e_r)}$
left wing	tip loss	40%	1	(β, p, ϕ)	120	sea level	$E_{(e_1,\dots e_r)}$
	tip loss	60%	2	(β, p, ϕ)	130	5000	$E_{(e_1,\dots e_r)}$
vertical tail	tip loss	20%	1	(β, r, ψ)	90	10000	$E_{(e_1,\dots e_r)}$
	tip loss	40%	2	(β, r, ψ)	100	5000	$E_{(e_1,\dots e_r)}$

The safe flight envelope can be considered as a set-valued result of an optimal-control based reachability problem. The resulting reachable set is represented as the zero-level set of an implicit surface function φ, i.e., a set of points where $\varphi = 0$. Without an explicit analytic expression, the surface function is approximated by values in grid points, which are propagated from an initial set in a certain velocity field. Therefore, the envelope can be regarded as a closed lower-dimensional interface that divides the state space into interior and exterior regions [12]. For a certain point $P(i, j)$, the sign of its value function $\varphi_{i,j}$ determines which side of the interface the point is on. That is, $P(i, j)$ is inside the interfaces when $\varphi_{i,j} < 0$ and outside when $\varphi_{i,j} > 0$. If $P(i, j)$ and its neighboring grid points satisfy [45]:

$$\max(\varphi_{i,j}, \varphi_{i+1,j}, \varphi_{i,j+1}, \varphi_{i+1,j+1}) < 0 \qquad \text{OR} \qquad \min(\varphi_{i,j}, \varphi_{i+1,j}, \varphi_{i,j+1}, \varphi_{i+1,j+1}) > 0 \tag{4.23}$$

it means that $P(i, j)$ is guaranteed to be inside or outside the interface. Such points are ignored and the rest of the grid points are regarded to lie on or in the vicinity of the interface. In this way, a narrow band around the interface is formed by the points that approximate the boundary.

Envelopes stored as grid points can be readily used for further calculation, but may suffer from bad scaling with the dimension. Therefore, it is also important to design the number of data points for each attribute so that the database can provide as much information as possible while keeping a reasonable data volume for onboard devices.

4.4.2. FLIGHT ENVELOPE INTERPOLATION

In real applications, safety should be included as the primary consideration. Since the finite number of safe flight envelopes in the database is in accordance with the number

of abnormal cases and discrete flight states, there are inevitably situations where the true flight envelope falls in between the two neighboring categories in the database. In this case, it is necessary to interpolate between two envelopes to fill in the gaps in Table. 4.2 and obtain more accurate results [39].

Interpolation that is commonly used in look-up tables mostly works with two points. However, in this application, interpolation needs to be done between two envelopes based on certain connections. It can be observed that the safe flight envelopes of different damage severity or flight conditions often share similar geometrical shapes with different scales of expanding, shrinking or shifting. Since flight envelopes can be considered as contours and surfaces, the method used for interpolation in this thesis is inspired by research on surface reconstruction and image matching using the level set method and the fast marching method [46–49]. The basic idea of these methods is to build up the geometrical features of contours and surfaces and track the propagation of their fronts made up of data points.

For two envelopes composed of two sets of data points, the mapping is implemented pair-wisely through the optimal path between each two points calculated by the fast marching method. For simplicity and a proof of concept, only two-dimensional envelopes are investigated in this chapter, since a three-dimensional envelope can be projected into a $2D$ plane. The extension to higher-dimensional hyper-surfaces will be included in future work.

Generally, given two points in $\Re^n$, the path in between can be defined by a vector-valued function $\gamma(\tau) : [0,\infty) \rightarrow \Re^n$, i.e., each dimension of $\gamma(\tau)$ is defined by a separate function parameterized by τ. If τ is the arclength parameterization of γ, then it has the property of $||\frac{d\gamma(\tau)}{d\tau}||_2 = 1$.

In two dimensions, given a cost function $F(x,y)$, one goal in optimal path planning is to construct the path between (x_0,y_0) and (x,y) that minimizes the cost of travel between these two points. Let $T(x,y)$ be the minimal cost, which is:

$$T(x,y) = \min_{\gamma} \int_{(x_0,y_0)=\gamma(0)}^{(x,y)=\gamma(L)} F(\gamma(\tau))d\tau \tag{4.24}$$

where L is the total arclength of path. The level set $T(x,y) = c$ is the set of all points that can be reached from (x_0,y_0) with minimal cost c, and the minimal cost paths are orthogonal to the level curves. Hence,

$$||\nabla T||_2 = F(x,y) \cdot ||\frac{d\gamma(\tau)}{d\tau}||_2 = F(x,y) \tag{4.25}$$

which forms an Eikonal equation [50]. The equation can be interpreted in another way. Imagine a wave front expanding from the starting point (x_0,y_0) with unit speed $F = 1$ until it reaches the end point (x,y). Then the solution $T(x,y)$ is the distance to the starting point, and the level curve of $T(x,y) = c$ denotes the wave front that is located a distance c away. The gradient $||\nabla T||_2$ must be orthogonal to these level curves, implying that the path followed by the wave is the shortest path in time. If the end point is not specified and we let the wave propagate through the entire grid, then each grid point should have a value of optimal distance from the starting point, and these values form a distance map of the grid.

The fast marching method provides a numerical scheme for computing solutions to the Eikonal equation based on entropy-satisfying upwind schemes and fast sorting techniques [50]. Readers can refer to Refs. [47, 50] for more details. In this thesis, the single starting point A is extended to a set of starting points located on the boundary of one retrieved envelope E_0. For each grid point (x, y), $T(x, y)$ is computed, which denotes the shortest travel distance from point (x, y) to its nearest starting point. The values of $T(x, y)$ thus formulate a distance map, which is stored and retrieved together with its envelope E_0 correspondingly. The size of distance should be designed to cover the largest envelope in the database so that for any envelope E_1, the shortest path can be constructed for points on the boundary through tracing along the smallest value of $T(x, y)$ until one of the points on E_0 is reached.

Once optimal path planing is repeated for each point on E_1, linear interpolation can be implemented on each optimal path between data points of the two envelopes. It is assumed that points forming the interpolated contour also lie on the optimal path, and their specific locations along the path are determined by the interpolation weights. These weights are heuristically chosen based on different conditions in which the envelopes are computed.

In Fig. 4.6, the lateral envelopes under wing damage are used as the first example for demonstration. Figure. 4.6(a) shows three 2D envelopes in (p, ϕ) computed by the level set method. The largest contour is computed without any damage and the smallest one is computed with 20% wing tip loss. The contour in between them corresponds to the envelope of 10% tip loss, which is used and displayed to test the performance of the interpolation with the method proposed in this section. The retrieved envelopes of zero damage and 20% damage are approximated by data points (fig. 4.6(b)) based on Eq. (4.23). Then, optimal paths between the points on the largest and the smallest contour are computed, which are represented in yellow dashed lines in fig. 4.6(b). After the mapping is built between two envelopes, linear interpolation is performed to find the points on the optimal path that approximate the intermediate envelope, which is shown in 4.6(b). It can be observed in fig. 4.6(c) that the interpolated contour accurately approximates the envelope of 10% wing damage computed by the level set method.

Damage level is not the only decisive factor in the database. Some other attributes, like true airspeed, pressure altitude and time horizon are also important in building the database. As shown in Table. 4.2, the value of these attributes are also discrete, which means that interpolation is necessary when specific values of certain states are required. The second example demonstrated in Fig. 4.7 deals with envelopes of different velocities. Figure. 4.7(a) shows three 2D envelopes in (β, r) computed by the level set method. The inner and outer envelopes correspond to $V_{TAS} = 60m/s$ and $V_{TAS} = 100m/s$ respectively. The task is to find out the contour of $V_{TAS} = 80m/s$ by interpolating between the two known contours. Following the similar steps of the fast marching method used in the first example, the intermediate contour is found, which approximates the contour computed by the level set method with satisfying accuracy, as shown in Fig. 4.7(c).

The performance of interpolation can be influenced by the geometric characteristics of the envelopes/contours. It is noticed in the figures that each established path starts from one point on the outer contour and traces back to one of the inner contour along the distance map. Since the distance map is computed based on the inner contour, each

"wave front" that propagates from each point on the inner contour may reach more than one point on the outer contour. In this way, not all of the inner points are connected to the outer contour since multiple paths may end up in the same inner point. This may result in some areas with concentrated paths and others with sparse paths. Such inconsistency gives rise to the accumulation of error, especially around the corners of the shape. It is also important to note that there is no direct relation between the computation of optimal path γ and the dynamics models of the aircraft, since the establishment of F and T of the fast marching method treats flight envelopes as ordinary geometric shapes.

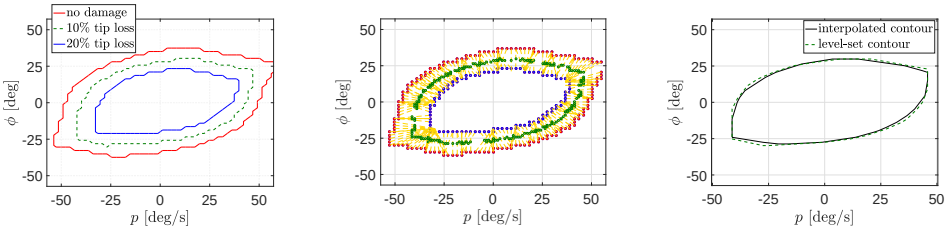

(a) Two-dimensional (p,ϕ) envelopes computed by the level set method

(b) Computed optimal paths and the resulting interpolated contour

(c) Comparison between the interpolated contour and the true contour of 10% wing damage

Figure 4.6: Interpolation between envelopes of different damage levels based on the fast marching method

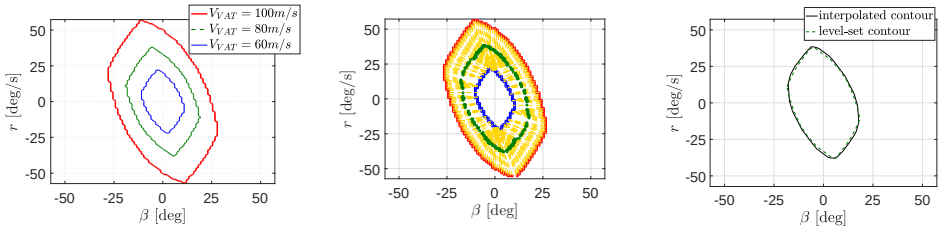

(a) Two-dimensional (β,r) envelopes computed by the level set method

(b) Computed optimal paths and the resulting interpolated contour

(c) Comparison between the interpolated contour and the true contour of $V = 80m/s$

Figure 4.7: Interpolation between envelopes of different velocities based on the fast marching method

4.4.3. INTERPOLATION ACCURACY

As mentioned earlier, the interpolation of flight envelopes in our research is initiated by a safety-related problem [39]. Take structural damage for example, it is desired to have more damage levels so that more accurate safe flight envelopes can be predicted. On the other hand, the number of designed damage levels is restricted by physical limitations of modeling experiments like wind-tunnel tests and simulations. Additionally, volume limitations on the database also exist if it needs to be carried onboard. Therefore, in order to obtain a better design of the database, it is important to determine the num-

ber of envelopes needed for each damage location by evaluating the performance of the interpolation under different database configurations.

Given two envelopes, one is interpolated from two neighboring envelopes retrieved from the database, and the other envelope for comparison is directly computed from the level set method. The interpolation error is calculated point-wise between the interpolated envelope and the compared envelope. For any point (x_i, y_i) on a 2D interpolated envelope, the error between (x_i, y_i) and any point (x_j, y_j) on the compared envelope is calculated by:

$$err(i,j) = \frac{\sqrt{(x_i - x_j)^2 + (y_i - y_j)^2}}{\sqrt{x_j^2 + y_j^2}} \tag{4.26}$$

Among all the $err(i,j)$, the point that gives the smallest $err(i,j)$ is regarded as the nearest point to (x_i, y_i) on the compared envelope, and this smallest error is defined as the error of point (x_i, y_i) on the interpolated envelope, which is: $err(i) = \min_j\{err(i,j)\}$. The calculated errors for each point on the interpolated envelope form a data set $\{err(i)\}$ that represents its interpolation error set. The interpolation errors of certain damage cases are evaluated on four database configurations.

In this thesis, the interpolation errors are evaluated on four database configurations based on the number of damage cases, as shown in Fig. 4.8(a). Between the damage scale of 0% and 60% tip loss, the number of stored envelopes can be reduced by enlarging the interval between two stored envelopes. In Fig. 4.8(a), four databases (denoted as DB-1 to DB-4 in the figure) are designed to store different numbers of envelopes. The notations E0 to E6 in the figure represent envelopes of different damage scales ranging from no damage (0%) to 60% tip loss for each damage location.

Based on these four configurations, the envelope interpolation errors of 25% and 45% wing tip loss calculated by Eq. 4.26 are shown in the box chart in Fig. 4.8(b). Significant increase of variance and outliers (denoted by cross mark) is observed in database 4 with the maximum scale interval. The interpolations on DB-1 and DB-2 show similar results in both cases, which indicates that the design with 4 damage levels (DB-2) is sufficient for obtaining accurate safe flight envelopes through interpolation. In this way, a lot of storage space can be saved, and the accuracy can be guaranteed at the same time.

4.5. COMPLEXITY ANALYSIS

In order to prove the feasibility of online application of the database approach, it is necessary to compare its computational complexity with that of the level set method. *Computational complexity theory* is concerned with how much computational resources in terms of time and space are required to solve a given task [51]. In this research, the complexity analysis is focused on the time complexity, or computational efficiency of the algorithm. The efficiency of an algorithm is quantified by the number of basic operations as a function of input size [51]. Basic operations, also called primitive operations, correspond to low-level instructions (e.g., addition, multiplication) with constant execution time. Thus, the actual running time of an algorithm is expected to be proportional to the number of primitive operations [52].

(a) Four databases with different number of envelopes stored

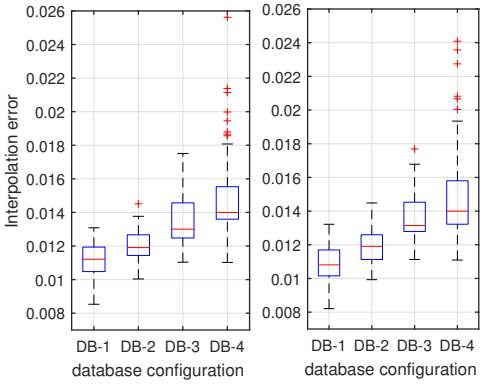

(b) The interpolation error of 25% wing tip loss (left) and 45% wing tip loss (right) evaluated on different database configurations

Figure 4.8: Database design of envelope numbers based on interpolation error

4.5.1. ANALYSIS OF THE LEVEL SET METHOD

For a given computational grid of d dimensions with equal resolution of n for each dimension, it takes at least $N(n,d) = K_{ls}(d) \cdot n^{d+1}$ primitive operations to compute a reachable set using the level set method, where $K_{ls}(d)$ denotes the number of primitive operations required for each grid point ("ls" represents "level set"). It should be noted that the increase of dimension d means that more complex system models might be used with an increased number of flight states as well as control inputs. If nonlinear programming is required to compute optimal control inputs, the complexity will grow significantly compared with the simple linear cases. Therefore, $K_{ls}(d)$ is an implicit, monotonically increasing function of dimension d, which may increase with more state equations of a higher-dimensional system model as well as with the complexity of the optimal controller.

The implementation of the level set method can be divided into five parts. Since it evolves solving for an ODE, the calculation is repeated for every time step. We first need to count the number of primitive operations for each time step. For a given grid of d dimensions with the same resolution of n for each dimension, the number of primitive operation can be roughly calculated.

1. If K_1 denotes the number of primitive operations of calculating the spatial derivatives $p_i = \frac{\partial \varphi_i}{\partial x_i}$ for each dimension i [12], the total number of operations for the

entire grid at each time step should be $d\,K_1\,n^d$.

2. Calculating the analytic Hamilton-Jacobi (HJ) functions $H(x,p) = \min_u F(p,x,u)$ needs $K_2 \cdot n^d$ primitive operations. The function to be minimized is defined as [8]:

$$F(p,x,u) = \sum_{i=1}^{d} p_i\, f_i(x,u) \tag{4.27}$$

where $f(x,u)$ is the aircraft system model and u is the control input. For each grid point with given values of x and p, K_2 largely depends on the optimization of $F(u)$ using optimal control input u, which is determined by $\frac{dF(u)}{du}$. For linear function where $\frac{dF(u)}{du}$ = constant, the control input is either maximum or minimum value (bang-bang solution in optimal control). For nonlinear function where $\frac{dF(u)}{du} = h(u)$, and $h(u)$ can be polynomial or trigonometric functions. In this case, nonlinear programming methods need to be taken to find the optimal value and the corresponding control inputs, which will significantly increase the computational load of the method.

3. The numerical approximation of HJ function with dissipation coefficients α using Lax-Friedrichs scheme is [12, 30]:

$$\hat{H}(x,p) = H(x,p) - \alpha(x) \tag{4.28}$$

The calculation of Lax-Friedrichs needs $(3+K_3)\cdot n^d$ primitive operations, where $K_3 = \sum_{i=1}^{d} K_{3_i}$ denotes the total number of steps taken to evaluate the dissipation coefficients α at each grid point. For each dimension i, K_{3_i} steps are required to determine $\alpha_i = \max_u |\frac{\partial H}{\partial p_i}|$ [30], which also depends on the relation between system states and control inputs.

4. Calculating the step bound for CFL condition of integration takes in the value of the calculated dissipation coefficient in [12]:

$$\Delta t_{max} = \frac{1}{\max_x(\sum_{i=1}^{d} \frac{\alpha_i(x)}{\Delta x_i})} \tag{4.29}$$

Therefore, the determination of time step requires $3d \cdot n^d$ primitive operations in total.

5. For each time step, the above calculation of $\hat{H}(x,p)$ is repeated for each grid point as the right hand side of the ordinary differential equation [12]:

$$\frac{d\varphi(x)}{dt} = -\hat{H} \tag{4.30}$$

The number of operations required to solve this ODE is K_4, which depends on the integration scheme. Take Euler method for example:

$$\varphi(t+\Delta t) = \varphi(t) - \Delta\hat{H} \tag{4.31}$$

where $K_4 = 5$ for each grid point. As stated before, the length of time step Δt is bounded by CFL condition $\Delta t \leq \frac{\Delta x}{\max|V|}$, where V denotes the external velocity that drives the propagation of the implicit surfaces. Hence, the total number of time steps can be calculated as:

$$N_t = \frac{T}{\Delta t} \geq \frac{T \cdot \max(|V|)}{\min_i \Delta x_i} = \frac{T \cdot \frac{\sqrt{\Sigma_{i=1}^{d} X_i^2}}{T}}{\frac{\min_i X_i}{n}} = \frac{\sqrt{\Sigma_{i=1}^{d} X_i^2}}{\min_i X_i} \cdot n \tag{4.32}$$

where T denotes the time horizon and X is the range of each dimension. Following the discussion above, the total number of primitive operations required to implement the level set method is $N(n,d) = (d \cdot K_1 + K_2 + K_3 + K_4 + 3\,d)\, n^d\, N_t = K_{ls}(d)\, n^d\, N_t$. Since $N_t > n$, the lower bound of $N(n,d)$ is $K_{ls}(d)\, n^{d+1}$.

4

4.5.2. COMPARISONS WITH THE DATABASE APPROACH

If the envelope is retrieved from the database instead of computed, the time complexity is not dependent on n or d but only the structure of the database, which is trivial compared to the level set method. When interpolation between two retrieved envelopes is required, instead of computing to the entire grid like the level set method, only a subset of points on the envelope boundary are needed. We first consider the simplest two-dimensional case, in which the interpolation between two envelopes, E_1 and E_2, requires $N(n) = M(n) \cdot N_{in}(n)$ primitive operations. $M(n) = \lambda \cdot n$ denotes the number of points on the boundary of E_1, which is proportional to the input size n with a scale factor λ. For each point on the boundary of E_1, the computation of the optimal path between two contours based on the offline generated distance map of E_2, requires $N_{in}(n) = K_{in} \cdot n$ primitive operations with $K_{in} < 1$ ("in" indicates "interpolation"). Therefore, the total number of primitive operation is $N(n) = K_{in} \cdot \lambda n^2$. Since a 3D envelope can be decomposed into slices of 2D envelopes, the total number of primitive operations can be approximated by:

$$N(n) = \sum_{i=1}^{n} K_{in}(i) \cdot \lambda(i)\, n^2 \leq n^3 \cdot \max_i K_{in}(i) \cdot \max_i \lambda(i) \tag{4.33}$$

where i is the index to the grid point of the third dimension. Based on this, the interpolation between higher dimensional envelopes approximately requires $N(n,d) = K_{in} \cdot \lambda\, n^d$ primitive operations by decomposing them into lower-dimensional envelopes, where $K_{in} \cdot \lambda$ is the average value over the whole grid.

For example, to obtain a yawing envelope of vertical tail damage with two states (β, r) (as shown in Fig. 4.7), the level set method takes approximately $3 \cdot 10^8$ ($K_{ls} = 307$) primitive operations on a 100×100 two-dimensional grid, whereas the database approach only needs 7695 ($K_{in} = 0.27$, $\lambda = 2.85$) primitive operations by interpolating between two envelopes retrieved from the database with the same grid resolution and dimension. Based on this aircraft model, Fig. 4.9(a) shows the number of primitive operations $N(n)$ of using interpolation and the level set method with respect to grid resolution ($n \in [10, 100]$, $d = 2$). The figure also shows the plot of n^2 and n^3 for comparison. It can be clearly seen that the database approach using interpolation method requires much less computation

load compared with the level set method. To make a more straightforward comparison of both methods in terms of dimension, the speedup ratio of the database approach is thus defined as:

$$S_{db}(n,d) = \frac{K_{ls}(d)\cdot n^{d+1}}{K_{in}\cdot\lambda\, n^{d}} = \frac{K_{ls}(d)}{K_{in}\cdot\lambda}\cdot n \tag{4.34}$$

The influence of dimension is mostly on the computation of the level set method described by $K_{ls}(d)$. Based on different models of 2, 3, and 4 dimensions respectively, the results of the speedup ratio for different d and n are displayed in Fig. 4.9(b). It can be observed that the speedup ratio grows significantly when the dimension reaches 4, indicating that the level set method becomes significantly more complex compared with the database approach. This is largely due to the increased complexity of solving a higher-order optimal control problem, which results in the non-linearity of $K_{ls}(d)$. Despite the high speedup ratio with dimension 4, it indicates the results in relatively simple cases where nonlinear programming is not involved during the computation. Therefore, The results shown in Fig. 4.9(b) should be interpreted as a lower bound to the speedup ratio of the database method. For more complex case where nonlinear programming is needed, the complexity of the level set method will increase as well as the speedup ratio. The computation of envelopes of such models with dimensions higher than 4 is out of the scope of this research, but we will look into it in future work.

A key advantage of the database approach is that the required computational load does not depend on the complexity of aircraft system model, which makes it a method that covers a wider spectrum of cases and models. It should be noted that the level set method is not the only way to compute reachable sets and flight envelopes, and the scope of this method is limited. For example, when models of over-actuated aircraft with highly-redundant control effectors are involved [53], the level set method is incapable of computing the flight envelopes since there's no analytic solutions to optimal control inputs. Instead, other theoretical and practical methods have been proposed and utilized for envelope computation of this kind of model. However, these methods also have high computational complexity that increase with the dimension [54], which can not be used online. Therefore, a database is always needed no matter what method is used offline to compute the safe flight envelopes.

This important feature also guarantees that when the aircraft model is changed due to faults and damage (within the range of the database), the running time of retrieving a different envelope remains unchanged, while the time taken to compute a new envelope using the level set method (if it is possible) increases significantly due to the changed model of the damaged aircraft.

REFERENCES

[1] N. Govindarajan, *An Optimal Control Approach for Estimating Aircraft Command Margins*, Ph.D. thesis, Delft University of Technology (2012).

[2] L. Tang, M. Roemer, J. Ge, J. Prasad, and C. Belcastro, *Methodologies for Adaptive Flight Envelope Estimation and Protection,* in *AIAA Guidance, Navigation and Control Conference* (2009).

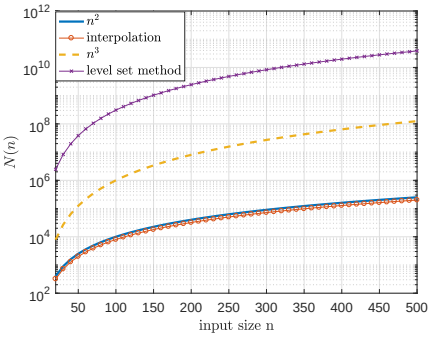

(a) The increase of primitive operations with different n on a two-dimensional grid

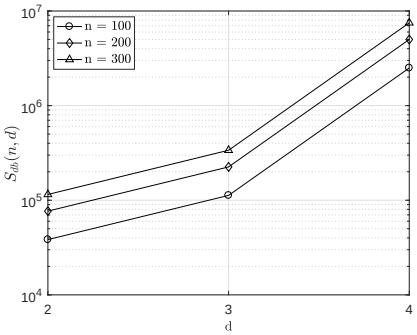

(b) The increase of speedup ratio with different model dimensions

Figure 4.9: Comparisons of the time complexity between the database interpolation approach and the level set method

[3] C. M. Belcastro, *Validation and Verification of Future Integrated Safety-critical Systems Operating Under Off-nominal Conditions,* in *AIAA Guidance, Navigation, and Control Conference* (2010).

[4] H. G. Kwatny, J.-E. T. Dongmo, B.-C. Chang, G. Bajpai, M. Yasar, and C. M. Belcastro, *Aircraft Accident Prevention : Loss-of-Control Analysis,* in *AIAA Guidance Navigation and Control Conference* (2009).

[5] H. G. Kwatny, J.-E. T. Dongmo, R. C. Allen, B.-C. Chang, and G. Bajpai, *Loss-of-Control: Perspectives on Flight Dynamics and Control of Impaired Aircraft,* in *AIAA Guidance, Navigation, and Control Conference* (2010).

[6] H. G. Kwatny, J.-E. T. Dongmo, B.-C. Chang, G. Bajpai, M. Yasar, and C. M. Belcastro, *Nonlinear Analysis of Aircraft Loss of Control,* Journal of Guidance, Control, and Dynamics **36**, 149 (2013).

[7] K. McDonough and I. Kolmanovsky, *Fast Computable Recoverable Sets and Their Use for Aircraft Loss-of-Control Handling,* Journal of Guidance, Control, and Dynamics **40**, 934 (2017).

[8] J. Lygeros, *On Reachability and Minimum Cost Optimal Control,* Automatica **40**, 917 (2004).

[9] E. R. Van Oort, *Adaptive Backstepping Control And Safety Analysis For Modern Fighter Aircraft*, Ph.D. thesis (2011).

[10] T. J. J. Lombaerts, S. Schuet, D. Acosta, J. Kaneshige, K. Shish, and L. Martin, *Piloted Simulator Evaluation of Safe Flight Envelope Display Indicators for Loss of Control Avoidance,* Journal of Guidance, Control, and Dynamics **40**, 948 (2016).

[11] I. M. Mitchell, A. M. Bayen, and C. J. Tomlin, *A time-dependent Hamilton-Jacobi Formulation of Reachable Sets for Continuous Dynamic Games,* IEEE Transactions on Automatic Control **50**, 947 (2005).

[12] R. Fedkiw and S. Osher, *Level Set Methods and Dynamic Implicit Surfaces* (Springer, 2003).

[13] J. Chongvisal and D. Talleur, *Loss-of-control Prediction and Prevention for NASA's Transport Class Model,* in *AIAA Guidance, Navigation, and Control Conference*, AIAA Paper 2014-0784 (2014).

[14] E. M. Atkins, I. A. Portillo, and M. J. Strube, *Emergency Flight Planning Applied to Total Loss of Thrust,* Journal of Aircraft **43**, 1205 (2006).

[15] C. M. Belcastro, *Validation of Safety-Critical Systems for Aircraft Loss-of-Control Prevention and Recovery,* in *AIAA Guidance Navigation and Control Conference* (2012).

[16] F. J. V. Belcastro, Christine M., *Aircraft Loss-of-Control Accident Analysis,* in *AIAA Guidance, Navigation and Control Conference* (2010).

[17] G. Shah, *Aerodynamic Effects and Modeling of Damage to Transport Aircraft,* AIAA Guidance, Navigation and Control Conference and Exhibit (2008).

[18] S. Kaynama, I. M. Mitchell, M. Oishi, and G. A. Dumont, *Scalable safety-preserving robust control synthesis for continuous-time linear systems,* IEEE Transactions on Automatic Control **60**, 3065 (2015).

[19] J. H. Gillula, G. M. Hoffmann, Haomiao Huang, M. P. Vitus, and C. Tomlin, *Applications of Hybrid Reachability Analysis to Robotic Aerial Vehicles,* The International Journal of Robotics Research **30**, 335 (2011).

[20] M. Althoff and B. H. Krogh, *Reachability analysis of nonlinear differential-algebraic systems,* IEEE Transactions on Automatic Control **59**, 371 (2014).

[21] J. Lygeros, C. J. Tomlin, and S. Sastry, *Controllers for Reachability Specifications for Hybrid Systems,* Automatica **35**, 349 (1999).

[22] C. J. Tomlin, J. Lygeros, and S. Sastry, *A Game Theoretic Approach to Controller Design for Hybrid Systems,* Proceedings of the IEEE **88** (2000), 10.1109/5.871303.

[23] M. Oishi, I. M. Mitchell, C. Tomlin, and P. Saint-Pierre, *Computing Viable Sets and Reachable Sets to Design Feedback Linearizing Control Laws Under Saturation,* in *Proceedings of the 45th IEEE Conference on Decision and Control* (2006) pp. 3801–3807.

[24] H. N. Nabi, T. J. J. Lombaerts, Y. Zhang, E. van Kampen, Q. P. Chu, and C. C. de Visser, *Effects of Structural Failure on the Safe Flight Envelope of Aircraft,* Journal of Guidance, Control, and Dynamics **41**, 1257 (2018).

[25] I. M. Mitchell, *Comparing Forward and Backward Reachability as Tools for Safety Analysis,* in *Hybrid systems: computation and control*, edited by A. Bemporad, A. Bicchi, and G. Buttazzo (Springer Berlin Heidelberg, 2007) pp. 428–443.

[26] N. Meuleau, C. Plaunt, D. E. Smith, and T. Smith, *An Emergency Landing Planner for Damaged Aircraft,* Artificial Intelligence **1000**, 114 (2009).

[27] G. Yi, J. Zhong, E. M. Atkins, and C. Wang, *Trim State Discovery with Physical Constraints,* Journal of Aircraft **52**, 90 (2015).

[28] A. Melikyan, A. Akhmetzhanov, and N. Hovakimyan, *On initial value and terminal value problems for Hamilton-Jacobi equation,* Systems and Control Letters **56**, 714 (2007).

[29] C. J. Tomlin, I. M. Mitchell, A. M. Bayen, and M. Oishi, *Computational Techniques for The Verification of Hybrid Systems,* Proceedings of the IEEE **91**, 986 (2003).

[30] I. M. Mitchell, *A Toolbox of Level Set Methods (Version 1.1)*, Tech. Rep. (2007).

[31] M. Chen, S. Herbert, and C. J. Tomlin, *Exact and Efficient Hamilton-Jacobi Guaranteed Safety Analysis via System Decomposition,* Proceedings - IEEE International Conference on Robotics and Automation , 87 (2017).

[32] T. J. J. Lombaerts, S. Schuet, and K. Wheeler, *Safe Maneuvering Envelope Estimation Based on A Physical Approach,* in *Guidance, Navigation, and Control and Co-located Conferences* (2013).

[33] T. J. J. Lombaerts, S. Schuet, D. Acosta, and J. T. Kaneshige, *Piloted Simulator Evaluation of Maneuvering Envelope Information for Flight Crew Awareness,* in *AIAA Guidance, Navigation, and Control Conference* (2015).

[34] A. M. Bayen, I. M. Mitchell, M. Oishi, and C. Tomlin, *Aircraft Autolander Safety Analysis Through Optimal Control-Based Reach Set Computation,* Journal of Guidance, Control, and Dynamics **30**, 68 (2007).

[35] G. Shah, J. Foster, and K. Cunningham, *Simulation Modeling for Off-Norminal Conditions - Where Are We Now?* in *AIAA Modeling and Simulation Technologies Conference* (2010).

[36] T. J. J. Lombaerts, H. Huisman, Q. P. Chu, J. Mulder, and D. Joosten, *Nonlinear Reconfiguring Flight Control Based on Online Physical Model Identification,* Journal of Guidance, Control, and Dynamics **32**, 727 (2009).

[37] B. Stevens and F. Lewis, *Aircraft Control and Simulation* (Wiley, 1992) pp. 81–90.

[38] G. Shah and M. Hill, *Flight Dynamics Modeling and Simulation of a Damaged Transport Aircraft,* AIAA Modeling and Simulation Technologies (2012).

[39] Y. Zhang, C. C. de Visser, and Q. P. Chu, *Aircraft Damage Identification and Classification for Database-Driven Online Flight-Envelope Prediction,* Journal of Guidance, Control, and Dynamics **41**, 449 (2018).

[40] K. Cunningham, D. Cox, D. Murri, and S. Riddick, *A Piloted Evaluation of Damage Accommodating Flight Control Using a Remotely Piloted Vehicle,* in *AIAA Guidance, Navigation, and Control Conference* (2011).

[41] N. T. Frink, P. C. Murphy, H. L. Atkins, S. A. Viken, J. L. Petrilli, A. Gopalarathnam, and R. C. Paul, *Computational Aerodynamic Modeling Tools for Aircraft Loss of Control,* Journal of Guidance, Control, and Dynamics **40**, 789 (2017).

[42] NASA, *Flight Dynamics Simulation of a Generic Transport Model,* (2016), https://software.nasa.gov/software/LAR-17625-1.

[43] N. T. Nguyen, K. S. Krishnakumar, J. T. Kaneshige, and P. Nespeca, *Flight Dynamics and Hybrid Adaptive Control of Damaged Aircraft,* Journal of Guidance, Control, and Dynamics **31**, 751 (2008).

[44] J. D. Boskovic, N. Knoebel, R. K. Mehra, and I. Gregory, *An Integrated Approach to Damage Accommodation in Flight Control,* in *AIAA Guidance, Navigation and Control Conference and Exhibit*, AIAA 2008-6504 (2008).

[45] R. Malladi, J. Sethian, and B. Vemuri, *Shape Modeling with Front Propagation: A Level Set Approach,* IEEE Transactions on Pattern Analysis and Machine Intelligence **17**, 158 (1995).

[46] H.-k. Zhao and R. Fedkiw, *Fast Surface Reconstruction Using the Level Set Method,* Variational and Level Set Methods in Computer Vision , 194 (2001).

[47] J. A. Sethian, *Evolution, Implementation, and Application of Level Set and Fast Marching Methods for Advancing Fronts,* Journal of Computational Physics **169**, 503 (2001).

[48] J. A. Sethian, *A Fast Marching Level Set Method for Monotonically Advancing Fronts,* Pnas **93**, 1591 (1996).

[49] D. Adalsteinsson and J. Sethian, *The Fast Construction of Extension Velocities in Level Set Methods,* Journal of Computational Physics **148**, 2 (1999).

[50] J. A. Sethian, *Fast Marching Methods,* SIAM Review **41**, 199 (1999).

[51] S. Arora and B. Barak, *Computational Complexity: A Modern Approach* (Cambridge University Press, 2009).

[52] M. T. Goodrich and R. Tamassia, *Algorithm Design: Foundations, Analysis, and Internet Examples* (Wiley, 2002) pp. 3–47.

[53] I. Matamoros and C. C. de Visser, *Incremental Nonlinear Control Allocation for a Tailless Aircraft with Innovative Control Effectors,* in *AIAA Guidance, Navigation, and Control Conference* (2018).

[54] N. Govindarajan, C. C. de Visser, and K. Krishnakumar, *A Sparse Collocation Method for Solving Time-dependent HJB Equations Using Multivariate B-splines,* Automatica **50**, 2234 (2014).

5

SAFE FLIGHT ENVELOPE PROTECTION

"Come close the loop !"

Prof. dr ir M.Mulder

Once a complete database is built, the final step is to integrate it into a flight envelope protection system with a fault tolerant controller. This chapter will close the loop of the whole system and achieve the main research goal by connecting all the separate modules discussed in previous chapters together. Simulations with in-flight damage cases are conducted to test the performance of the database-driven safe flight envelope protection system. Simulation results indicate that the proposed system can be implemented online and can help prevent the damaged aircraft from flying into loss-of-control conditions.

This chapter is based on:
Y. Zhang, C. C. de Visser, and Q. P. Chu, *Database-driven Online Flight Envelope Protection for Damaged Aircraft*, Journal of Guidance, Control, and Dynamics, 2019. (to be submitted)

5.1. INTRODUCTION

The function of a flight envelope protection system is two-fold: an augmentation of the flight controller to monitor and maintain the aircraft within its flight envelope (e.g., maximum angle of attack) [1–3]; and an auxiliary system to inform pilots of the current flight envelopes (e.g., minimum speed) via human-machine interactions such as haptics and visual displays [4–7]. The first function prevents pilots from over-steering the aircraft by limiting the commands to the flight controller, and the second function directly provides safety-related information to the pilots so that they can make unconventional control strategies without violating the envelope boundaries. These two functions work in cooperation to enhance the flight safety.

Sudden occurrence of abnormal cases, like structural damage and system failures, may cause an abrupt change of the inherit flight dynamics as well as control authority, leading to a potential loss of stability and control [8]. In many cases, fast responses and high-frequency control inputs from new control strategies are required, which are difficult for human pilots. Instead, a fault tolerant controller can be reconfigured to regain the stability of the aircraft given the knowledge of the new flight envelope.

This chapter mainly focuses on the first function of the flight envelope protection system, which integrates the prediction of the new flight envelope into a fault tolerant controller. In this way, commands from pilot/autopilot as well as flight states are constrained within new limits in abnormal situations.

In the database-driven flight envelope prediction system proposed in this thesis, the flight envelope is an explicit set of data, separate from the baseline controller as an independent module. With modular design of the flight envelope protection system, only envelopes that are explicitly referred to by the system need to be retrieved from the database, and the re-design of the overall protection and control system is not necessarily needed.

The implementation of system identification, fault/damage diagnosis and database building have been individually discussed in the previous chapters. However, none of these have practical meanings if they are not connected and run in a loop, providing new envelope information to the succeeding flight envelope protection and flight control. Hence, the main focus of this chapter is the implementation of the closed-loop fault tolerant control with flight envelope prediction and protection.

Abnormal situations can be roughly categorized as either catastrophic or moderate. A catastrophic case indicates the situation where the flight envelope is too small for aircraft to recover from upset conditions and perform maneuvers. For example, under total loss of actuators and strong gust wind, the aircraft may immediately lose its control without any effective control. Therefore, discussions on severely-impaired aircraft and extreme external disturbances are excluded from the scope of this thesis.

Under moderate abnormal cases, *internal* control problems may lead to aircraft loss-of-control (LOC), which is the main issue this chapter aims to solve. When, for instance, the magnitude of faults/damage is not too large, it is still possible to control the aircraft back to trim condition given appropriate control strategies. However, LOC is still likely to happen when new maneuvers are initiated without the knowledge of the current abnormal condition and reduced flight limits. Therefore, flight envelope protection plays an important role in preventing the aircraft from entering the LOC condition after the

change of system dynamics and control authorities.

5.2. RECONFIGURATION OF FLIGHT CONTROL

A fault tolerant controller (FTC) is designed to reconfigure the flight control when there are system faults and damage. The reconfigured controller is expected to achieve the control object and satisfactory performance by using remaining control authorities to adapt to the changed system dynamics and mitigate the adverse impact of faults and damage. This can either be achieved passively with elaborate controller design, or actively with onboard detection of fault/damage. A general review of FTCs and their comparisons can be found in [9, 10].

Among various adaptive fault tolerant controllers for highly nonlinear systems, incremental nonlinear dynamic inversion (INDI) control method [11, 12] has been intensively applied to different types of aircraft. The INDI method can be considered as an incremental form of the widely used nonlinear dynamic inversion (NDI) method [13, 14]. The NDI method only works fine with systems of which the models are perfectly modeled without mismatch. The advantage of the INDI method over the NDI method is that it makes the controller significantly less sensitive to model mismatch with simpler control design. In situations of system faults, failures and especially structural damage, the present of model mismatch is inevitable. The INDI method uses sensor information to replace a large part of the model including its unmodeled uncertainties, making it much less model-dependent and very suitable for fault tolerant control. In practice, the high performance and adaptiveness of the INDI controller has been proved by many published results from simulations as well as real flight tests. In [12], a flight control strategy based on the INDI method has been applied to a T-tailed UAV simulation model, which showed increased robustness of the system. Real-world flight tests on a quadrotor UAV have demonstrated high performances of the INDI controller with very coarse knowledge of model parameters in advance [15]. Highly nonlinear and inherently unstable models of helicopters [16] as well as over-actuated tailless aircraft [17] also utilized the INDI method in controller design to achieve efficient tracking of the commands under model uncertainties. Most significantly, real flight tests have been successfully conducted on a Cessna Citation II aircraft (PH-LAB) [18]. The INDI control method was integrated with the fly-by-wire and sensor system, and has performed satisfying results with robustness to a certain amount of model mismatch [18]. In accordance with previous chapater, the simulation work conducted in this chapter is based on the Cessna Citation model in DASMAT [19].

5.2.1. CONTROLLER STRUCTURE

The aircraft is controlled in a multi-loop structure based on its dynamics model. The number of loops is decided by the states that are directly given commands to. In abnormal situations, maintaining control of attitude and aerodynamic angles is primarily considered, thus is implemented in this section. As illustrated in Fig. 5.1, the control system consists of two loops: an outer loop of roll angle ϕ, angle of attack α, and side-slip angle β; an inner loop of angular rates $\boldsymbol{\omega} = [p, q, r]^T$ corresponding to roll, pitch and yaw respectively. The engine throttle is controlled by a separated auto-throttle loop to keep

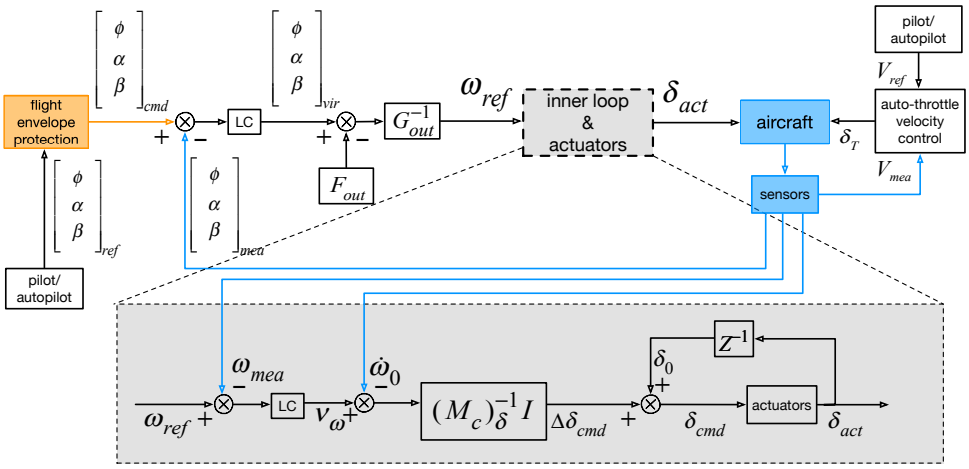

Figure 5.1: A multi-loop NDI/INDI control structure

the aircraft at a certain level of velocity. The commands of $[\phi, \alpha, \beta, V]$ are given by the pilots/autopilots. The dynamics of $[\phi, \alpha, \beta]$ can be written in the form:

$$\begin{aligned} \begin{bmatrix} \dot{\phi} \\ \dot{\alpha} \\ \dot{\beta} \end{bmatrix} &= F_{out} + G_{out}\boldsymbol{\omega} \\ &= \begin{bmatrix} 0 \\ f_\alpha \\ f_\beta \end{bmatrix} + \begin{bmatrix} 1 & \sin\phi\tan\theta & \cos\phi\tan\theta \\ \frac{-uv}{u^2+w^2} & 1 & \frac{-vw}{u^2+w^2} \\ \frac{w}{\sqrt{u^2+w^2}} & 0 & -\frac{u}{\sqrt{u^2+w^2}} \end{bmatrix} \begin{bmatrix} p \\ q \\ r \end{bmatrix} \end{aligned} \tag{5.1}$$

where,

$$f_\beta = \frac{1}{\sqrt{u^2+w^2}}\left[-\frac{uv}{V^2}(A_x - g\sin\theta) + (1-\frac{v}{V^2})(A_y + g\sin\phi\cos\theta) - \frac{vw}{V^2}(A_z + g\cos\phi\cos\theta)\right] \tag{5.2}$$

$$f_\alpha = \frac{1}{u^2+w^2}\left[u(A_z + g\cos\phi\cos\theta) - w(A_x - g\sin\theta)\right] \tag{5.3}$$

and A_x, A_y, A_z denotes the specific forces along the body X/Y/Z axis; u, v, w are the velocity components along the body X/Y/Z axis. The values of these states as well as the Euler angles are measured from onboard sensors. These measurements are estimated by Kalman filters so that they are not contaminated by sensor noise and biases.

Since eq. 5.1 and 5.2 contains little model uncertainties, the classic NDI controller is applied to the outer loop. The desired input to the inner-loop control $\boldsymbol{\omega}_{ref} = [p, q, r]^T_{ref}$ is solved by introducing a virtual input $[\phi, \alpha, \beta]^T_{vir}$ to the outer-loop controller:

$$\boldsymbol{\omega}_{ref} = G^{-1}_{out}\left([\phi, \alpha, \beta]^T_{vir} - F_{out}\right) \tag{5.4}$$

Substituting Eq. 5.4 into the dynamics quation Eq. 5.1 yields a decoupled linear relation:

$$[\dot{\phi}, \dot{\alpha}, \dot{\beta}]^T = [\phi, \alpha, \beta]^T_{vir} \tag{5.5}$$

The virtual input $[\phi, \alpha, \beta]^T_{vir}$ can be solved by a linear controller (LC), as shown in Fig. 5.1.

The resulting $\boldsymbol{\omega}_{ref}$ is used for controlling the inner-loop of angular rates, where the Euler equations of motion are used [12]:

$$\mathbf{M} = \mathbf{I}\dot{\boldsymbol{\omega}} + \boldsymbol{\omega} \times \mathbf{I}\boldsymbol{\omega} \tag{5.6}$$

where $\mathbf{M} = [L, M, N]^T$ are the angular moments acting on the aircraft, and the inertia matrix is denoted by $\mathbf{I}$.

The moments $\mathbf{M}$ can be specified as a combination of flight-states-related moments $\mathbf{M}_a$ generated by airframe aerodynamics, and actuator-related moments $\mathbf{M}_c$ generated by the control surface deflections. Solving the above equation for $\dot{\boldsymbol{\omega}}$ yields [12]:

$$\dot{\boldsymbol{\omega}} = \mathbf{I}^{-1}(\mathbf{M}_a + \mathbf{M}_c - \boldsymbol{\omega} \times \mathbf{I}\boldsymbol{\omega}) \tag{5.7}$$

by assuming on the linear relation between $\mathbf{M}_c$ and actuator deflections $\boldsymbol{\delta} = [\delta_a, \delta_e, \delta_r]^T$, which is:

$$\mathbf{M}_c = (\mathbf{M}_c)_\delta \boldsymbol{\delta} = \frac{1}{2}\rho V^2 S \begin{bmatrix} bC_{l_{\delta_a}} & 0 & bC_{l_{\delta_r}} \\ 0 & \bar{c}C_{m_{\delta_e}} & 0 \\ bC_{n_{\delta_a}} & 0 & bC_{n_{\delta_r}} \end{bmatrix} \begin{bmatrix} \delta_a \\ \delta_e \\ \delta_r \end{bmatrix} \tag{5.8}$$

where $(\mathbf{M}_c)_\delta = \frac{\partial}{\partial \boldsymbol{\delta}}\mathbf{M}_c$. If NDI is applied to the inner-loop, the actuator deflections $\boldsymbol{\delta}$ can be solved by introducing a virtual input $\boldsymbol{\nu}_\omega$ to the inner-loop, which yields:

$$\boldsymbol{\delta} = \mathbf{M}_c^{-1}(\mathbf{I}\boldsymbol{\nu}_\omega + \boldsymbol{\omega} \times \mathbf{I}\boldsymbol{\omega} - \mathbf{M}_a) \tag{5.9}$$

where $\boldsymbol{\nu}_\omega$ corresponds to the virtual input of the inner loop shown in Fig. 5.1. Similar to the outer-loop, the introduction of $\boldsymbol{\nu}_\omega$ yields a linear system $\dot{\boldsymbol{\omega}} = \boldsymbol{\nu}_\omega$, of which a linear controller is used to generate $\boldsymbol{\nu}_\omega$ depending on the error between the measured and desired value of $\boldsymbol{\omega}$, as shown in Fig. 5.1.

It is noticed in Eq. 5.9 that the control law depends on the full aerodynamic model of $\mathbf{M}_a$ and $\mathbf{M}_c$. Hence, the uncertainties of the aerodynamic model will have an undesired impact on the performance of the controller. Alternatively, it is considered to only compute the increments of actuator deflections at each execution, which is only influenced by $\mathbf{M}_c$. The incremental part is obtained by a first-order Taylor approximation of $\dot{\boldsymbol{\omega}}$ in Eq. 5.7[12]:

$$\dot{\boldsymbol{\omega}} \approx \dot{\boldsymbol{\omega}}_0 + \frac{\partial}{\partial \boldsymbol{\omega}}\left[\mathbf{I}^{-1}(\mathbf{M}_a - \boldsymbol{\omega} \times \mathbf{I}\boldsymbol{\omega})\right]_{\boldsymbol{\omega}_0, \boldsymbol{\delta}_0}(\boldsymbol{\omega} - \boldsymbol{\omega}_0) + \frac{\partial}{\partial \boldsymbol{\delta}}\left[\mathbf{I}^{-1}\mathbf{M}_c\right]_{\boldsymbol{\omega}_0, \boldsymbol{\delta}_0}(\boldsymbol{\delta} - \boldsymbol{\delta}_0) \tag{5.10}$$

where $\boldsymbol{\omega}_0$ and $\boldsymbol{\delta}_0$ are the measured values of the previous time step. For small time increments, the change rate of angular $(\boldsymbol{\omega} - \boldsymbol{\omega}_0)$ is considered to be negligible compared to the change of actuator deflection. Hence, by denoting $(\boldsymbol{\delta} - \boldsymbol{\delta}_0)$ as $\Delta\boldsymbol{\delta}$, Eq. 5.10 can be simplified as:

$$\dot{\boldsymbol{\omega}} = \dot{\boldsymbol{\omega}}_0 + \left[\mathbf{I}^{-1}(\mathbf{M}_c)_\delta\right]\Delta\boldsymbol{\delta} \tag{5.11}$$

It can be observed that a large part of the aerodynamic model $\mathbf{M}_a$ is canceled when only the incremental form is considered. On the assumption of accurate sensor information

of angular accelerations, the commanded incremental deflections of actuators can be solved by:

$$\Delta\boldsymbol{\delta}_{cmd} = (\mathbf{M}_c)_{\delta}^{-1}\mathbf{I}(\boldsymbol{\nu}_{\omega} - \dot{\boldsymbol{\omega}}_0) \tag{5.12}$$

which yields the commanded control input to the aircraft:

$$\boldsymbol{\delta}_{cmd} = \boldsymbol{\delta}_0 + \Delta\boldsymbol{\delta}_{cmd} \tag{5.13}$$

It should be noted that the derivation of the INDI method requires actuators with fast deflection responses and linear relationship between $\boldsymbol{\delta}$ and M_c, so the performance of the controlled may be degraded when the actuator saturated due to system faults or aircraft damage, which will be discussed later in this chapter.

5.3. ONLINE IMPLEMENTATION

Figure 5.2 shows the complete loop to be implemented online, which is designed to enhance aircraft safety under the adverse impact of sudden faults/damage. Each building block of the loop has been discussed separately, what remains left is implementing the complete loop online.

The flight after faults/damage can be divided into two phases, and the first phase ends with the new trimmed flight. During the first phase, the initial trim condition is disturbed by the sudden faults/damage and the aircraft is quickly re-stabilized by the onboard fault tolerant controller and actuators. Meanwhile, the system identification and diagnosis system provides information on the current abnormal situation of the aircraft as well as the reduced control authorities. Based on the current velocity and damage case, a flight envelope is retrieved from the database.

The second phase starts when the aircraft tries to maneuver (e.g. turning). This phase is more safety-related, since the maneuver may cause incremental forces and moments that are beyond the current control authority and lead to loss-of-control. Therefore, during phase 2, it is extremely important to consider the remaining control power and the boundary of reduced flight envelope when giving commands to the controller.

As illustrated in Fig. 5.2, half of the loop on the right is more active during phase 1, where the re-stabilization and diagnosis of the impaired aircraft is achieved. The left side of the loop is more important during phase 2, where flight envelope prediction and protection are connected to ensure that the maneuver is always kept within the safe flight envelope.

5.3.1. PHASE 1: FROM DAMAGE TO TRIM

When unexpected hazards, like structural damage suddenly occur, passive fault tolerant control is used to allocate the actuators to re-stabilize the aircraft. The advantage of passive control is that it responds faster to abnormal situations than human pilots. Hence, in phase 1, the mitigation of unexpected hazards is quickly achieved by passive fault tolerant control if sufficient control authority is available. The quick reaction of the controller alleviates the work load of pilots so that they can focus more on the situation analysis and higher-level decision-makings.

In case of loss of vertical tail, for example, it is hardly possible to maintain directional stability via rudder. Instead, research shows that alternate control methods like differ-

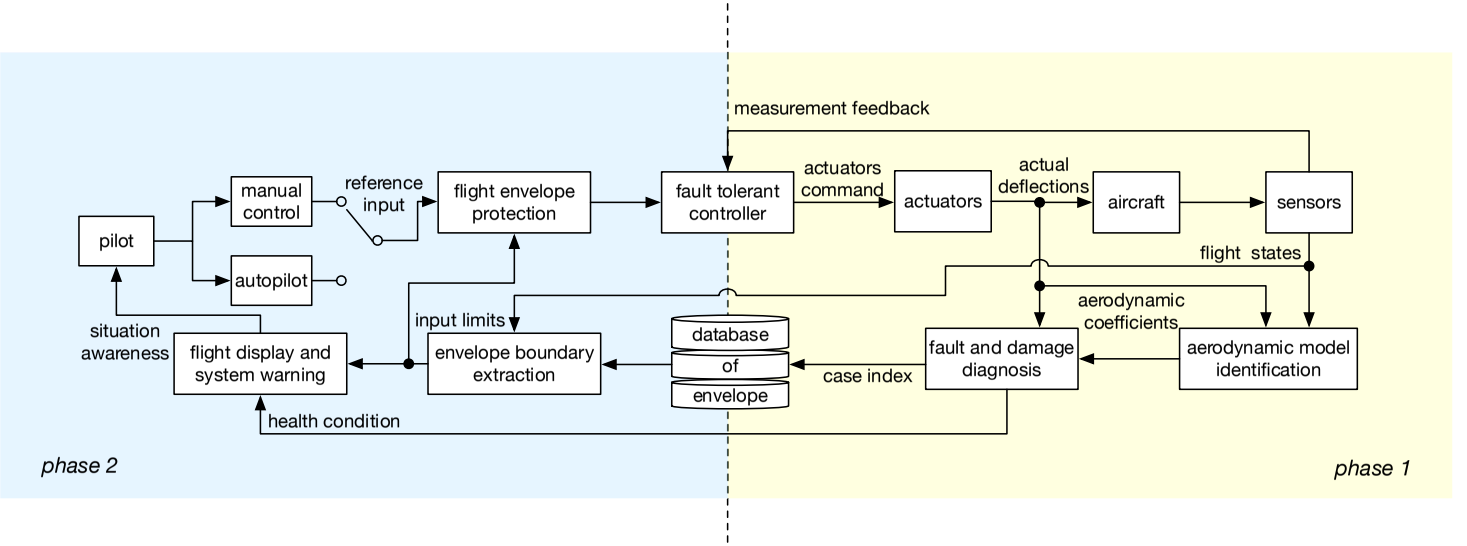

Figure 5.2: An overview of the complete loop to be implemented online

ential thrust and combined use of ailerons can be applied automatically by flight control systems [20]. A more frequently occurred case is engine failure, which imposes a sudden asymmetric side force and a non-zero side-slip angle (β) followed by a roll motion. Under such emergencies, with the help of automatic flight controller, a rudder deflection is used to mitigate the adverse yaw and maintain a zero β.

In Chapter 2, aerodynamic model identification is excited by a designed open-loop doublet maneuver to show the performance of the re-identification process. In a closed-loop controller, the excitation input $\boldsymbol{\delta}$ is generated in a more practical manner. When normal flight is disturbed by sudden faults or damage, the controller will try to re-stabilize the aircraft and keep it under control. Meanwhile, the detection alarm is generated to trigger the re-identification. During the process, actuator commands $\boldsymbol{\delta}_{cmd}$ are generated and measured, which are used for the excitation input for the identification of control effectiveness. Triggered by the detection alarm, the covariance matrix is reset to its initial value so that the re-identification is mostly influenced by new data in the changed situation. Once the identification error and covariance matrix converge to sufficiently small values, the identified parameters converge to their new values, which are used for the diagnosis system.

Persistently exciting input is one of the key issues in system identification. In normal situations, inputs from various flight states are expected to be as sufficient as possible to obtain accurate global results. In abnormal situations where aircraft is more likely to lose its control with maneuvers, excitation inputs, if required, should be given with safety considerations, so the identification accuracy needs to be compromised. Due to the highly generalization ability of support vector machines (SVM) used in the diagnosis system, both safety and accuracy can be achieved.

The diagnosis system is composed of several parallel classifiers, each of which corresponds to one of pre-defined damage and fault cases. The classification is based on the off-line training functions stored in the system, and each classifier may have different aerodynamic coefficients as input. Based on the results produced by all the classifiers running in parallel, the decision-making process determines the type, location and severity of faults and damage.

The classification and decision-making results will then generate the case index to retrieve the corresponding flight envelopes in the database. If the diagnosis system indicates that there are multiple damage locations, or there is necessity for flight envelope interpolation, more than one flight envelopes will be retrieved from the database.

5.3.2. PHASE 2: FROM TRIM TO MANEUVER

In the second phase when the re-stabilized aircraft tries to maneuver to another state, active control strategies can be applied. However, during this phase, the loss of aircraft control can be caused by aggressive commands. In an icing scenario simulated in [21], even though ice accretion did not initiate immediate LOC of the aircraft, the maximum achievable flight states had greatly changed. If the protection system had not taken these changes into account, a combined pitch up and roll maneuver after icing could have easily steered the aircraft over its physical limits and caused LOC.

Similarly, faults and damage to the aerodynamic surfaces and actuators lead to reduced stability margin and control authority. If the aircraft is subjected to incremental

moments due to asymmetric damage and faults, it will cause further reduction of available control power during the maneuver. All these changes are reflected in the shrunken flight envelopes. If the maneuver command is given without considering the changed envelopes, the aircraft may fly into unrecoverable states. In some cases, for instance, excessive input may generate incremental moments that the remaining control authorities can not counteract, leading to the saturation of actuators and irreparable LOC condition. Therefore, flight envelopes retrieved from the database are incorporated in the control and warning system to protect the aircraft from LOC situations.

5.4. CASE STUDY AND SIMULATION RESULTS

In this section, online implementation of the whole system shown in Fig. 5.2 is simulated in the DASMAT model, where the flight envelope database is built in the form of look-up tables. The overall objective of the simulation is to investigate if the flight envelope can be successfully retrieved online, and if the envelope protection can prevent aircraft from potential LOC conditions.

It is argued in [20] that lateral control limitation are less familiar to pilots than longitudinal control limitations. A possible reason is that aircraft in normal flight will have adequate roll and yaw control until stall speed. This means that longitudinal control hazard will normally manifest itself before lateral control becomes an issue. However, this situation changes when stability and control of roll and yaw axis are influenced by hazards (e.g., structural damage, ice accretion) on wing and vertical tail. In such cases, excessive commands on angle of attack can over-steer the aircraft into LOC conditions before it reaches stall limits.

In order to show the importance of envelope protection, two structural-damage cases are modeled in the DASMAT model for simulation, as shown in Fig. 5.3. The first case is symmetrical damage to the rudder, and the second case is asymmetrical damage to the left wing and aileron. The combination of both wing and rudder damage is also simulated and discussed. Due to the coupling between roll and yaw motion, the loss of directional control will generate rolling moment that may lead to the loss of lateral control if the available control power runs out. The simulation is performed in DASMAT under normal and abnormal flight conditions. During each simulated flight, the aircraft is initially trimmed at $100 m/s$ and $5000 m$ with $\alpha = 3.7°$.

5.4.1. RUDDER DAMAGE

Rudder is commonly used to maintain zero sideslip angle under side force and adverse yaw moment. Normally, rudder is not used for turning, except for crosswind landings, where it is necessary to align the aircraft with the runway and a certain (non-zero) sideslip angle is given as the reference input by the pilot/autopilot. When the aileron control is limited, however, rudder can be used as an alternative for turning [20].

When rudder is damaged, in order to maintain the same value of β, more rudder deflections are required compared to normal situations. If the reference input of β is given without considering the reduced control effectiveness, the damaged rudder may soon saturate and lead to the loss of directional control. The aim of β-protection is to prevent such aggressive use of rudder controls.

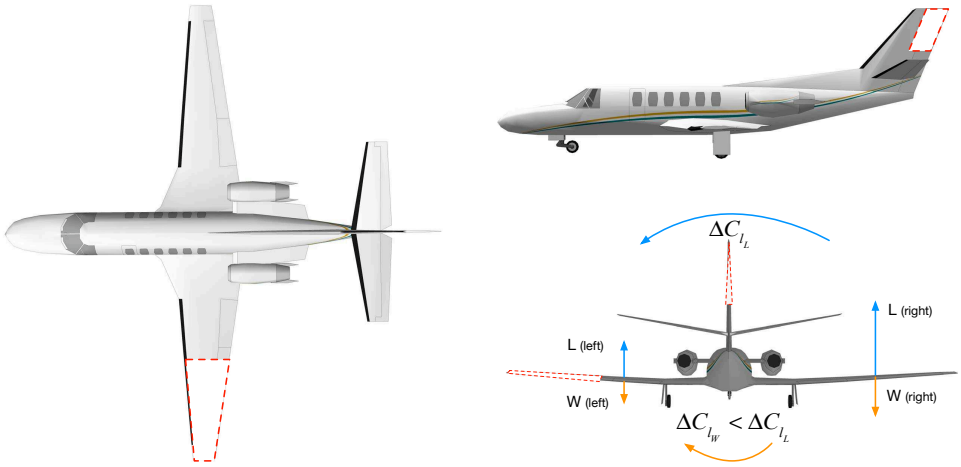

Figure 5.3: A three-view illustration of a damaged Cessna Citation aircraft

As discussed in the previous section, re-identification and classification form the primary phase of envelope prediction and protection. The re-identification is triggered when the error between measured and modeled output exceeds a certain threshold. The triggering threshold is pre-defined based on the slightest damage scale modeled in the simulation. For asymmetrical damage (e.g., wing damage), the detection errors are induced by unequal forces and increments of moments.

Ruder damage, however, is symmetrical, which does not induce constant increments of yawing moment, unless it is combined with rudder hard-over or asymmetric engine failures. Nevertheless, it is still possible to detect the error if the damaged rudder deflects to, for instance, maintain a non-zero β command. Additionally, reports on past flight accidents reveal that rudder and vertical tail damage is often accompanied, or induced by sudden external disturbances and turbulence, when rudder deflects to re-trim the aircraft.

The covariance matrix is an indication of the convergence of the re-identified parameters to their new values, which are closely related to the sufficiency of each state input. In abnormal situations, recovering and re-stabilizing maneuvers only excite a limited range of states, resulting in an updated local model of the current flight condition. Observing the variance of each estimated parameter, it is found that not all parameters are fully excited and re-identified. Nevertheless, the advantage of using classification is that it does not require all changed parameters to be accurately re-estimated. Only parameters that quickly converge are selected as the classification features. This advantage naturally circumvents the safety concerns associated with obtaining global models in abnormal situations.

The classification of damage is based on the training results by the SVM method discussed in chapter 3. Two parameters, C_{n_β} and $C_{n_{\delta_r}}$, are selected as the classification features. They can either be trained as two individual features, which yields two separate classifiers, or as a feature set of one classifier. As shown in Fig. 5.4, the training is

based on a feature set, and the boundaries of every two of the three classes are trained by a linear kernel.

Similar to Chapter 3, data points of different classes in the training set are denoted by different symbols in Fig. 5.4. Based on these data points, the decision function f is trained. The decision boundary between two classes (solid line) is $f = 0$, as shown between two dotted lines with $f = -1$ and $f = 1$ respectively. The whole state space is divided by different color scales according to their values of decision scores.

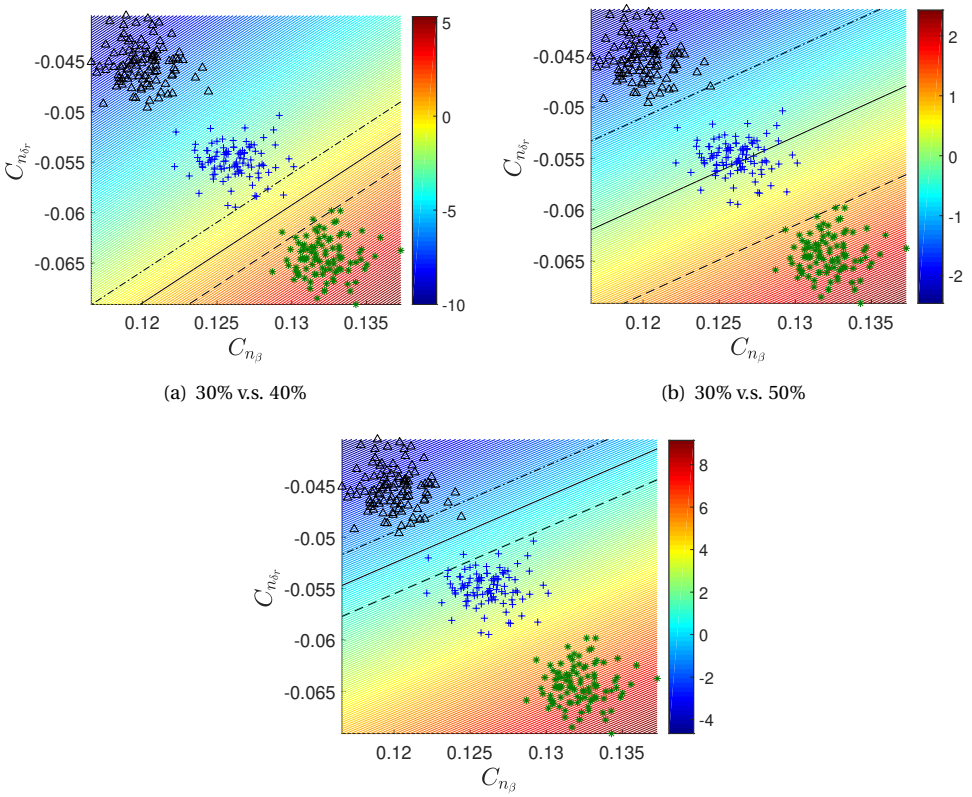

(a) 30% v.s. 40%

(b) 30% v.s. 50%

(c) 40% v.s. 50%

Figure 5.4: SVM training results of three damage levels denoted by % of tip loss ($*$: 30%, $+$: 40%, $\triangle$: 50%)

In this section, a 50% tip loss of rudder is simulated by changing the values of aerodynamic parameters in the look-up tables of the DASMAT simulation model. The original values of these parameters and their changed values after damage are listed in Table 5.1.

In the simulation shown in Fig. 5.5, the rudder damage is triggered at 15s. An impulse of external yaw moment ΔC_n is added at 15s and lasts for 2 seconds to simulate the effect of disturbances and turbulence, which causes an immediate rise of averaged error of C_n. As shown in Fig. 5.5(a), $\bar{\Delta} C_n$ exceeds the triggering threshold (3×10^{-7}) twice. Under the influence of external yaw moment, β deviates from zero and rudder immediately

Table 5.1: The values of aerodynamic coefficients before and after damage

	C_{n_β}	$C_{n_{\delta_r}}$	C_{n_r}
original value	0.153	-0.1	-0.21
value after damage	0.122	-0.05	-0.168

deflects in response to the sudden change, which excites the identification of C_{n_β} and $C_{n_{\delta_r}}$ respectively. In Figs. 5.5(e)(f), the value of C_{n_β} changes from 0.147 to 0.12, and $C_{n_{\delta_r}}$ from -0.095 to -0.046.

It can be observed from Fig. 5.5(d) that even though both parameters converge to their changed values, the variance of estimated C_{n_β} converges a bit slower than that of $C_{n_{\delta_r}}$. This is due to different excitation inputs of β and δ_r.

In the damage assessment system, each classifier correspond to one damage case, and the output of each classifier is represented by the value (0/1) of one indication flag. Whichever flag becomes unity, its corresponding damage case is declared as the current damage case. Based on the identification results shown on the left y-axis, the flag of the expected damage case is shown on the right y-axis of Figs. 5.5(e)(f).

In the simulation shown in Fig. 5.6, the amplitude of the added impulse signal is reduced to simulate the situation where the re-stabilizing response of β is not enough to fully excite the identification of C_{n_β}. As shown in Fig. 5.6(b)(c), at the time of damage occurrence, β deviates from zero and the controller gives commands of δ_r to maintain zero sideslip angle, which generates the excitation input to the re-identification of C_{n_β} and $C_{n_{\delta_r}}$. Figure 5.6(d) shows that before $20s$, the variance of the estimated C_{n_β} did not converge to a small value as that of $C_{n_{\delta_r}}$, since the excitation of β is not sufficient.

From the point of identification, more β-maneuvers are required for higher accuracy, but this may also increase the risk of LOC in the current abnormal situation that has yet been fully identified. Safety is always the first priority when it comes to flight, so small maneuvers are suggested when giving excitation inputs. However, the criteria for "small" is hard to define. In this chapter, we choose a limit of $\pm 2°$ for β command to numerically suggest how small the maneuvers should be. The limit is based on the most severe but still recoverable rudder-damage case modeled in the simulation, in order to prevent the aircraft from entering LOC condition during the identification process.

As shown in Fig. 5.6, after $20s$, a series of β-command is manually given within the limits, which provides more excitations for the estimated C_{n_β} to approach its expected value around $25s$. It can be observed that under damage conditions, the uncertainty of identification is magnified due to limited maneuvers and the insufficiency of excitations.

When the identification of C_{n_β} can hardly be fully excited within the safe maneuvering limits, decision will be made based on the value of its variance of estimation. If the variance is under a certain threshold, it means that the estimation is close to the expected value. Given the high generalization ability of SVM classification, C_{n_β} can still generate the expected classification results, as shown in Fig. 5.6(e). If the variance of estimation remains at a value above the threshold, it means that the estimated C_{n_β} deviates too far from the expected value, and can not be included as a feature input in the classification. Under this condition, the classification will only depend on the identification

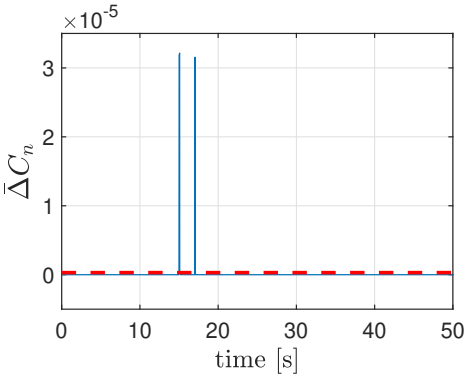

(a) threshold: 3×10^{-7} (red dotted line)

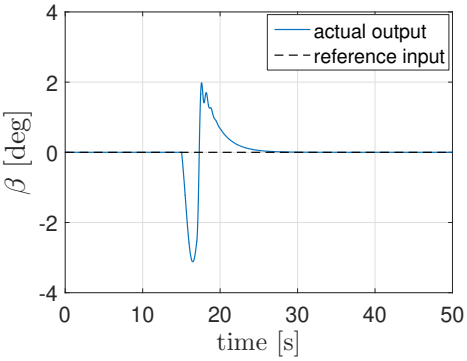

(b)

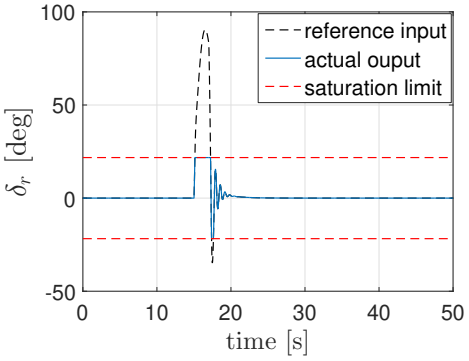

(c)

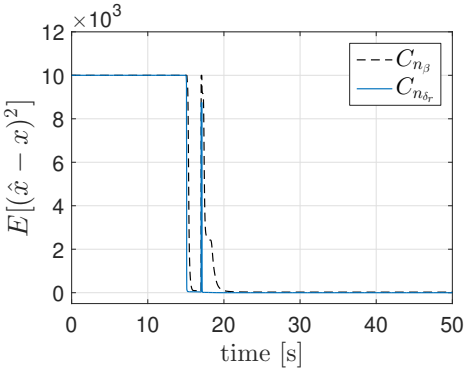

(d)

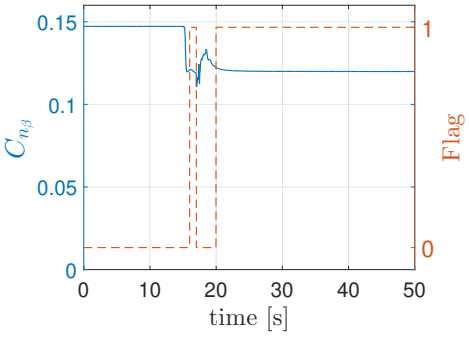

(e)

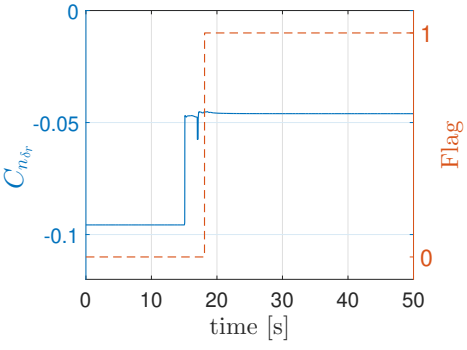

(f)

Figure 5.5: Identification without further maneuvers

of $C_{n_{\delta_r}}$, which converges more easily since rudder deflections δ_r in the inner loop have faster dynamics and thus generate sufficient excitations.

The comparison between flights with and without β protection after rudder damage

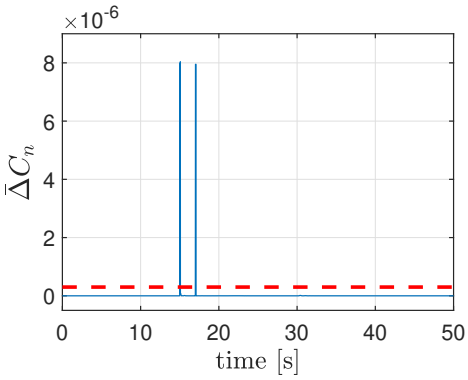

(a) threshold: 3×10^{-7} (red dotted line)

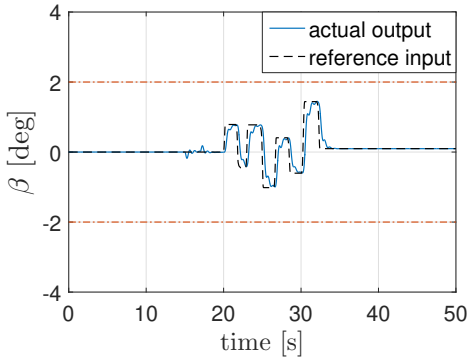

(b)

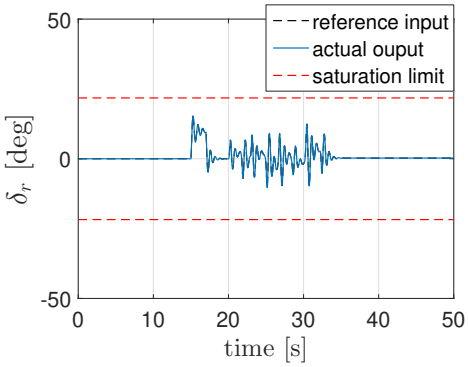

(c)

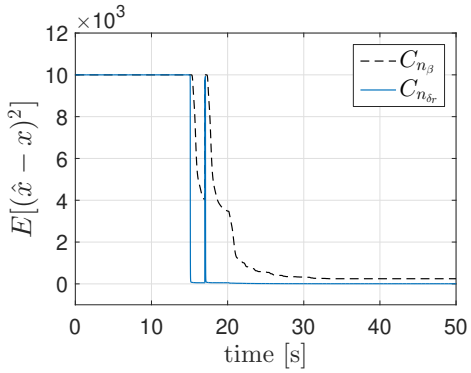

(d)

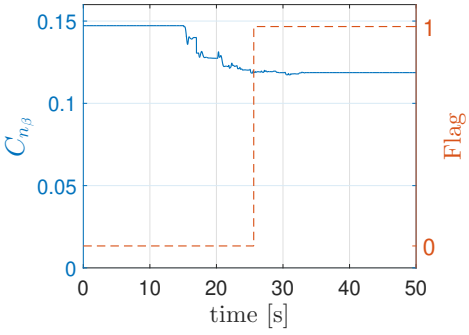

(e)

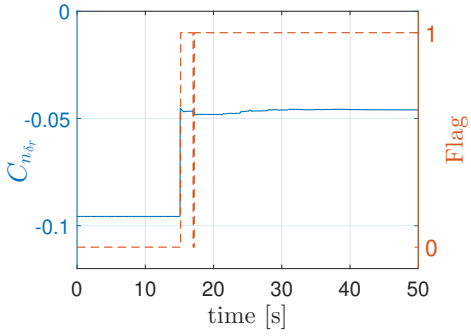

(f)

Figure 5.6: Identification with further maneuvers

is shown in Fig. 5.7. Before damage occurs, the sideslip angle β is maintained around $-5°$. In this simulation, external yawing moment is not added at the time of damage ($15s$). Instead, the deflection of rudder experienced an increase at the time of damage

to maintain the same value of β, which generates the error shown in Fig. 5.7(a). The magnitude of the error exceeds the pre-defined threshold, though it is much smaller than that in Figs. 5.5(a) and 5.6(a).

Based on the identified $C_{n_{\delta_r}}$ in Fig. 5.7(b), rudder damaged is quickly classified and confirmed after the damage. As shown in Figs. 5.7(c)(d), after $20s$ the reference input of β continues to increase until the damaged rudder begins to saturate. Under excessive β-command without protection of the new envelope, the directional control is not regained until $42s$, which is more than 10 seconds after the β-command is reduced at $30s$. Even though the saturation cannot cause the aircraft to flip over, strong forces at extreme positions may trigger more severe damage, like the total loss of rudder and vertical stabilizer. With updated information on the changed envelope, the same excessive input command is limited within the bound of envelope, as shown in Figs. 5.7(e)(f), which makes sure that the rudder deflections are always kept within the saturation limit.

5.4.2. LEFT WING AND AILERON DAMAGE

Unlike rudder damage, wing damage is asymmetrical, which generates an incremental rolling ΔC_l from unequal lift force (ΔC_{l_L}) and weight (ΔC_{l_W}) of two wing spans, as shown in the lower right subplot of Fig. 5.3. Since the reduction of weight is much less compared to lift force, its contribution to ΔC_l is neglected.

Figure 5.8 shows data from NASA wind-tunnel experiments [8], which indicates how incremental rolling moment change with angle of attack under wing damage. It is observed that ΔC_l can be approximated by a linear function of α. This can be explained by the fact that for general aircraft like Cessna Citation, lift force can be linearly determined by α in low-angle-of-attack region between $\alpha = -5°$ and $\alpha = 10°$. Hence, ΔC_l in DASMAT can be modeled as:

$$\Delta C_l = C_{l_\alpha} \cdot \alpha \tag{5.14}$$

The damage also induces reduction in the stability and control authority of the aircraft, which are reflected in the changed value of aerodynamic coefficients like control effectiveness $C_{l_{\delta_a}}$ and roll damping C_{l_p} [8]. The value of C_{l_α} and other aerodynamic coefficients influenced by the damage is modeled in the DASMAT so that their original values change once the damage is triggered in the simulation. In this section, a damage case of 50% tip loss of left wing is simulated. Table 5.2 lists the original values of most influenced coefficients in the look-up table and their modeled values after damage. It should be noted that C_{l_α} is not necessarily included as a classification feature, since the re-identification of this parameter requires sufficient input of α, which poses potential risk to the flight after damage. Similar to Fig. 5.4, the training results of three different wing damage levels using SVMs are shown in Fig. 5.9.

Table 5.2: The values of aerodynamic coefficients before and after damage

	C_{l_p}	$C_{l_{\delta_a}}$	C_{l_α}
original value	-0.46	-0.186	0
value after damage	-0.345	-0.093	0.6

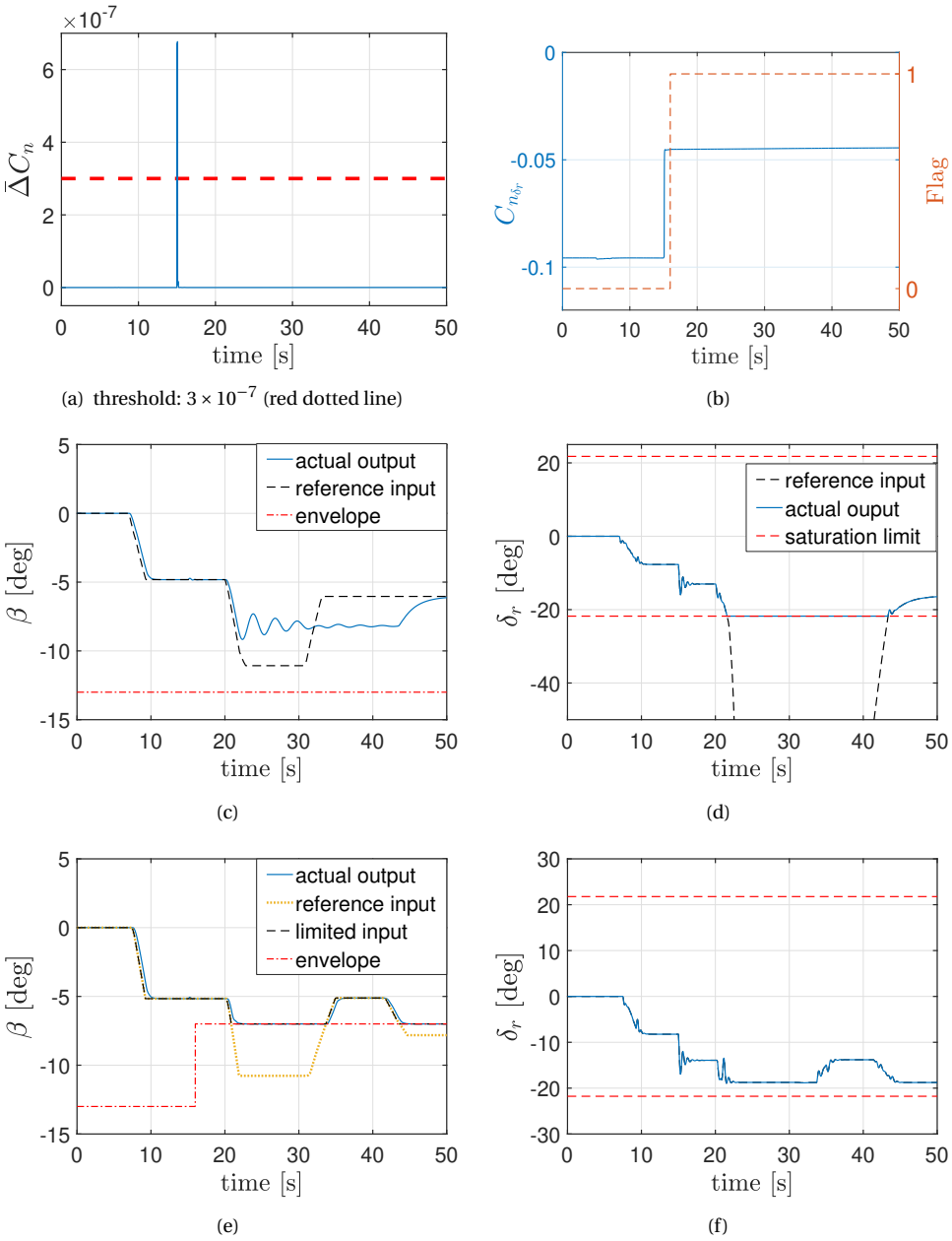

(a) threshold: 3×10^{-7} (red dotted line)

(b)

(c)

(d)

(e)

(f)

Figure 5.7: The identification of single rudder damage and the comparison between flights with and without envelope protection under yaw maneuvers

As shown in Fig. 5.10(a), the damage is initiated at 5s, and the averaged error of rolling moment $\bar{\Delta}C_l$ suddenly increases above the threshold, which triggers the re-identification.

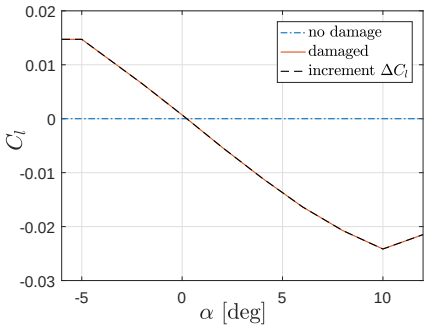

(a) $\beta = 0$

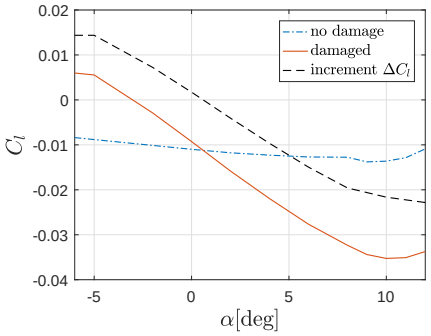

(b) $\beta = 5°$

Figure 5.8: Wind-tunnel data of incremental rolling moment with respect to angle of attack

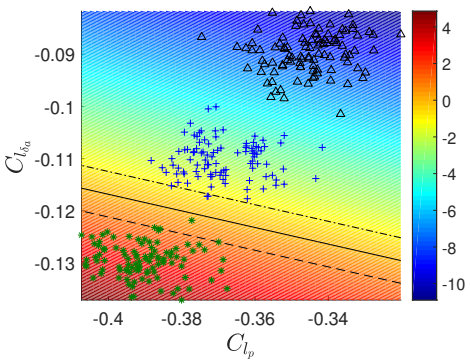

(a) 30% v.s. 40%

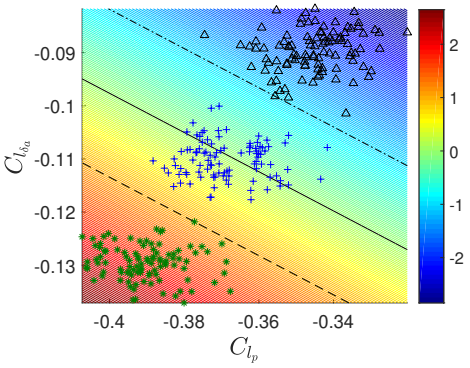

(b) 30% v.s. 50%

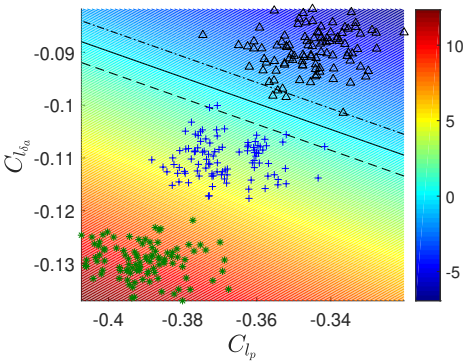

(c) 40% v.s. 50%

Figure 5.9: SVM training results of three damage levels denoted by % of tip loss ($*$: 30%, $+$: 40%, $\triangle$: 50%)

Sufficient excitation for identification is less an issue compared with rudder damage, due to the existence of incremental moment. In response to the sudden roll motion at $5s$ (Fig. 5.10(c)), the undamaged (right) aileron deflects in an effort to re-trim the aircraft and compensate for the incremental moment ΔC_l, as shown in Fig. 5.10(b). Meanwhile, the aileron deflections and roll motions have provided sufficient input excitation to the re-identification of aerodynamic coefficients. The identified C_{l_p}, $C_{l_{\delta_a}}$ are shown on the left y-axis of Figs. 5.10(d)(e).

As shown in Figs. 5.10(b), in the course of re-stabilizing the aircraft, the aileron needs to deflect about 25° to keep the roll angle to be zero, leaving limited authority (13°) for further roll control. If ΔC_l continues to increase, the right aileron will saturate and the aircraft may potentially lose control if velocity does not increase in a short period of time.

According to the previous analysis of wing damage and Eq. 5.14, the increase of α may generate too much rolling moment that saturates the actuator and lead to uncontrollable roll motions. Under normal condition without damage, as shown in Fig. 5.11(a), the angle of attack can be controlled to increase above 8° during pitch maneuver, and the roll motion is barely influenced (Fig. 5.11(b)) due to decoupled effect of α. In the wing damage scenario shown in Figs. 5.11(c), the command of α starts to increase at 30s after the damaged aircraft has been re-trimmed. Under the coupled influence of wing damage, the value of δ_a increases with α. As shown in Figs. 5.11(c)(d), when α increases to about 5.5°, δ_a meets the upper limit and the aircraft starts rolling to one side under the incremental rolling moment that can not be counteracted. This indicates that the angle of attack needs to be protected within the envelope, so that the damaged aircraft is not subjected to uncontrollable rolling moment.

The flight under envelope protection is shown in Figs. 5.11(e)(f), where the envelope is retrieved based on the current damage case and flight states. The reference input of α given by pilots/autopilot is not directly sent to the controller, but restricted by the retrieved envelope to about 5.2° before the deflection of δ_a is computed by the INDI controller. As shown in Figs.5.11(e)(f), δ_a is kept within the limit so that there is no unwanted roll motion during pitching maneuvers.

5.4.3. COMBINED RUDDER AND WING DAMAGE

Based on the analysis of these two cases, it is observed that asymmetrical damage is more critical than symmetrical damage, due to additional moments that are constantly generated by unequal forces. Under asymmetrical damage, the aircraft is always at the risk of LOC once the actuators reach their limits. In the simulation shwon in Fig. 5.12, the situation of wing damage deteriorates after the occurrence of rudder damage.

For single rudder damage, rudder saturation will cause deviations of β-command, but not total loss of aircraft control. However, when rudder damage is combined with wing damage, the envelope protection of β becomes critical, due to the coupling between directional and lateral motion.

In the extreme situation shown in Fig. 5.12(a), the α-command is beyond the safe limit and the actual α is maintained within the envelope boundary. It can be observed in Fig. 5.12(e) that aileron deflection is on the edge of saturation. Due to the typically large effective dihedral (C_{l_β}) of swept-wing transport aircraft, the sideslip excursions will result in potentially large uncommanded rolling motions that require more aileron de-

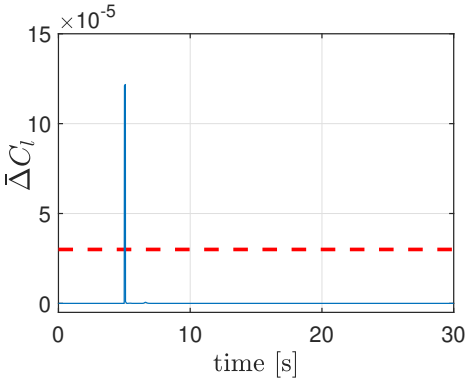

(a) threshold: 3×10^{-5} (red dotted line)

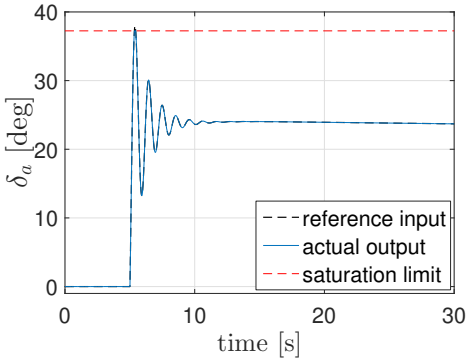

(b)

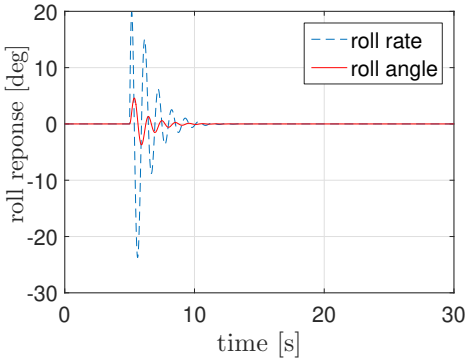

(c)

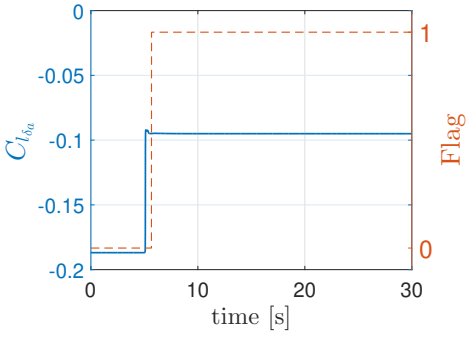

(d)

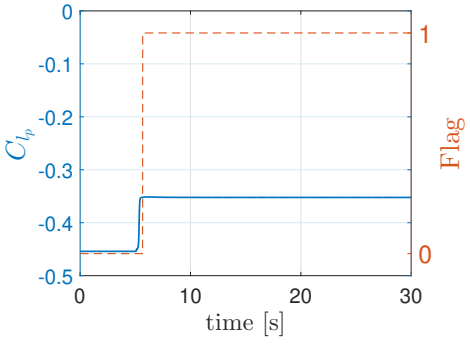

(e)

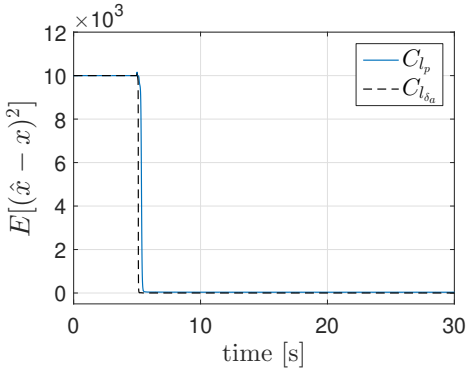

(f)

Figure 5.10: Aerodynamic identification and damage classification results under wing damage, without further maneuvers

flections.

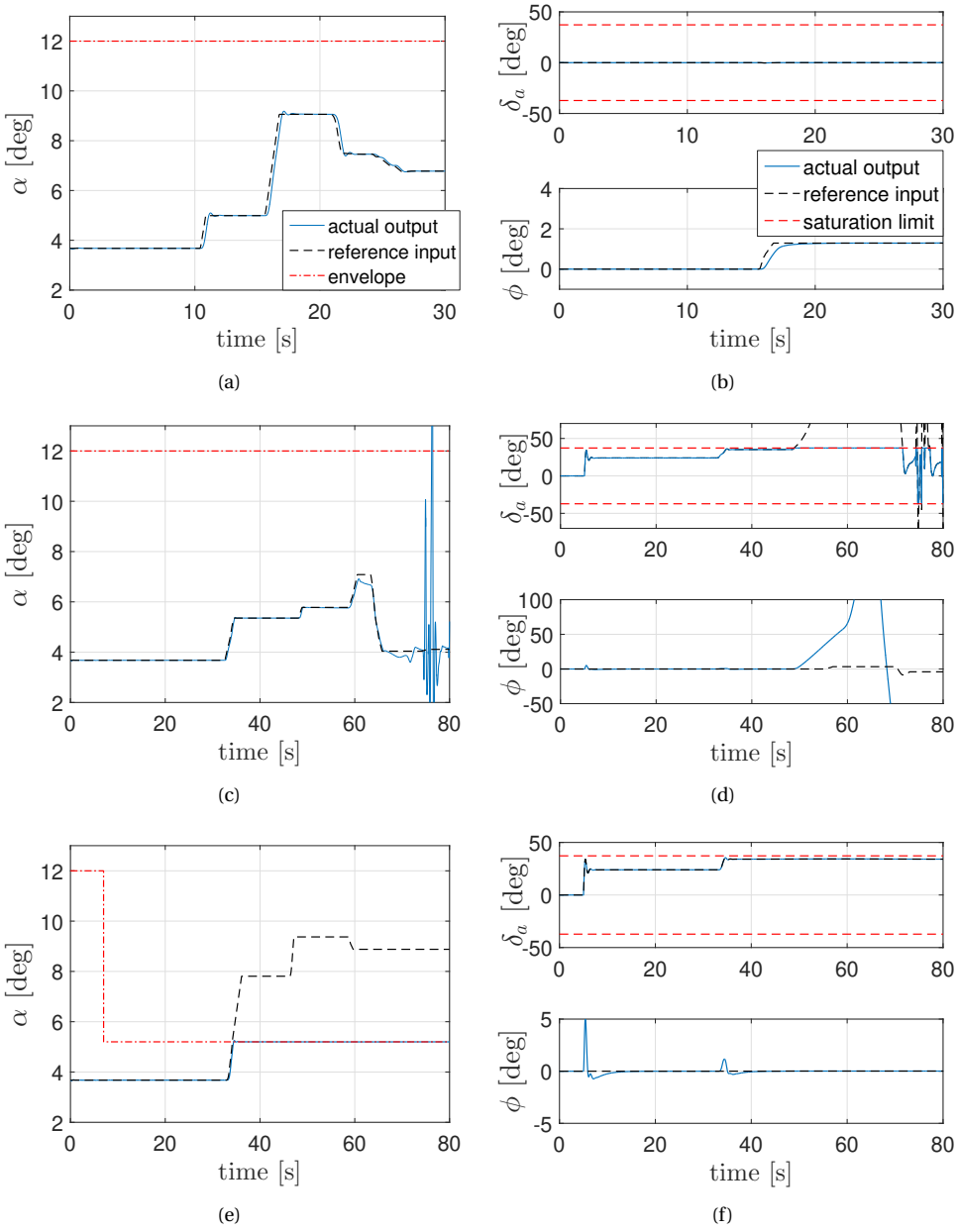

Figure 5.11: The influence of wing damage and envelope protection under pitch maneuvers

As shown in Fig. 5.12(c), the excursion of β occurs at around $20s$, when the control authority of rudder is completely lost without β protection. The uncontrolled β and saturated rudder generates more incremental rolling moment that cannot be mitigated

by the aileron, which causes the aircraft to roll to one side until it crashes to the ground. It can be observed that the protection of α can no longer prevent the aircraft from LOC if β is not effectively protected. As shown in the right column of Fig. 5.12, the utilization of both β and α envelope protection can effectively prevent LOC situation when pilots give excessive commands to the controller under emergencies.

5.4.4. DISCUSSION

Among all the LOC hazards that have a fundamental influence on flight envelopes, structural damage discussed in this chapter is only one category. Combination with other abnormal cases can lead to further change of flight envelopes and more stringent protection strategies. For example, icing-induced LOC incidents and accidents have occurred on all classes of aircraft [21]. The primary aerodynamic effect of icing is the increased drag force and reduced lift force on the icing part. Normally the ice accretion is not symmetrical, thus inducing moments from unequal forces. Based on these analysis, icing can be regarded as a reformation of airframe outline, which is similar to the impact of structural damage. Due to the lack of aerodynamic modeling data, icing is not modeled and simulated in this chapter. The determination and protection of flight envelopes in icing situations has been thoroughly discussed in [21, 22].

Engine failure is another important research topic related to LOC recovery, where velocity plays a vital role between life and death. Rudder is applied when asymmetric thrust generates non-zero side-slip angle. Another critical category is actuator faults, like rudder jam or hardover, which not only result in loss of control effectiveness but also induces unwanted moments. In these situations, flight envelope protection on automatic controller is not enough to guarantee safe flight, but the cooperation between pilots and machines. This also implies that the protection strategy discussed in this chapter has its scope and limitations. For other LOC prevention and recovery strategies under engine failure and rudder jam, readers can refer to Refs. [20, 23].

REFERENCES

[1] N. Tekles, J. Chongvisal, E. Xargay, R. Choe, D. A. Talleur, N. Hovakimyan, and C. M. Belcastro, *Design of a Flight Envelope Protection System for NASA's Transport Class Model,* Journal of Guidance, Control, and Dynamics **40**, 863 (2017).

[2] H. Lee, S. Snyder, and N. Hovakimyan, *L1 Adaptive Control Within a Flight Envelope Protection System,* Journal of Guidance, Control, and Dynamics **40**, 1013 (2017).

[3] D. Briere and P. Traverse, *AIRBUS A320/A330/A340 Electrical Flight Controls - A Family of Fault-tolerant Systems,* FTCS-23 The Twenty-Third International Symposium on Fault-Tolerant Computing , 616 (1993).

[4] K. A. Ackerman, D. A. Talleur, R. S. Carbonari, E. Xargay, B. D. Seefeldt, A. Kirlik, N. Hovakimyan, and A. C. Trujillo, *Automation Situation Awareness Display for a Flight Envelope Protection System,* Journal of Guidance, Control, and Dynamics **40**, 964 (2017).

[5] T. J. J. Lombaerts, G. Looye, J. Ellerbroek, and M. R. y. Martin, *Design and Piloted*

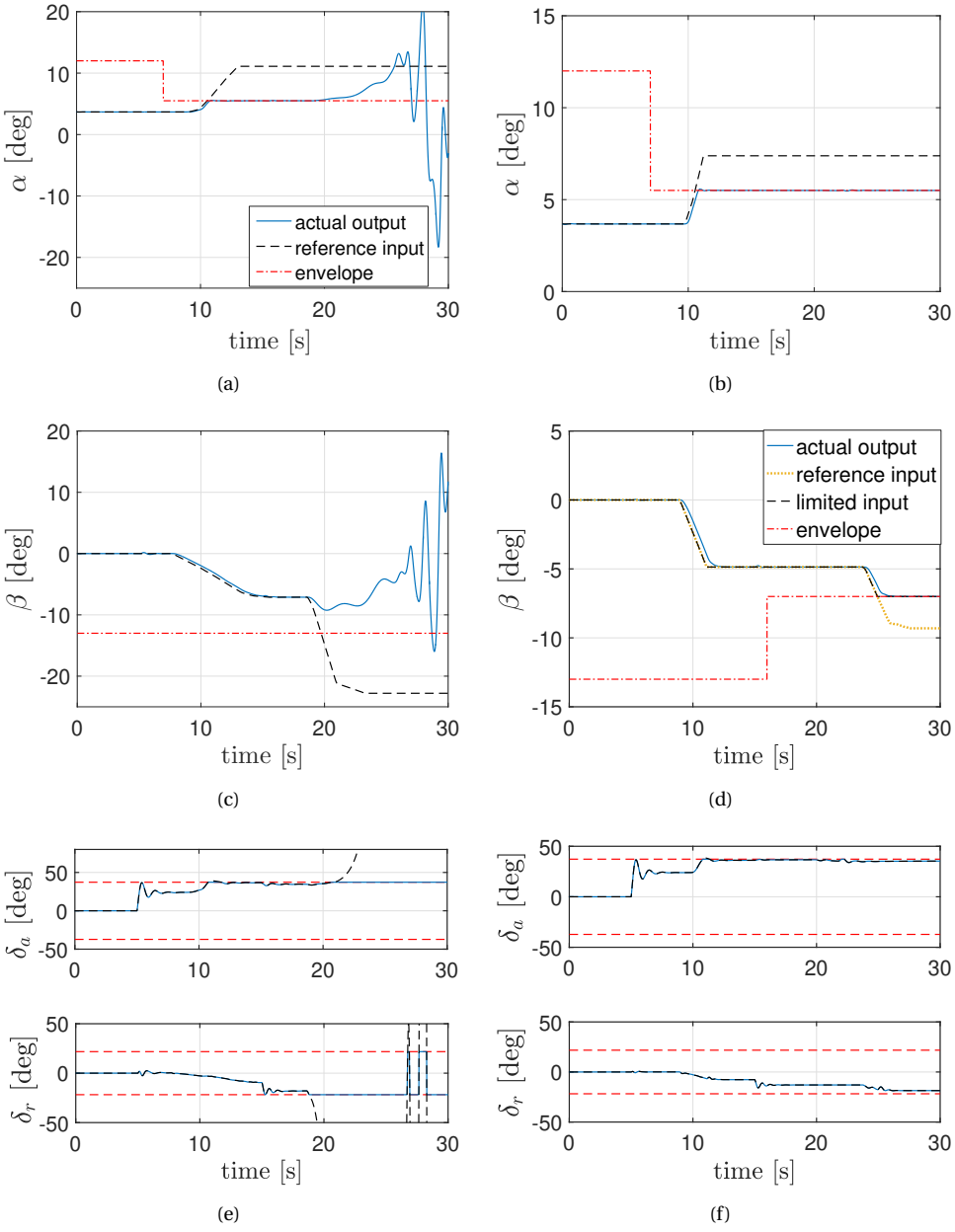

Figure 5.12: Comparison between flight with and without envelope protection under combined wing and rudder damage

Simulator Evaluation of Adaptive Safe Flight Envelope Protection Algorithm, Journal of Guidance, Control, and Dynamics **40**, 1902 (2017).

[6] D. Van Baelen, J. Ellerbroek, M. M. van Paassen, and M. Mulder, *Design of a Haptic Feedback System for Flight Envelope Protection,* in *AIAA Modeling and Simulation Technologies Conference* (2018).

[7] J. Ellerbroek, M. J. Martin, T. J. J. Lombaerts, M. M. van Paassen, and M. Mulder, *Design and evaluation of a Flight Envelope Protection haptic feedback system,* IFAC-PapersOnLine **49**, 171 (2016).

[8] G. H. Shah, *Aerodynamic Effects and Modeling of Damage to Transport Aircraft,* AIAA Guidance, Navigation and Control Conference and Exhibit (2008).

[9] R. J. Patton, *Fault-Tolerant Control: The 1997 Situation,* in *Proc. of the IFAC Symp. SAFEPROCESS 97* (Kingston Upon Hull, UK, 1997) pp. 1033–1055.

[10] Y. Zhang and J. Jiang, *Bibliographical review on reconfigurable fault-tolerant control systems,* Annual Reviews in Control **32**, 229 (2008).

[11] B. Bacon, A. J. Ostroff, and S. Joshi, *Reconfigurable NDI Controller Using Inertial Sensor Failure Detection & Isolation,* Aerospace and Electronic Systems, IEEE Transactions on **37**, 1373 (2001).

[12] S. Sieberling, Q. P. Chu, and J. A. Mulder, *Robust Flight Control Using Incremental Nonlinear Dynamic Inversion and Angular Acceleration Prediction,* Journal of Guidance, Control, and Dynamics **33**, 1732 (2010).

[13] T. Lombaerts, H. Huisman, P. Chu, J. A. Mulder, and D. Joosten, *Nonlinear Reconfiguring Flight Control Based on Online Physical Model Identification,* Journal of Guidance, Control, and Dynamics **32**, 727 (2009).

[14] H. J. Tol, C. C. D. Visser, L. G. Sun, E. V. Kampen, and Q. P. Chu, *Multivariate Spline-Based Adaptive Control of High-Performance Aircraft with Aerodynamic Uncertainties,* Journal of Guidance, Control, and Dynamics **39**, 781 (2016).

[15] E. J. J. Smeur, Q. Chu, and G. C. H. E. de Croon, *Adaptive Incremental Nonlinear Dynamic Inversion for Attitude Control of Micro Air Vehicles,* Journal of Guidance, Control, and Dynamics **39**, 450 (2016).

[16] P. Simplício, M. D. Pavel, E. van Kampen, and Q. P. Chu, *An acceleration measurements-based approach for helicopter nonlinear flight control using incremental nonlinear dynamic inversion,* Control Engineering Practice **21**, 1065 (2013).

[17] I. Matamoros and C. C. de Visser, *Incremental Nonlinear Control Allocation for a Tailless Aircraft with Innovative Control Effectors,* in *AIAA Guidance, Navigation, and Control Conference* (2018).

[18] F. Grondman, G. Looye, R. O. Kuchar, Q. P. Chu, and E.-J. Van Kampen, *Design and Flight Testing of Incremental Nonlinear Dynamic Inversion-based Control Laws for a Passenger Aircraft,* in *2018 AIAA Guidance, Navigation, and Control Conference* (2018).

[19] P. Lu, E. J. van Kampen, C. de Visser, and Q. Chu, *Aircraft fault-tolerant trajectory control using Incremental Nonlinear Dynamic Inversion,* Control Engineering Practice **57**, 126 (2016).

[20] H. Koolstra, *Preventing Loss of Aircraft Control: Aiding pilots in manual recovery from roll-limited situations*, Ph.D. thesis, Delft University of Technology (2017).

[21] D. Gingras, R. Ranaudo, B. Barnhart, T. Ratvasky, and E. Morelli, *Envelope Protection for In-Flight Ice Contamination,* in *AIAA Aerospace Sciences Meeting* (2009).

[22] T. Lombaerts, G. Looye, A. Seefried, M. Neves, and T. Bellmann, *Proof of concept simulator demonstration of a physics based self-preserving flight envelope protection algorithm,* Engineering Applications of Artificial Intelligence **67**, 368 (2018).

[23] P. F. A. Di Donato, S. Balachandran, K. McDonough, E. M. Atkins, and I. Kolmanovsky, *Envelope-Aware Flight Management for Loss of Control Prevention Given Rudder Jam,* Journal of Guidance, Control, and Dynamics **40**, 1027 (2017).

6

Discussion, Conclusions and Recommendations

6.1. DISCUSSION AND CONCLUSIONS

This research is motivated by the practical significance and technical challenges of loss of control (LOC) prevention. The thesis started with a statistical summary of aircraft accidents in recent years, addressing the importance of LOC prevention. Since LOC can be defined as an aircraft moving outside its safe flight envelope [1], one of the keys to LOC prevention is the ability of prediction and protection of these safe flight envelopes, which motivates the main focus of this thesis.

As a dynamics and control problem, LOC is highly complex in that there are many causal and contributing factors that happen in solo or in sequence [1, 2]. Among the most challenging contributing factors, some factors fundamentally change the dynamics, and the control authority of the aircraft. As a result, the flight envelopes are different from that of a nominal aircraft. The scope of this research is limited to the envelope prediction of such incidents, which includes airframe damage, icing, and actuator failures.

The main research goal formulated in Chapter 1 was:

Research Goal

To develop an online safe flight envelope prediction system for aircraft subject to in-flight faults and damage.

The key words of the research question are “online”, “prediction” and “in-flight”, indicating that the to-be developed system is required to predict the changed flight envelope *during* (abnormal) flight. This requirement poses several challenges to the research. The fundamental challenges in the online computation of flight envelopes lie in the fundamental impossibility of obtaining a *global* model of an in-flight damaged aircraft, as well as in the heavy computational load of online envelope updates. To circumvent these challenges, the concept of using a database is proposed in this research, which solves the problem of a large amount of online computations by using fast database retrieval. The core of this research is to develop this online system, the “Database-driven safE Flight ENvelope preDiction (DEFEND)” system [3].

In order to design and implement such a database-driven prediction system, the research is divided into two parts: offline envelope computation and online envelope prediction. The offline work focuses on the preparation for online implementations; together they form the main content of this thesis.

This final chapter summarizes the main results and contributions of this thesis. The proposed methodologies are evaluated in terms of their advantages and limitations. Recommendations for further research are given, as extensions of the current work, but also potential applications in the field of aircraft safety and LOC prevention.

6.1.1. OFFLINE PREPARATION

The work to be accomplished offline includes three aspects: 1) aircraft dynamics modeling, 2) flight envelope computation, and 3) database building. The offline preparation lays the foundation of the envelope prediction system.

DAMAGE MODELING

Modeling of aircraft dynamics effects under realistic LOC hazards is important but challenging work. The main challenge to tackle is data acquisition from impaired aircraft or during abnormal flight. One feasible and safe solution is through conducting wind-tunnel experiments as well as CFD modeling work on a sub-scale generic aircraft model under several pre-defined LOC cases [4–7]. In these experiments, values of stability and control derivatives under different abnormal cases are obtained and compared with normal aircraft flight. It can be drawn from these experiments that structural damage significantly reduces the stability of the aircraft as well as its control authorities.

The main focus of Chapter 3 is to incorporate the aerodynamic characteristics of various damage cases into the original mathematical model of a normal Cessna Citation aircraft, based on data from the aforementioned experiments, to establish a model of a partially damaged Cessna Citation. The severity level of damage is defined as the length ratio of damaged/lost tip to the total span. The model derived in Chapter 3 covers a range of five severity levels (10% - 50%) at three different parts (wing, horizontal stabilizer, vertical tail) and their affiliated actuators.

During the modeling process, it is found that the original model structure no longer holds under asymmetric damage, which needs additional terms that represent the changed aerodynamic effects. It is also found that damage to different parts on aircraft results in different aerodynamic characteristics, which are reflected in changes of different model parameters. For a certain damaged part, the change scale of each model parameter is related to the damage scale . By analyzing experimental data obtained from [4–7], the quantitative relation between change scales of model parameters and severity levels of the damage is approximated by a linear function.

In this way, each damage case is modeled by a predefined model structure with parameters that linearly change with the damage severity. By incorporating the modeling into DASMAT, the aerodynamic effects of different damage cases can be simulated under various flight conditions. Open-loop simulation results demonstrate that the derived model reflects the change of aerodynamic characteristics, as well as a change in control authority due to damage.

However, the models used in this research can not be verified by real flights or wind-tunnel tests, since it is practically infeasible to conduct such experiments with a passenger aircraft under damage conditions. Despite this, the modeling still accurately reflects how aircraft model changes, because the trends of stability reductions can be explained by flight dynamics principles. The only difference between the aerodynamic models of two similar aircraft types is in the numerical values of their aerodynamic coefficients. This is the primary assumption on which the modeling of the damage Cessna Citation aircraft can be based upon.

FLIGHT ENVELOPE COMPUTATION AND DATABASE BUILDING

In Chapter 4, safe envelopes for both longitudinal and lateral motions are computed using the level set method. It is shown that the shape and size of the computed envelopes depend on the time horizon, initial trim set, input values and most importantly, the current aircraft model. From damage modeling in Chapter 2, it is found that structural dam-

age directly influences the aircraft model. Therefore, the damage condition becomes a decisive factor of a flight envelope.

Flight envelopes computed under 20% wing damage and 30% horizontal stabilizer damage show obvious reductions in size and variations in shape compared with the nominal flight envelope. These results not only show the large impact of structural damage and the resulting aerodynamic model changes, but also confirm the necessity of computing the shrunken flight envelopes during flight after the occurrence of damage. It is also shown that flight envelopes are influenced by the flight condition, which for example expand with increasing true airspeed. This finding inspires further research on aircraft upset conditions(e.g., abnormal velocity and altitude).

Although the full aircraft model has been decoupled into longitudinal and lateral models to reduce the high computational burden, online envelope computation using the level set method is still extremely time consuming. Both theoretical analysis on computational complexity and numerical implementations demonstrate the infeasibility of direct envelope computation during flight even if the global model is available after a failure. These findings give rise to the idea of using a database for envelope look-up.

In Chapter 4, a database is designed to store the offline computed flight envelopes under different flight conditions and damage cases. Each flight envelope stored in the database can be retrieved by referring to the corresponding case index and current flight condition. However, physical limitations on database volume and damage modeling restricts the number of envelopes stored, which yields the need for interpolation. It is important to note that it is neither necessary nor feasible to interpolate between any two envelopes that are randomly retrieved from the database. In this dissertation, interpolation is only applied between envelopes that have connections in their physical origins and share similar geometric features. For example, envelopes of two different levels of tip loss of the same damage part, or envelopes of two different values of the same flight state or input.

Two examples are shown in Chapter 4, one is the interpolation between envelopes of two different damage scales, and the other is the interpolation between envelopes under two different values of airspeed. The interpolated envelopes are compared with the ones computed by the level set method, and the results show that the interpolation can approximate the result of the level set method with high accuracy.

In order to demonstrate the feasibility of online application of the database approach, it is necessary to evaluate the computational efficiency of the algorithm used for envelope interpolation. Compared to the level set method, the improvement in computational efficiency of the proposed database approach and interpolation is quantified by the speedup ratio, which is shown to increase with model dimension and computational grid resolution. For a simple 2D example, a significant enhancement in computational efficiency is demonstrated with a speedup ratio of 40000. This ratio can even increase up to 10^6 for a more complicated problem with 4 states. The complexity analysis indicates that envelope interpolation allows for quick prediction of flight envelopes based on database retrieval.

Furthermore, it is also discussed that envelopes obtained by experimental and computational methods other than the level set method can all be included in the database, regardless of the complexity of the methods applied offline. Given its high versatility and

efficiency, the database approach is demonstrated to be essential in online LOC prevention system, where available computational power and storage volume is limited.

Among all the contributing factors of LOC accidents, the database design and envelop computation in this thesis is only applied to aircraft damage cases. For some other factors, such as sensor and software faults, aircraft upsets, wind gust, inappropriate crew operations, the flight envelopes defined and computed in this thesis may not change. For such cases, alternative ways of determining envelopes and other protection strategies are required. Therefore, the proposed approach in its current form can not prevent all LOC accidents, but can be of great importance in situations where the safe flight envelopes have reduced. It should be noted that the proposed database-driven approach can be potentially extended to include more abnormal cases, both failure and non-failure, with flight envelopes defined and computed in different ways.

6.1.2. ONLINE IMPLEMENTATION

Based on offline-prepared database and models, the online system of envelope prediction can be established. To formulate the entire loop from sensor measurements to control inputs, several modules need to be designed and connected to the database.

AERODYNAMIC COEFFICIENT IDENTIFICATION

The adverse impact of unexpected structural damage on aircraft dynamics is reflected in the abrupt change of stability and control derivatives in the aerodynamic model, as revealed by wind-tunnel tests. The change of these coefficients can also be explained by basic flight dynamics, since the stability derivatives of the aircraft depend on the level in which airframe and control surfaces are complete and functioned.

Mathematically, the changed coefficients can be identified from the aircraft model. Since the damage/failure is activated in-flight, the changed model parameters need to be re-identified online and replace their original values. After the re-identification is initiated, the co-variance matrix is increased to enhance the influence of new incoming data. Then, sufficient excitation is provided to the system so that the parameters can converge to new values.

The re-identification is triggered by the signal of model change, which is generated when the discrepancy between measured output and expected output rises above a predefined threshold. From flight simulations in different scenarios, it is observed that the sudden activation of asymmetric damage generates unequal forces and subsequent incremental moments, which yield large errors in the original model of the undamaged aircraft. It is also found that the values of errors depend on the scale of damage as well as the level of external noise. Hence, the determination of the detection threshold for a certain damage part is based on the slightest level of damage severity and the highest level of noise modeled in the simulation environment. Different values of thresholds are simulated and results compared. It is found that higher threshold yields more false negatives (missed detections), while lower threshold results in more false positives (false alarms). The threshold that achieves a balance between false positives and false negatives is chosen as the detection threshold.

Sufficient excitation input is the crux of parameter identification, which can be generated either in an active way or in a passive way. During open-loop simulations in Chap-

ter 2, the excitation inputs to the aircraft are the deflections of elevators, ailerons and rudder, which are directly given by pilots. A balance needs to be achieved between safety and sufficiency when giving excitation inputs, especially after the occurrence of damage and failures. Therefore, small maneuvers are desired when giving excitation inputs.

However, current discussions on how small the maneuvers should be are more focused on pilot experience and intuition instead of the quantification of input constraints. In this thesis, pilot commands for excitation are constrained by the computed flight envelopes to guarantee safety. Since no information of the current damage condition can be provided before identification, the system will go for the most pessimistic one. This means that the excitation input starts with the boundary of the smallest envelope, which corresponds to the most severe damage case in the database. If the aircraft is still in control and more excitation is required, the input can be gradually increased to the boundary value of a larger envelope, until an updated local model around the current flight condition is successfully identified.

In Chapter 5, the aircraft is controlled by an automatic fault tolerant controller, so the excitation input is not directly given by the pilots but by the controller. Under this closed-loop configuration, the excitation is less of an issue than it is in the open-loop flight, especially when the damage is severe. The reason is that when trimmed flight is disturbed by sudden damage, the fault tolerant controller will automatically re-stabilize the aircraft, generating actuator commands that excite the identification. The closed-loop controlled flight is simulated in Chapter 5, and the aircraft is in trim flight when damage occurs. It is found that in the process of re-trimming the aircraft, sufficient excitation has been generated for parameter identification, and no additional maneuver commands are required from the pilot. The more severe the damage, the more the system is sufficiently excited as long as the actuators will not saturate and the aircraft is still under control. If the damage is too slight to fully excite the system, moderate commands will be given by pilots based on the most pessimistic envelope, as previously described.

System identification is implemented in open-loop and closed-loop simulations in Chapter 2 and Chapter 5, respectively. It is clearly shown that the identified stability derivatives quickly converge to the changed values after maneuvers and excitation. The identified parameters are used to capture the aerodynamic characteristics of the damaged aircraft as a preparation for damage case classification.

DAMAGE ASSESSMENT SYSTEM

This part of the research is motivated by the need for retrieving flight envelopes from the database. Since different abnormal cases result in different safety boundaries during flight, the type, location and severity of the damage and failures are used as the search key for retrieving various flight envelopes. In the database, each abnormal case is assigned an index number, which corresponds to a multi-dimensional data set of computed flight envelopes. Based on the current flight condition (e.g., velocity, altitude), the data set is decomposed and the desired flight envelope can be retrieved.

Among various abnormal cases, the identification of large-scale structural damage is barely discussed in literature. The main challenge of this issue is that there is no explicit mapping, i.e., a precise analytic mathematical function that describes the relationship between the damage condition of the aircraft and the changed aerodynamic character-

istics of the damaged aircraft. To tackle this problem, machine-learning is used to formulate the relationship from training data. Since the target of training is a set of pre-defined discrete events, the training is aimed at classifying the data into one of the categories defined by these events.

Two methods have been applied for damage case classification, namely neural networks (NN) and support vector machines (SVM). The classifiers normally produce a score that represents the degree of which an instance is a member of a class. The score is then used with a threshold to produce a discrete result. Each class is described by the percentage of tip loss of wings and tails. In Chapter 3, the performance of the neural network classification is evaluated by calculating the number and rate of true positive, false negative, true negative and false positive in a cross-validation. These evaluation results give us an insight into the balance between accuracy and generalization achieved by the classifier under a certain level of uncertainties and disturbances.

For database retrieval, it is found out that SVMs have better generalization ability, which provides additional information on the area between two neighboring classes. When the target classes are sparsely located, this feature is used to trigger envelope interpolation in the database, which is beneficial for safety. When the training classes are closely located, both SVMs and NNs give similar classification and evaluation results.

Apart from damage classification, the current condition can be assessed in a more descriptive way, such as 'moderate damage', 'severe damage', etc, which is achieved by applying fuzzy logic (FL). The FL represents the current situation in a more qualitative and descriptive manner, which may contribute to enhancing the situation awareness of pilots. Unlike machines, humans may not need numerically precise results, but would rather have a general qualitative idea of the current situation. Therefore, FL can be used as an auxiliary part in loss-of-control prevention systems, where pilots can be warned of the current situation by the diagnosis and assessment system.

FLIGHT ENVELOPE PROTECTION

By connecting online identification and classification to the offline-built database, an online flight envelope prediction system is established. The utilization of such a system is for online flight envelope protection, which closes the loop by feeding the safe boundaries to the online fault tolerant controller. Through online implementation of the complete loop, the feasibility of the database-driven flight envelope prediction is proved.

The aircraft is controlled in a multi-loop structure by pilot commands. In this research, commands on roll angle ϕ, angle of attack α and side-slip angle β are given to the controller as the reference input, and are transformed into deflections of ailerons, elevators and rudder, respectively, through NDI/INDI. On occurrence of sudden damage, the controller will try to re-stabilize the aircraft within its control authority. Simulation results show that during the period of re-stabilization, parameter re-identification, damage assessment and flight envelope retrieval can indeed be achieved.

It is observed from simulations that after the sudden occurrence of damage, the aircraft will be quickly re-stabilized by actions of a passive fault tolerant controller. As a consequence, part of the actuators will be used to mitigate the adverse effect of damage, which reduces the control authority of the aircraft. Simulation results show that LOC is still likely to happen when a new maneuver is initiated by pilots without providing them

with updated information of the current damage condition and reduced flight envelope limits to the control system. It can therefore be concluded that even though flight envelope prediction and protection cannot *directly* save the aircraft from LOC after sudden damage, it can actively prevent the aircraft from entering the LOC condition *again* after it is trimmed.

Hence, the main function of flight envelope protection in this research is to limit maneuvering commands and protect the re-trimmed aircraft from LOC. In Chapter 5, comparisons between simulated flights with and without envelope protection under the same damage case reveal the importance of online flight envelope prediction and protection. Simulation results also indicate that online implementation of flight envelope prediction and protection is feasible based on the offline-built databases.

From closed-loop simulations, it is found that the aircraft can not be protected from all damage cases. When the damage is so severe that the remaining actuators have reached their maximum control limits given the largest possible speed/thrust, the recovery of the aircraft is beyond the reach of the envelope prediction and protection techniques developed in this dissertation.

6.2. MAIN CONTRIBUTIONS

This thesis describes a method for online safe flight envelope prediction and addresses the issue of loss-of-control in transport-type aircraft. This work is unique in that it proposes referencing a database of damage/failure scenarios based on in-flight identification, rather than identification of a global model and direct envelope computations for any damage/failure condition.

With significantly reduced computational effort compared to existing methods, the proposed system is shown to be feasible for onboard real time implementation within the aircraft control laws. The research advances the state of the art in online damage/failure detection and safe envelope prediction of general fixed-wing aircraft.

Based on the above discussion, the main contributions of this thesis can be summarized as follows:

- An approach to online safe flight envelope prediction is proposed, which is based on the retrieval of information from offline-assembled databases.
- The aerodynamic model of a structurally damaged Cessna Citation aircraft is estimated and added to the flight simulation model.
- An online damage assessment system is designed to determine the structural damage of the state of the aircraft by using identification, detection, and classification methods. The concept of classification based on changes in aerodynamic derivatives is an innovative concept.
- A database is constructed offline, storing flight envelopes of different flight conditions and damage cases that are computed using the level set method.
- A method for interpolating between two pre-computed safe-flight envelopes is presented, which is less computationally expensive than directly using the level

set method. With the ability to interpolate between envelopes, the database can be used to establish an online flight envelope prediction system.

- The database-driven flight envelope prediction method is integrated with an online fault tolerant controller, to formulate a closed-loop flight envelope protection system. The implementation of the system in flight simulation illustrates the feasibility of its onboard application.

6.3. RECOMMENDATIONS FOR FUTURE WORK

This thesis has provided answers to the research questions posed in Chapter 1, yet in the course of obtaining results, many new questions and opportunities for further research have emerged. Recommendations for future work are summarized here.

MODELING AND SIMULATION OF VARIOUS LOC HAZARDS

Among all the contributors to LOC accidents, only fault and damage cases are modeled and simulated in this thesis as examples of representative abnormal cases based on wind-tunnel and CFD data. The modeling and simulation work of other LOC hazards, like stall, onboard icing and engine failures conducted in other research work [1, 6] is not included in this thesis. Therefore, it is recommended to develop an integrated real-time LOC simulation, covering a wide range of LOC scenarios and realistic combinations.

One limitation of this thesis is the lack of data, for our source of data is mainly from wind tunnel tests conducted by NASA [4, 5] on a generic transport model. To enable a more thorough study on the aerodynamic characteristics of a damaged Cessna Citation aircraft and establish its mathematical model in the DASMAT, wind tunnel tests on subscale model or CFD computation is recommended in future work.

Compared with the modeling process discussed in this thesis, the modeling method can be improved in future work to include not only aerodynamic effects, but also influential factors like propulsion and mass properties. The improvements on the modeling and simulation of LOC hazards will enhance the fidelity of the computed flight envelopes as well as the whole prediction and protection system. In addition, it will also benefit pilot training and the design of re-configurable flight control systems.

DEVELOPING INTERFACE SYSTEMS ON FLIGHT ENVELOPE PROTECTION

Generally, the application of safe flight envelopes should be focused on two aspects. One is on automatic flight control systems, and another equally important aspect is on human factors. This thesis mainly focuses on the former one, while the significance of situation awareness of pilots should not be ignored. Under highly-complex LOC conditions, a lack of situation awareness may result in inappropriate or delayed pilot response, counteracting the effectiveness of the controller and exacerbating the current situation.

Therefore, it is recommended in future work to apply the database-driven flight envelope prediction system to the development of flight deck interfaces. Based on dynamic flight envelopes retrieved from the database, better anticipatory guidance and improved situation awareness can be achieved either by modifying current displays [8–10] or designing new ones [11]. The abstract numerical limitation of flight envelopes can be transformed into interfaces designed in visual, verbal or haptic forms [12], which are more

easily understood and interpreted by human pilots.

EXPERIMENTAL TESTING FOR TECHNOLOGY VALIDATION

The DEFEND system developed in this thesis is only implemented through software simulation, while it is not yet validated by real-time hardware experiments. Hardware tests of closed-loop safety-critical systems are normally implemented on a robotic motion flight simulator [13], or more advanced subscale aircraft [1].

Based on the facilities available in TU Delft, it is recommended to conduct human-in-the-loop experiments on the six-degree-of-freedom SIMONA Research Simulator (SRS). Compared with desktop software simulations, the SRS provides a much more realistic environment that incorporates more practical considerations as well as human factors issues. In future work, various LOC scenarios can be simulated in the SRS, combined with an operational DEFEND system. Evaluations on flight performance and pilot work load in specific flying tasks (e.g., take off and landing) is recommended.

Although real flight tests on large passenger aircraft cannot be flown into high-risk LOC conditions, tests on small unmanned aircraft are possible to evaluate the performance of the DEFEND system and optimize the database based on the onboard memory capacity. Currently, experiments on a damaged quadrotor drone are being conducted, where one rotor is removed from the drone and the flight is maintained by an INDI controller [14]. Future work is recommended to define and compute flight envelopes that can be applied to damaged drones in the framework of the database approach.

TOWARD FUTURE AUTONOMOUS SYSTEMS

With the rise of self-driving cars, conceptual electric air taxis and intelligent robots etc., future research is moving towards more autonomous systems and operations [1], which pose critical safety-related issues. The concept of reachability can be applied to such systems, to guarantee a certain level of safety in autonomous operations. For example, the safe driving envelope can be computed for autonomous cars to reduce crash probability in a planned trajectory [15, 16]. Obstacle avoidance for drones may possibly be achieved by computing the reachable sets in more complex environments.

Furthermore, the concept of reachability can be extended to stochastic reachability analysis [17], which computes the probability of reaching a target set under the inevitable presence of disturbances. The combination of reachability and stochastic process is suitable for autonomous systems in complicated environment full of uncertainties and disturbances. Additionally, future autonomous systems will need to be adapted to a wide spectrum of adverse conditions and hazards. Therefore, database technology developed in this thesis may provide a set of safe operation envelopes for these systems in various abnormal scenarios with advanced intelligent and decision-making methods.

REFERENCES

[1] C. M. Belcastro, J. V. Foster, G. H. Shah, I. M. Gregory, D. E. Cox, D. A. Crider, L. Groff, R. L. Newman, and D. H. Klyde, *Aircraft Loss of Control Problem Analysis and Research Toward a Holistic Solution,* Journal of Guidance, Control, and Dynamics **40**, 733 (2017).

[2] S. Jacobson, *Aircraft Loss of Control Causal Factors and Mitigation Challenges,* in *AIAA Guidance, Navigation, and Control Conference* (2010).

[3] Y. Zhang, C. C. de Visser, and Q. P. Chu, *Aircraft Damage Identification and Classification for Database-Driven Online Flight-Envelope Prediction,* Journal of Guidance, Control, and Dynamics **41**, 449 (2018).

[4] G. H. Shah, *Aerodynamic Effects and Modeling of Damage to Transport Aircraft,* in *AIAA Atmospheric Flight Mechanics Conference* (2008).

[5] G. H. Shah and M. Hill, *Flight Dynamics Modeling and Simulation of a Damaged Transport Aircraft,* in *AIAA Modeling and Simulation Technologies Conference* (2012).

[6] D. Gingras, R. Ranaudo, B. Barnhart, T. Ratvasky, and E. Morelli, *Envelope Protection for In-Flight Ice Contamination,* in *AIAA Aerospace Sciences Meeting* (2009).

[7] H. N. Nabi, T. J. J. Lombaerts, Y. Zhang, E. van Kampen, Q. P. Chu, and C. C. de Visser, *Effects of Structural Failure on the Safe Flight Envelope of Aircraft,* Journal of Guidance, Control, and Dynamics **41**, 1257 (2018).

[8] R. Ranaudo, B. Martos, and B. Norton, *Piloted Simulation to Evaluate the Utility of a Real Time Envelope Protection System for Mitigating In-Flight Icing Hazards,* in *Atmospheric and Space Environments Conference* (2010).

[9] T. J. J. Lombaerts, S. Schuet, D. Acosta, J. Kaneshige, K. Shish, and L. Martin, *Piloted Simulator Evaluation of Safe Flight Envelope Display Indicators for Loss of Control Avoidance,* Journal of Guidance, Control, and Dynamics **40**, 948 (2016).

[10] S. Schuet, T. J. J. Lombaerts, D. Acosta, J. Kaneshige, K. Wheeler, and K. Shish, *Autonomous Flight Envelope Estimation for Loss-of-Control Prevention,* Journal of Guidance, Control, and Dynamics **40**, 847 (2017).

[11] A. D. T. Rijndorp, C. Borst, C. C. De Visser, O. Stroosma, M. Mulder, and M. M. Van Paassen, *Aviate, Navigate: Functional Visualizations of Asymmetric Flight Envelope Limits,* in *AIAA Information Systems* (2017).

[12] D. Van Baelen, J. Ellerbroek, M. M. van Paassen, and M. Mulder, *Design of a Haptic Feedback System for Flight Envelope Protection,* in *AIAA Modeling and Simulation Technologies Conference* (2018).

[13] T. J. J. Lombaerts, G. Looye, A. Seefried, M. Neves, and T. Bellmann, *Proof of concept simulator demonstration of a physics based self-preserving flight envelope protection algorithm,* Engineering Applications of Artificial Intelligence **67**, 368 (2018).

[14] S. Sun, L. Sijbers, X. Wang, and C. C. de Visser, *High-speed flight of quadrotor despite loss of single rotor,* IEEE Robotics and Automation Letters **3**, 3201 (2018).

[15] M. Althoff and B. H. Krogh, *Reachability analysis of nonlinear differential-algebraic systems,* IEEE Transactions on Automatic Control **59**, 371 (2014).

[16] M. Althoff and J. M. Dolan, *Online verification of automated road vehicles using reachability analysis,* IEEE Transactions on Robotics **30**, 903 (2014).

[17] R. van den Brandt, *Safe Flight Envelope Uncertainty Quantification using Probabilistic Reachability Analysis*, Master's thesis, Delft University of Technology (2017).

ACKNOWLEDGEMENTS

The past four and a half years of my PhD experience have been an unforgettable adventure in my life. Apart from all the scientific results and knowledge that constitutes this thesis, what makes this life period so wonderful is the cheerful and lovely people I met along these years. Therefore, it is my pleasure to conclude this book with this acknowledgement, to express my deep gratitude and appreciation.

My first thanks goes to my promotor, Prof. Max Mulder, for giving me the opportunity to pursue my career in this loving group. I am impressed by your energetic and enthusiastic way of work as well as your caring and thoughtful support. Thanks to your cheerfulness, being in the C&S group feels just like home. I enjoyed following your quick minds when discussing my thesis work with you. Thank you for all the wise remarks and interesting comments that greatly improved my work.

My deep gratitude also goes to another promotor of mine, Dr. Chu, who is as inspiring as a supervisor, and as caring as a friend to me. You are always available and approachable whenever I felt confused. Thank you for giving so many courageous and supportive suggestions on my research as well as my life. I will always cherish the happy moments when we exchanged research ideas and shared our common hobbies on photography. You showed me what an ideal relationship between a student and teacher would look like, which, in Chinese is, "yi shi yi you" (a teacher in class and a friend in life).

I also would like to express my profound appreciation toward my co-promotor, my daily supervisor, Dr. Coen de Visser. Coen, thank you for patiently reviewing my journal papers and giving valuable comments so that they were so much improved that finally got accepted. I couldn't thank you more for helping me achieve the first scientific paper of my research career. You are always bright and cheerful with your relaxing smiles and humorous comments, which makes it enjoyable working with you. I would never forget the happy memories we share during daily work as well as travelling abroad.

My thanks also goes to all the other staff members: Prof. Bob Mulder, Prof. Jacco Hoekstra, René van Paassen, Daan Pool, Erik-Jan van Kampen, Clark Borst, Joost Ellerbroek, Guido de Croon, Olaf Stroosma, Marilena Pavel, Alexander in't Veld, Hans Mulder, Bertine Markus, Ferdinand Postema, Andries Muis, Harold Thung, Alwin Damman, who gave me a lot of technical and academic supports during my study, and I learned a lot from them. A particular thank to Bertine, for always being so kind and helpful whenever I have questions.

Next, my deep gratitude goes to my dear colleagues, whom I have spent a lot of good time working and having fun with: Xuerui Wang, Sihao Sun, Wei Fu, Junzi Sun, Shuo Li, Shushuai Li, Ye Zhou, Bo Sun, Ying Yu, Yingfu Xu, Sophie Armanini, Dyah Jatiningrum, Jaime Junell, Kimberley McGuire, Isabel Metz, Diana Olejnik, Matěj Karásek, Kirk Scheper, Ivan Miletović, Dirk Van Baelen, Jelmer Reitsma, Daniel Friesen, Mario Coppola, Emmanuel Sunil, Ewoud Smeur, João Caetano, Tommaso Mannucci, Yazdi Je-

nie, Henry Tol, Kasper van der El, Hann Woei Ho, Peng Lu, Lei Yang, Liguo Sun, Tao Lu, Jerom Maas, Julia Rudnyk, Sarah Baarendswaard, Tom van Dijk, Rolf Klomp, Annemarie Landmann, Federico Paredes Vallés. I will miss you, with all those hilarious coffee breaks, tasty cakes, daily complaints, “gezellige” drinks and unforgettable summer sailings and BBQs.

Special thanks go to my dear Chinese friends - thanks for all the fun time and unforgettable moments in amazing travelings, countless hot-pot dinners and movie nights, crazy world-cup parties, heart-warming Chinese new year’s eves. I miss all the stupid jokes you made and bright advises you gave. To Sherry and Sihao, for all the happy memories we share during these years, and for your encouragement and inspirations; to Ye Zhou, for all the interesting long talks in and outside office hours; to Wei Fu and Gehua Wen, for the amazing trip to Austria and all the get-together dinners; to Junzi and your lovely family, for hosting us on each Chinese New Year’s eve and all the interesting discussions we had during lunch time; to Shuo, who is busy all the time but still kindly offers to be our defence photographer with Yingfu, for always being so generous and sweet; to Shushuai and Mel, for being such a sweet and lovely couple and giving us so much happiness; to Ying, for the tasty snacks you brought from China and the amazing meals you cooked for us; to Peng and Xiang, for being so inspiring and courageous even after you graduated; to Lei, who had seated behind me for two years, for being so lively and cheerful all the time; to newly-come young friends Bo and Yingfu; for adding more liveliness to the party with your fresh ideas...Your accompanies along these years make me feel like home even in darkest hours.

Special thanks also goes to my old and new friends that comes from all around the world. To Sophie, for all the interesting talks and correspondences we had about life and study; to Jamie, for giving so many amazing performances with Sophie, Tommaso and Tao, and the happiness you brought to the office; to my desk-mate Kimberley, for always being so cheerful and humorous, who lightens up my day; to my ex-desk-mate Henry, for hosting us to your lovely home in Volendam; to Dyah, for all the nice experiences together in the US and Poland; to Ivan, for all the cheering conversations we had; to Kirk, for being so energetic and enthusiastic around; to Diana, for your lively spirit and fancy styles, which I like a lot; to Jemer, for all the fun talks during coffee breaks; to Matěj for your amazing adventures that inspired me, and all the Czech desserts you brought from home; to Dirk, for all the good times in the US, and for translating my summary into Dutch; to Isabel for all the happy talks in “de Atmosfeer”; to Daniel for your hilarious jokes and to Jerom for your interesting stories in the coffee corner; to João and Susanna for leaving us such a nice apartment and being cheerful and sweet all the time...I will cherish the happy memories of you all throughout my whole life.

I want to express my deepest gratitude toward my parents, for your unconditional love and support and all the exciting, anxious, happy and frustrating moments we share through Skype. Your endless encouragement, concerns and suggestions on my research and career have greatly helped me through my ups and downs. My PhD would not be so smooth without your enduring love and care!

And finally, Yingzhi, my dearest friend, my most trusted companion, my beloved husband. We have known each other and been working together for ten years. Your unwavering support and ever present love, optimism, determination and above all, your

irreplaceable cooking skills, pulled me through. Thank you for being a part of my life. Together with you, I see a bright future full of happiness.

I will remember these four and a half years as one of the most amazing times I have ever had. I will miss Delft and all the people I am so fortunate to meet. Thank you very much!

Delft, March 2019

CURRICULUM VITÆ

Ye ZHANG

23-12-1990 Born in Xi'an, China.

EDUCATION

2008–2012 B.Sc.
Northwestern Polytechnical University, China
Guidance, Navigation and Control
Faculty of Astronautic Engineering
Thesis : Visual Servo Technology in Space Rendezvous and Docking

2012–2014 M.Sc.
Northwestern Polytechnical University, China
Guidance, Navigation and Control, Faculty of Astronautic Engineering
Thesis: Particle Filter Theory and Its Application in Multi-target Tracking

2014 Ph.D.
Delft University of Technology, The Netherlands
Control and Simulation, Faculty of Aerospace Engineering
Thesis : Database-driven Online Safe Flight Envelope Prediction and Protection for Enhanced Aircraft Fault Tolerance

AWARDS

2012 Distinguished undergraduate student

2012 Best graduation thesis

2014 Distinguished graduate student

List of Publications

Journal Papers

5. **Y. Zhang**, C. C. de Visser, and Q.P. Chu. *Database Building and Interpolation for an Online Safe Flight Envelope Prediction System.* Journal of Guidance, Control and Dynamics, 2019. (published)

4. **Y. Zhang**, C. C. de Visser, and Q.P. Chu. *Aircraft Damage Identification and Classification for Database-driven Online Safe Flight Envelope Prediction.* Journal of Guidance, Control and Dynamics, Vol. 41, No. 2, 2018, pp. 449–460.

3. H. N. Nabi, T.J.J. Lombaerts, **Y. Zhang**, E. van Kampen, Q.P. Chu, and C. C. de Visser. *Effects of Structural Failure on the Safe Flight Envelope of Aircraft.* Journal of Guidance, Control, and Dynamics, Vol. 41, No. 6 (2018), pp. 1257-1275.

2. M. Yin, Q.P. Chu, **Y. Zhang**, M. Niestroy, C. C. de Visser. *Probabilistic Flight Envelope Estimation with Application to Unstable Over-Actuated Aircraft.* Journal of Guidance, Control and Dynamics, 2019. (under review)

1. **Y. Zhang**, C. C. de Visser, and Q.P. Chu. *Database-driven Online Flight Envelope Protection for Damaged Aircraft.* Journal of Guidance, Control and Dynamics, 2019. (to be submitted)

Conference Papers

7. **Ye Zhang**, Coen C. de Visser, and Q.P. Chu. *Aircraft Damage Pattern Recognition Using Aerodynamic Coefficients and Fuzzy Logic.* Advances in Aerospace Guidance, Navigation and Control. Springer, 2018

6. **Ye Zhang**, Coen C. de Visser, and Q.P. Chu. *Database Building and Interpolation for a Safe Flight Envelope Prediction System.* AIAA Information Systems, 2018.

5. **Ye Zhang**, Coen C. de Visser, and Q.P. Chu. *Online Aircraft Damage Case Identification and Classification for Database Information Retrieval.* AIAA Atmospheric Flight Mechanics Conference, 2018.

4. **Ye Zhang,** Coen C. de Visser, and Q.P. Chu. *Aircraft Damage Identification and Classification for Database-driven Safe Flight Envelope Prediction.* AIAA Atmospheric Flight Mechanics Conference. 2017.

3. **Ye Zhang**, Coen C. de Visser, and Q.P. Chu. *Online Safe Flight Envelope Prediction for Damaged Aircraft: A Database-driven Approach.* AIAA Modeling and Simulation Technologies Conference. 2016.

2. **Ye Zhang**, Coen C. de Visser, and Q.P. Chu. *Online Physical Model Identification for Database-driven Safe Fight Envelope Prediction of Damaged Aircraft.* AIAA Atmospheric Flight Mechanics Conference. 2016

1. M. Yin, Q.P. Chu, **Y. Zhang**, M. Niestroy, C. C. de Visser. *Probabilistic Flight Envelope Estimation with Application to Unstable Over-Actuated Aircraft.* AIAA Scitech Forum, 2019.